UC-32
LBL-22086
c.2

Lawrence Berkeley Laboratory

UNIVERSITY OF CALIFORNIA

Physics Division

RECEIVED
LAWRENCE
BERKELEY LABORATORY

OCT 13 1986

LIBRARY AND
DOCUMENTS SECTION

Mathematics Department

A NUMERICAL STUDY OF SUPERFLUID TURBULENCE
IN THE SELF-INDUCTION APPROXIMATION

T.F. Buttke
(Ph.D. Thesis)

August 1986

TWO-WEEK LOAN COPY

This is a Library Circulating Copy
which may be borrowed for two weeks.

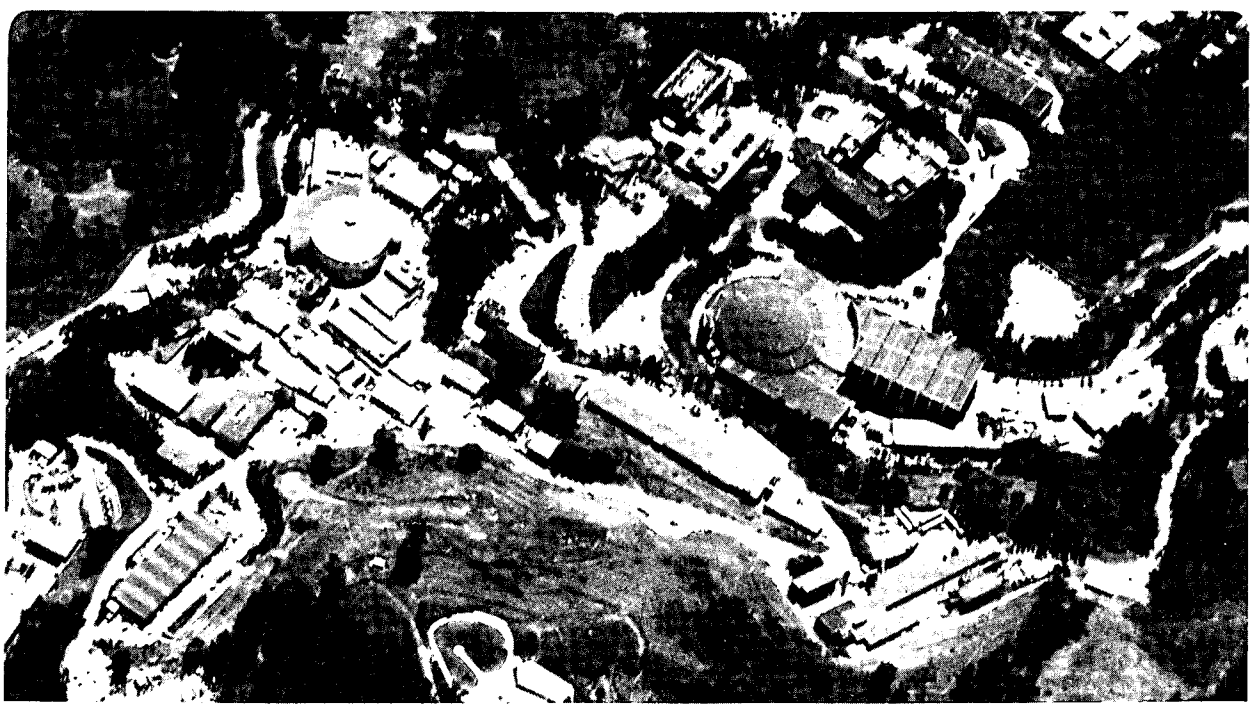

LBL-22086
c.2

Prepared for the U.S. Department of Energy under Contract DE-AC03-76SF00098

DISCLAIMER

This document was prepared as an account of work sponsored by the United States Government. While this document is believed to contain correct information, neither the United States Government nor any agency thereof, nor the Regents of the University of California, nor any of their employees, makes any warranty, express or implied, or assumes any legal responsibility for the accuracy, completeness, or usefulness of any information, apparatus, product, or process disclosed, or represents that its use would not infringe privately owned rights. Reference herein to any specific commercial product, process, or service by its trade name, trademark, manufacturer, or otherwise, does not necessarily constitute or imply its endorsement, recommendation, or favoring by the United States Government or any agency thereof, or the Regents of the University of California. The views and opinions of authors expressed herein do not necessarily state or reflect those of the United States Government or any agency thereof or the Regents of the University of California.

LBL-22086

A NUMERICAL STUDY OF SUPERFLUID TURBULENCE IN THE SELF-INDUCTION APPROXIMATION[1]

Thomas F. Buttke

Department of Mathematics and Lawrence Berkeley Laboratory
University of California
Berkeley, California 94720

Ph.D. Thesis

August 1986

[1]Supported in part by the Applied Mathematical Sciences Subprogram of the Office of Energy Research, U.S. Department of Energy under contract DE-AC03-76SF00098.

A Numerical Study of Superfluid Turbulence in the Self-Induction Approximation

Thomas F. Buttke

Abstract

We present a numerical method that determines the evolution of a superfluid vortex, and use it to calculate some properties of turbulent superfluid vortex systems. We find substantial disagreements with previous calculations.

We derive a stable finite difference method for solving the self-induction equation in vortex dynamics. The self-induction equation is equivalent to a non-linear Schrödinger equation. We design our numerical method so that it preserves some of the invariants of the Schrödinger equation; this leads to stability. Our method is written in terms of the tangent field of the vortex lines. We are able to show that the approximate solutions exist for all times and for all initial conditions. As far as we know, this is the first stable numerical method for solving the self-induction equation.

We also find a new exact self-similar solution of the self-induction equation and use this solution along with the previously known soliton solutions to validate our method. We conclude that the method is second order accurate in space and time.

We view the equations which govern the evolution of a superfluid vortex as a perturbation of the self-induction equation and develop a method for determining the evolution of a superfluid vortex. We incorporate the reconnection ansatz of Schwarz into our method. We validate our method by comparison with known exact solutions and by a careful convergence check for cases where the exact solution is not known. We find that if the spatial step in the approximation is chosen too large the approximate solutions become inaccurate. Following the work of Schwarz we perform experiments on vortex systems to find the line length density of a turbulent superfluid. We find that the turbulence produced is not homogeneous, and we find line length densities and critical properties that disagree with earlier results. We

Acknowledgements

I wish to thank my advisor, Alexandre Chorin, without whose mathematical guidance and insights this thesis would have been impossible. More importantly I thank Alexandre for his humanity and personal guidance at a critical point in my life.

I am also deeply grateful to Harry Morrison for his encouragement and guidance.

I thank Ole Hald for his instructive conversations and his patience.

In addition I would like to thank Andy Majda, Murray Protter and Marina Ratner; from each of them I learned much.

I am also grateful to Gerry Puckett for many helpful discussions.

Finally I would like to thank K. W. Schwarz for his helpful conversation.

Table of Contents

Introduction 1

1. The Self-Induction Approximation 5

1.1 The Self-Induction Approximation 5

1.2 The Betchov Equations 11

1.3 The Non-Linear Schrödinger Equation 15

1.4 Invariants 19

1.5 Exact Solutions 21

1.6 The Self-Similar Solution 25

1.7 Existence and Uniqueness of Solutions 27

2. Numerical Schemes for the Self-Induction Equation 28

2.1 The Finite Difference Equations 29

2.2 Methods for Solving the Finite Difference Equations 33

2.3 Stability 37

2.4 Accuracy 39

2.5 Summary of the Method 41

3. Numerical results for the Self-Induction Equation 43

Tables 3.1-3.3 49

Figures 3.1-3.18 52

4. Self-Induction Plus Stretching for Superfluid Helium 70

4.1 The Two Fluid Equations 71

4.2 Quantized Vortices 74

4.3 The Model Equation 77

4.4 Exact Solutions of the Model Equation 80

Figures 4.1-4.6 83

5. Numerical Methods That Account for Stretching 89

5.1 The Finite Difference Equations 89

5.2 Stability 93

5.3 The Reconnection Ansatz 97

Figure 5.1 102

6. Numerical Results for Superfluid Helium 103

Figures 6.1-6.17 109

Bibliography 126

Introduction

We present a numerical method that determines the evolution of a superfluid vortex. We use our method to calculate some properties of turbulent superfluid vortex systems. We find substantial disagreement with previous calculations.

We first find a stable finite difference method for solving the self-induction equation. The self-induction equation is equivalent to a non-linear Schrödinger equation and thus the problems in solving the Schrödinger equation are also inherent to solving the self-induction equation. We are able to develop a successful method by designing our numerical method so that it preserves some of the invariants of the Schrödinger equation; this ultimately implies the stability of the numerical method. We then view the equation governing the evolution of the superfluid vortices as a perturbation of the self-induction equation and appropriately modify our approximation to take into account the additional complexities.

The self-induction approximation in vortex theory consists of setting the velocity of a vortex line proportional to the curvature of the vortex line and in the direction of the binormal to the line. For short times the self-induction approximation gives correct results for the motion of the vorticity [8]; however, the approximation allows for no stretching of the vorticity and thus cannot be expected to give accurate results over long periods of time. In spite of its inadequacies the self-induction approximation is attractive because of its simplicity.

In the first chapter we present a derivation of the self-induction approximation as given in Batchelor [4]. We then discuss properties of the self-induction equation. We present Betchov's equations [5] in which the self-induction approximation is written in terms of the evolution of the curvature and torsion of the vortex. We present the transformation, due to Hasimoto [24], which transforms the self-induction equation into a non-linear Schrödinger equation. We discuss the fact that the self-induction equation has an infinite number of integral invariants and present several of these invariants. We then present the known exact solutions of the self-induction equation. These exact solutions include the soliton solutions.

Next we present a new exact self-similar solution. This self-similar solution results from initial conditions which have a discontinuity in the tangent field of the vortex. This exact self-similar solution is important in validating the numerical method we develop in chapter 2.

Hama [22,23] was the first to attempt to approximate the self-induction equations numerically and was successful in developing a pseudo-stable numerical method. Hama's method is pseudo-stable in the sense that the approximate solutions appear to converge for a certain time interval before the instability becomes apparent. Schwarz [41] also attempted a numerical approximation and although he developed a method different from Hama's, Schwarz' method exhibited the same instabilities as Hama's. Aref and Flinchem [2] developed a numerical approximation to the self-induction equations and they saw no indication of any instability in their results, however, they generally carried out their results for times for which instabilities would not be expected. The fact that the self-induction equation is equivalent to a Schrödinger equation makes it difficult to find stable numerical methods [27].

In chapter two we present a finite difference method which we developed which, as far as we know, is the first stable numerical approximation of the self-induction equation. The method finds the tangent field of the vortex rather than the position of the vortex directly. We show that this approximation has three invariants that corresond to invariants of the Schrödinger equation. The conservation of these invariants implies the stability of the method. We then discuss methods for solving the non-linear finite difference equations which result from our finite difference approximation. We are able to show that numerical solutions to the finite difference equations exist for all initial conditions and for all times. We then show the stability and local linear stability of our method. Next we discuss the accuracy of our method and conclude that it is second order accurate in time and space. Following the discussion of the accuracy of our basic method we propose a modification to our basic method which is fourth order accurate; however, we have done no calculations with this

fourth order method.

In chapter three we present numerical results obtained with our method. First we compare our approximate solutions with exact soliton solutions and verify that the method is second order accurate in space and time for smooth solutions. Next we discuss the numerical solution of the self-similar problem and compare the exact solution with the approximate solution. The approximate solution converges to the exact solution, but the convergence is slower than it is for smooth solutions. We also present evidence indicating that derivatives of the approximate solution converge weakly to the derivatives of the exact solution.

As mentioned above, one of the inadequacies of the self-induction equation is that a vortex does not stretch when it evolves according to this approximation. In order to correct this problem, the self-induction approximation is sometimes used together with other approximations which cause the vortex to stretch [2,38]. We consider an approximation due to Schwarz [38], in which he uses the self-induction approximation along with phenomenological terms in order to approximate the motion of a superfluid vortex. In chapter four we present a brief introduction to the two fluid equations, introduced by Landau [28], which describe the flow of superfluid helium. We present Schwarz' work in which he obtains a local model for the evolution of a superfluid vortex. We then present the only known exact solutions to this model equation, which are circular vortices.

In chapter five we generalize our numerical method for solving the self-induction equations so that we can solve equations which are perturbations of the self-induction equation. In our numerical method for solving the self-induction equation we use arclength as our spatial variable; however, when stretching of the vortices is introduced we rewrite our equations in terms of a lagrangian variable labeling the fluid particles along the vortex. We develop our numerical approximation so that it preserves the important stability results obtained in chapter two for the self-induction equation. As a specific example we introduce a method for solving the equation introduced by Schwarz [39] for modeling superfluid vortices. We also

introduce the reconnection ansatz, implemented by Schwarz [39] to model superfluid turbulence, in which any two vortices which cross each other reconnect with each other. We then discuss the error which appears if the spatial approximation step is not small enough. We conclude the chapter by discussing the problems of implementing the reconnection ansatz.

In chapter six we present the results obtained by using the numerical method introduced in chapter five. We first validate the method by comparing approximate solutions with exact circular solutions. We then investigate the convergence of a problem in which we allow a reconnection to take place. We find that the spatial step in the approximation must be chosen small enough to approximate accurately the region of large curvature introduced by the reconnection. If the spatial step is too large there is a precipitous loss of accuracy. We then repeat the numerical experiments of Schwarz [39] to determine the line length density of superfluid helium vortices. We find that Schwarz' approximation together with the reconnection ansatz does produce a system of vortices which equilibrates to an equilibrium line length density for most initial conditions. Furthermore we find that if the system reaches a dynamical equilibrium, the value of the line length density is independent of the initial conditions of the system. Contrary to earlier results, however, we find that the resultant turbulence is not homogeneous. We also find that the numbers reported earlier for the line length density are in error, and we explain the source of the error. We conclude that the model used is inadequate to describe homogeneous turbulence in superfluid helium.

Chapter 1: The Self-Induction Approximation

In this chapter we introduce the self-induction approximation. We write the self-induction equation in three equivalent forms and present some properties that solutions of the self-induction equation satisfy. We present a family of exact soliton solutions as well as a new exact self-similar solution. The self-similar solution is important because it has the same singularity as the problems we shall be solving in chapter six.

1.1 The Self-Induction Approximation

We begin by considering an incompressible isentropic fluid of infinite extent in three dimensions. We wish to determine its time evolution by determining the evolution of the vorticity. We denote the velocity field by $\vec{v}$ and the vorticity field by $\vec{\omega}$.

$$\vec{\omega} \equiv \nabla \times \vec{v} \ .$$

We first derive an expression for the velocity field in terms of the vorticity [10]. A fluid is incompressible if and only if $\nabla \cdot \vec{v} = 0$. Given a field $\vec{v}$ satisfying $\nabla \cdot \vec{v} = 0$, there exists a vector field $\vec{A}$ such that $\nabla \cdot \vec{A} = 0$ and $\nabla \times \vec{A} = \vec{v}$ [44]. If we use the vector identity $\nabla \times \nabla \times \vec{v} = \nabla(\nabla \cdot \vec{v}) - \nabla^2 \vec{v}$, we obtain $\nabla^2 \vec{A} = -\vec{\omega}$. Let $\vec{x}$ and $\vec{x}'$ denote arbitrary points in $\mathbf{R}^3$. The Green's function for the three dimensional Laplacian is

$$G(\vec{x}, \vec{x}') = -\frac{1}{4\pi} \frac{1}{|\vec{x} - \vec{x}'|}$$

Using the Green's function for the Laplacian, we obtain the following result, which expresses $\vec{A}$ in terms of the vorticity, $\vec{\omega}$.

$$\vec{A}(\vec{x}) = \frac{1}{4\pi} \int_{\mathbf{R}^3} \frac{\vec{\omega}(\vec{x}')}{|\vec{x} - \vec{x}'|} \, d^3\vec{x}' \tag{1.1}$$

After taking the curl of both sides of equation (1.1), we find that

$$\vec{v}(\vec{x}) = -\frac{1}{4\pi} \int_{\mathbf{R}^3} \frac{(\vec{x} - \vec{x}') \times \vec{\omega}(\vec{x}')}{|\vec{x} - \vec{x}'|^3} \, d^3\vec{x}' \ . \tag{1.2}$$

We consider the case where the vorticity is nonzero only in a small neighborhood of a single vortex line. As a specific example consider a cylinder in the fluid; let the vorticity be

nonzero only inside the cylinder and parallel to the axis of the cylinder. If we consider any two planes, S_1 and S_2, which intersect the cylinder, we find that $\int_{S_1} \vec{\omega}\cdot d\vec{A} = \int_{S_2} \vec{\omega}\cdot d\vec{A}$, where $d\vec{A}$ denotes the differential directed area. If we let

$$\Gamma = \int_S \vec{\omega}\cdot d\vec{A} \ ,$$

then Γ is called the strength of the vortex.

We define a vortex line to be an integral curve of the vorticity. We define a vortex tube as a two dimensional surface S nowhere tangent to $\vec{\omega}$, with vortex lines drawn through each point of a bounding curve C of S. Helmholtz' Theorem [10] states: If C_1 and C_2 are any two curves encircling the vortex tube and S_1 and S_2 are surfaces whose boundaries are C_1 and C_2 respectively, then

$$\Gamma = \int_{S_1} \vec{\omega}\cdot d\vec{A} = \int_{S_2} \vec{\omega}\cdot d\vec{A} \ ,$$

furthermore, the strength Γ is constant in time as the tube moves with the fluid.

We wish to look at a vorticity distribution which can be approximated by assuming the vorticity to be localized to a small region near a curve in $\mathbf{R}^3$; we call this distribution a vortex filament. The vorticity associated with a vortex filament points in the direction of the tangent to the curve and its magnitude is characterized by the fact that $\int_S \vec{\omega}\cdot d\vec{A} = \Gamma$, where S is any surface which intersects the curve transversally at only one point. Γ is called the strength of the filament.

We now specialize equation (1.2) to the case of a vortex filament, described by the function $\vec{r}(s)$, where s is arclength measured along the filament. Γ denotes the strength of the filament. $\vec{t} \equiv \frac{d\vec{r}}{ds}$ is the tangent to the filament. From equation (1.2) we see that the velocity produced by this vortex filament can be written as

$$\vec{v}(\vec{x}) = -\frac{\Gamma}{4\pi} \int_0^L \frac{(\vec{x} - \vec{r}(s)) \times \vec{t}(s)}{|\vec{x} - \vec{r}(s)|^3} \, ds \tag{1.3}$$

where s is arclength along the filament and L is the length of the filament. In general we consider the filaments to be closed curves, although other possibilities exist.

We now proceed to determine the time evolution of the vorticity; in particular we are interested in the time evolution of the vortex filament. Consider a closed curve C_t encircling the filament. We let this curve evolve in time by moving it with the fluid velocity. By Stokes theorem the strength of the vorticity Γ_{C_t} can be represented as $\Gamma_{C_t} = \int_{C_t} \vec{v} \cdot d\vec{t}(s)$, where the integral is a line integral along C_t and the t subscript emphasizes the fact that the curve is moving with the fluid. Γ_{C_t} is a constant in time; the filament also moves with the fluid velocity. In order to determine the evolution of the filament, we must determine the fluid velocity on the filament. However, as $\vec{x}$ approaches the filament in equation (1.3), the velocity diverges logarithmically. We now proceed to investigate this singularity in more detail by means of an asymptotic expansion first introduced by Arms and used by Hama [22,23]. We follow closely the discussion presented in Batchelor [4].

We begin by considering a specific point on the filament. For convenience, let us assume that this point is the point $s=0$. Since we want to look at the velocity near the filament, we expand the function $\vec{r}(s)$ in a Taylor series about the point $s=0$. The result is $\vec{r}(s) = \vec{r}(0) + \vec{t}(0)s + \frac{d\vec{t}(0)}{ds}\frac{s^2}{2!} + \frac{d^2\vec{t}(0)}{ds^2}\frac{s^3}{3!} \cdots$. Expanding the tangent similarly, we obtain $\vec{t}(s) = \vec{t}(0) + \frac{d\vec{t}(0)}{ds}s + \cdots$.

We now introduce a local coordinate system whose origin is located at the point $\vec{r}(0)$. We take as the basis vectors the tangent $\vec{t}(0)$, the normal $\vec{n}(0)$, and the binormal $\vec{b}(0)$. For a curve $\vec{r}(s)$, these are defined in the following manner. The tangent is defined: $\vec{t} \equiv \frac{d\vec{r}}{ds}$. The curvature κ is defined as $\kappa \equiv \left|\frac{d\vec{t}}{ds}\right|$. The normal is defined by the expression: $\frac{d\vec{t}}{ds} = \kappa\vec{n}$. The binormal is defined as $\vec{b} \equiv \vec{t} \times \vec{n}$. We note that $\vec{t}$, $\vec{n}$, and $\vec{b}$ form an

orthonormal coordinate system at all points along the curve $\vec{r}(s)$. As mentioned above, we are using the coordinate system defined at the point $s=0$; we denote these coordinate vectors as $\vec{t}_0$, $\vec{n}_0$, and $\vec{b}_0$.

We wish to find the velocity close to the filament, so our small parameter in the asymptotic expansion will be σ, the distance of the point of observation from the filament. We define our point of observation $\vec{x}$ to be $\vec{x} = y\vec{n}_0 + z\vec{b}_0$, where $y=\sigma\cos\phi$ and $z=\sigma\sin\phi$. We substitute the expansions for $\vec{r}(s)$ and $\vec{t}(s)$ into equation (1.3) and, after dropping terms of order s^3 and higher, we find the following expressions for the integrand in equation (1.3):

$$(\vec{x} - \vec{r}(s))\times\vec{t}(s) \approx$$
$$-y\vec{b}_0 + z\vec{n}_0 - zs\,\kappa\vec{t}_0 + \frac{ys^2}{2}\vec{n}_0\times\vec{t}_0{}'' + \frac{zs^2}{2}\vec{b}_0\times\vec{t}_0{}'' - \frac{s^2}{2}\vec{t}_0\times\vec{t}_0{}' \tag{1.4}$$

In expression (1.4) the $'$ denotes a derivative with respect to arclength s and the subscript denotes evaluation at $s = 0$. The denominator in the integrand of equation (1.3) is approximated in the following form.

$$|\vec{x} - \vec{r}(s)|^2 \approx \sigma^2 + (1 - y\,\kappa)s^2 \tag{1.5}$$

We take as our variable of integration $\xi=\frac{s}{\sigma}$. In taking the limit we wish to let $\sigma\rightarrow 0$ while keeping ξ fixed. Using expressions (1.4) and (1.5) and keeping leading order terms, we find that

$$\vec{v}(\vec{x}) \approx \frac{\Gamma}{4\pi}\int_{-l_0/\sigma}^{l_0/\sigma} \frac{(\cos\phi\vec{b}_0 - \sin\phi\vec{n}_0)\sigma^{-1} + \xi\sin\phi\kappa\vec{t}_0 + \frac{\xi^2}{2}\vec{t}_0\times\vec{t}_0{}'}{(1+\xi^2)^{3/2}}\,d\xi$$

where l_0 is some small but fixed limit of integration. We ignore the contribution to the integral from points such that $|s| > l_0$, and only note that this contribution is bounded. Carrying out the integration in the limit as $\frac{l_0}{\sigma}\rightarrow\infty$, we find that

$$\vec{v} \approx \frac{\Gamma}{2\pi\sigma}(\vec{b}_0\cos\phi - \vec{n}_0\sin\phi) + \frac{\Gamma}{2\pi}\log\frac{2l_0}{\sigma}\,\vec{t}_0\times\vec{t}_0{}' + o(1)\,. \tag{1.6}$$

The first term in (1.6) represents the circular motion around a straight filament. The second term gives a correction to the velocity due to the fact that the filament is curved.

The third term represents the terms which have a lower order dependence on σ. An infinite straight filament would produce a velocity field identical to that given by the first term in (1.6), but it remains stationary in its own velocity field; thus we assume that the second term gives an approximation of the velocity on the filament itself. This approximation to the velocity of the filament is called the self-induction approximation. Using the self-induction approximation we write down an equation for the evolution of the filament:

$$\frac{\partial \vec{r}}{\partial t} = \frac{\Gamma}{2\pi} \log \frac{2l_0}{\sigma_0} \, \vec{t} \times \vec{t}' \quad ,$$

where σ_0 is generally taken as the true finite radius of the vortex filament and $'$ indicates a derivative with respect to arclength. We define the units of time in order to eliminate the constant appearing above and write:

$$\frac{\partial \vec{r}}{\partial t} = \vec{t} \times \vec{t}' \quad . \tag{1.7}$$

In practice the logarithmic term is not very large and as a result the self-induction approximation is valid only for short times before the neglected terms in equation (1.6) become important.

The correct way to parametrize $\vec{r}$ is by labeling the fluid particles on the filament; we use the variable ξ to label the particles along the filament. If the filament stretches as it evolves, then the arclength becomes a function of time as well as ξ. In equation (1.7) we are approximating the velocity of the fluid particle at a particular position on the filament, thus the partial derivative with respect to time in equation (1.7) is taken with ξ kept fixed.

We now proceed to show that for the self-induction equation, equation (1.7), the variables ξ and arclength s are linearly related. We do this by showing that the arclength is not a function of time; there is no stretching of the filament. We begin by defining a vector $\vec{\tau}$, which is not necessarily a unit vector, $\vec{\tau}(\xi,t) \equiv \frac{\partial \vec{r}(\xi,t)}{\partial \xi}$. We also define the functions $g(\xi,t)$ and $h(\xi,t)$; $g \equiv |\vec{\tau}| = \frac{\partial s(\xi,t)}{\partial \xi}$ and $h \equiv \frac{1}{g}$. In order to show that there is no stretching, we must show that $\frac{\partial g(\xi,t)}{\partial t} = 0$. Using equation (1.7) we find that

$\frac{\partial^2 \vec{r}}{\partial \xi \partial t} = \frac{\partial \vec{r}}{\partial t} = \frac{\partial}{\partial \xi}(\vec{t} \times \vec{t}\,')$. Since $' \equiv \frac{\partial}{\partial s} = h\frac{\partial}{\partial \xi}$, we have that $\frac{\partial}{\partial \xi}(\vec{t} \times \vec{t}\,') = \frac{\partial \vec{t}}{\partial \xi} \times h\frac{\partial \vec{t}}{\partial \xi} + \vec{t} \times \frac{\partial}{\partial \xi} h\frac{\partial \vec{t}}{\partial \xi}$. Thus we have that $\frac{\partial \vec{r}}{\partial t} = \vec{t} \times \frac{\partial}{\partial \xi} h\frac{\partial \vec{t}}{\partial \xi}$. It follows directly then that $g\frac{\partial g}{\partial t} = \vec{r} \cdot \frac{\partial \vec{r}}{\partial t} = 0$. Therefore ξ and s are related by an affine transformation and equation (1.7) does not change its form if we consider $\vec{r}$ to be a function of s and t instead of ξ and t.

One can either write the self-induction equation in terms of $\vec{r}$ or $\vec{t}$. In terms of $\vec{r}$ we have that $\frac{\partial \vec{r}}{\partial t} = \frac{\partial \vec{r}}{\partial s} \times \frac{\partial^2 \vec{r}}{\partial s^2}$. By differentiating both sides of the equation with respect to s, we obtain the equation written in terms of $\vec{t}$:

$$\frac{\partial \vec{t}}{\partial t} = \vec{t} \times \frac{\partial^2 \vec{t}}{\partial s^2} . \tag{1.8}$$

We consider the self-induction equation written as equation (1.8). We are motivated to use (1.8) by the fact that we are attempting to find stable numerical schemes to solve for the self-induced motion of a filament. If we linearize equation (1.7), the equation which results has both a hyperbolic and parabolic term, whereas the linearized version of equation (1.8) has only a parabolic term; thus a priori it appears simpler to consider (1.8).

Assuming that we have a solution to (1.8), we wish to show how the corresponding solution to (1.7) can be obtained. We start with the identity, $\vec{r}(s,t) = \vec{r}(0,0) + \vec{r}(0,t) - \vec{r}(0,0) + \vec{r}(s,t) - \vec{r}(0,t)$. We then use the facts that $\int_0^t \frac{\partial \vec{r}(0,\varsigma)}{\partial \varsigma}\, d\varsigma = \vec{r}(0,t) - \vec{r}(0,0)$ and $\int_0^s \frac{\partial \vec{r}(\varsigma,t)}{\partial \varsigma}\, d\varsigma = \vec{r}(s,t) - \vec{r}(0,t)$. Using (1.7) and the definition of $\vec{t}$, we find that

$$\vec{r}(s,t) = \vec{r}(0,0) + \int_0^t \vec{t}(0,\varsigma) \times \frac{\partial \vec{t}(0,\varsigma)}{\partial s}\, d\varsigma + \int_0^s \vec{t}(\varsigma,t)\, d\varsigma . \tag{1.9}$$

We take (1.9) as the defining relation for $\vec{r}(s,t)$. We have

$$\frac{\partial \vec{r}}{\partial t} = \vec{t}(0,t) \times \frac{\partial \vec{t}(0,t)}{\partial s} + \int_0^s \frac{\partial \vec{t}(\varsigma,t)}{\partial t}\, d\varsigma$$

$$= \vec{t}(0,t)\times\frac{\partial\vec{t}(0,t)}{\partial s} + \int_0^s \frac{\partial}{\partial\varsigma}\left(\vec{t}(\varsigma,t)\times\frac{\partial\vec{t}(\varsigma,t)}{\partial\varsigma}\right) d\varsigma$$

$$= \vec{t}(0,t)\times\frac{\partial\vec{t}(0,t)}{\partial s} + \vec{t}(s,t)\times\frac{\partial\vec{t}(s,t)}{\partial s} - \vec{t}(0,t)\times\frac{\partial\vec{t}(0,t)}{\partial s}$$

$$= \vec{t}(s,t)\times\frac{\partial\vec{t}(s,t)}{\partial s}.$$

Thus given a solution to (1.8), we have a corresponding solution to (1.7) given by (1.9).

1.2 The Betchov Equations

We now present the first of two alternate forms of equation (1.8). The first of these alternate forms is due to Betchov [5]. Betchov's equations describe the evolution of the curvature and torsion of a filament which evolves according to (1.8).

We begin by presenting some fundamental facts and definitions from the differential geometry of a curve [30]. We begin with a curve C described by a function $\vec{r}(\varsigma):\mathbf{R}\rightarrow\mathbf{R}^3$, where $0\leq\varsigma\leq\varsigma_0$ and where $\left|\frac{d\vec{r}(\varsigma)}{d\varsigma}\right| > 0$ for $0<\varsigma<\varsigma_0$. We first define the arclength s, of the curve C to be

$$s(\varsigma) \equiv \int_0^\varsigma \left|\frac{d\vec{r}(\xi)}{d\xi}\right| d\xi. \tag{1.10}$$

Since the integrand in (1.10) is positive, we know by the inverse function theorem that the function $s(\varsigma)$ has an inverse, which we denote as $\varsigma(s)$, $0\leq s\leq s_0$. Using $\varsigma(s)$, we now consider the curve C to be parameterized by s, by the function $\vec{r}(\varsigma(s))$. Following usual conventions, we also denote this function as $\vec{r}(s)$. The tangent vector $\vec{t}(s)$ is defined to be the derivative of $\vec{r}$ with respect to s,

$$\vec{t}(s) \equiv \frac{d\vec{r}}{ds} = \frac{d\varsigma}{ds}\frac{d\vec{r}}{d\varsigma}. \tag{1.11}$$

We see from the definition of $\varsigma(s)$ that $|\vec{t}(s)| = 1$. We define the curvature $\kappa(s)$, of the curve C to be

$$\kappa(s) \equiv \left|\frac{d\vec{t}(s)}{ds}\right|. \tag{1.12}$$

If $\kappa(s)>0$, we can define the normal $\vec{n}(s)$, to the curve C to be

$$\vec{n}(s) \equiv \frac{1}{\kappa(s)} \frac{d\vec{t}(s)}{ds} .$$

Since $|\vec{t}(s)| = 1$, we find that $0 = \frac{d\,|\vec{t}\,|^2}{ds} = 2\,\vec{t}\cdot\frac{d\vec{t}}{ds}$, and thus $\vec{n}(s)$ is perpendicular to $\vec{t}(s)$. We can define an orthonormal coordinate system along C by defining the third member, called the binormal $\vec{b}(s)$, to be

$$\vec{b}(s) \equiv \vec{t}(s) \times \vec{n}(s) . \tag{1.13}$$

As defined above, the normal vector and consequently the binormal vector are only defined when the curvature is nonzero. We can extend their definitions to all points along a smooth curve (smooth here means that $\vec{r}(s)$ has as many derivatives as required) by requiring that $\kappa(s)$, $\vec{t}(s)$, $\vec{n}(s)$, and $\vec{b}(s)$ all be continuous. In order for both the curvature and the normal to be continuous, we must allow the curvature to be negative. Thus (1.12) should have a $\pm$ sign in it, the correct sign being determined by the condition that $\vec{n}(s)$ be continuous. We clarify this point in the following paragraph, by describing $\vec{t}$, $\vec{n}$, and $\vec{b}$ in terms of $\kappa(s)$ and another function $\tau(s)$.

We now derive expressions for the derivatives of the orthonormal triad in terms of the triad itself. Since $\vec{t}\cdot\vec{n} = \vec{t}\cdot\vec{b} = \vec{n}\cdot\vec{b} = 0$, we find, by differentiating each expression in turn, that

$$\begin{aligned} \frac{d\vec{t}}{ds}\cdot\vec{n} &= -\vec{t}\cdot\frac{d\vec{n}}{ds} , \\ \frac{d\vec{t}}{ds}\cdot\vec{b} &= -\vec{t}\cdot\frac{d\vec{b}}{ds} , \\ \frac{d\vec{n}}{ds}\cdot\vec{b} &= -\vec{n}\cdot\frac{d\vec{b}}{ds} . \end{aligned} \tag{1.14}$$

In a likewise manner using the facts that $|\vec{t}\,|^2 = |\vec{n}\,|^2 = |\vec{b}\,|^2 = 1$, we find that

$$\begin{aligned} \vec{t}\cdot\frac{d\vec{t}}{ds} &= 0 , \\ \vec{n}\cdot\frac{d\vec{n}}{ds} &= 0 , \\ \vec{b}\cdot\frac{d\vec{b}}{ds} &= 0 . \end{aligned} \tag{1.15}$$

In view of (1.14), (1.15) and the definition of κ and $\vec{n}$, we have only one undetermined

component of the derivatives of the triad. We thus define the torsion $\tau(s)$ to be

$$\tau(s) \equiv \vec{b} \cdot \frac{d\vec{n}}{ds} . \tag{1.16}$$

Using (1.14), (1.15) and (1.16) we find the following system of differential equations describing $\vec{t}$, $\vec{n}$ and $\vec{b}$.

$$\frac{d}{ds}\begin{pmatrix} \vec{t} \\ \vec{n} \\ \vec{b} \end{pmatrix} = \begin{bmatrix} 0 & \kappa & 0 \\ -\kappa & 0 & \tau \\ 0 & -\tau & 0 \end{bmatrix} \begin{pmatrix} \vec{t} \\ \vec{n} \\ \vec{b} \end{pmatrix} \tag{1.17}$$

Equation (1.17) is called the Frenet-Seret formula. It shows that a curve is determined by its curvature and its torsion; thus if we determine the evolution of a curve's torsion and curvature, we determine the evolution of the curve itself.

We now resume the derivation of Betchov's equations. Using the definition of curvature, we find

$$\frac{1}{2}\frac{\partial \kappa^2}{\partial t} = \frac{1}{2}\frac{\partial}{\partial t}\left|\frac{\partial \vec{t}}{\partial s}\right|^2 = \frac{\partial \vec{t}}{\partial s} \cdot \frac{\partial^2 \vec{t}}{\partial t\, \partial s} . \tag{1.18}$$

Differentiating the terms of (1.8) we find that

$$\frac{\partial^2 \vec{t}}{\partial t\, \partial s} = \frac{\partial \vec{t}}{\partial s} \times \frac{\partial^2 \vec{t}}{\partial s^2} + \vec{t} \times \frac{\partial^3 \vec{t}}{\partial s^3} . \tag{1.19}$$

Using (1.18) and (1.19), we find that

$$\frac{1}{2}\frac{\partial \kappa^2}{\partial t} = -\frac{\partial}{\partial s}\left(\vec{t} \cdot \frac{\partial \vec{t}}{\partial s} \times \frac{\partial^2 \vec{t}}{\partial s^2}\right) . \tag{1.20}$$

Using the Frenet-Seret formula, we can write all derivatives of $\vec{t}$ in terms of τ and κ and their derivatives, and the orthonormal triad. We do this for the first three derivatives of $\vec{t}$.

$$\begin{aligned} \frac{d\vec{t}}{ds} &= \kappa \vec{n} \\ \frac{d^2\vec{t}}{ds^2} &= -\kappa^2 \vec{t} + \frac{d\kappa}{ds}\vec{n} + \kappa\tau\vec{b} \\ \frac{d^3\vec{t}}{ds^3} &= -\frac{3}{2}\frac{d\kappa^2}{ds}\vec{t} + \left(\frac{d^2\kappa}{ds^2} - \kappa\tau^2 - \kappa^3\right)\vec{n} + \left(2\frac{d\kappa}{ds}\tau + \kappa\frac{d\tau}{ds}\right)\vec{b} \end{aligned} \tag{1.21}$$

Using (1.20) and (1.21), we write the Betchov equation describing the time evolution of the curvature,

$$\frac{1}{2}\frac{\partial \kappa^2}{\partial t} = -\frac{\partial \kappa^2 \tau}{\partial s} . \tag{1.22}$$

In order to derive the second Betchov equation we look at $\frac{\partial \kappa^2 \tau}{\partial t}$. We have that

$$\frac{\partial \kappa^2 \tau}{\partial t} = \frac{\partial}{\partial t}\left(\vec{t}\cdot\frac{\partial \vec{t}}{\partial s}\times\frac{\partial^2 \vec{t}}{\partial s^2}\right) \tag{1.23}$$
$$= \frac{\partial \vec{t}}{\partial t}\cdot\frac{\partial \vec{t}}{\partial s}\times\frac{\partial^2 \vec{t}}{\partial s^2} + \vec{t}\cdot\frac{\partial^2 \vec{t}}{\partial t\,\partial s}\times\frac{\partial^2 \vec{t}}{\partial s^2} + \vec{t}\cdot\frac{\partial \vec{t}}{\partial s}\times\frac{\partial^3 \vec{t}}{\partial t\,\partial s^2} .$$

Differentiating the terms of (1.8) twice with respect to s , we find that

$$\frac{\partial^3 \vec{t}}{\partial t\,\partial s^2} = \vec{t}\times\frac{\partial^4 \vec{t}}{\partial s^4} + 2\frac{\partial \vec{t}}{\partial s}\times\frac{\partial^3 \vec{t}}{\partial s^3} . \tag{1.24}$$

Then after using (1.8), (1.19) and (1.24) to replace the time derivatives on the right side of (1.23), we find

$$\frac{\partial \kappa^2 \tau}{\partial t} = -\left(\vec{t}\times\frac{\partial^2 \vec{t}}{\partial s^2}\right)\cdot\left(\vec{t}\times\frac{\partial^3 \vec{t}}{\partial s^3}\right) + 2\left(\vec{t}\times\frac{\partial \vec{t}}{\partial s}\right)\cdot\left(\frac{\partial \vec{t}}{\partial s}\times\frac{\partial^3 \vec{t}}{\partial s^3}\right) \tag{1.25}$$
$$+ \left(\vec{t}\times\frac{\partial \vec{t}}{\partial s}\right)\cdot\left(\vec{t}\times\frac{\partial^4 \vec{t}}{\partial s^4}\right) .$$

After some algebraic manipulation, we find that we can rewrite the right side of equation (1.25). We find

$$\frac{\partial \kappa^2 \tau}{\partial t} = \frac{\partial}{\partial s}\left[\left(\vec{t}\times\frac{\partial \vec{t}}{\partial s}\right)\cdot\left(\vec{t}\times\frac{\partial^3 \vec{t}}{\partial s^3}\right) + \left(\frac{\partial \vec{t}}{\partial s}\times\frac{\partial^2 \vec{t}}{\partial s^2}\right)\cdot\left(\vec{t}\times\frac{\partial \vec{t}}{\partial s}\right)\right. \tag{1.26}$$
$$\left. - \left(\vec{t}\times\frac{\partial^2 \vec{t}}{\partial s^2}\right)\cdot\left(\vec{t}\times\frac{\partial^2 \vec{t}}{\partial s^2}\right) + \frac{\kappa^4}{4}\right] .$$

Using (1.21) to replace the spatial derivatives in (1.26), we obtain the second Betchov equation,

$$\frac{\partial \kappa^2 \tau}{\partial t} = \frac{\partial}{\partial s}\left(\frac{\kappa^4}{4} - 2\tau^2\kappa^2 + \kappa^2\frac{\partial^2 \ln\kappa}{\partial s^2}\right) . \tag{1.27}$$

By integrating (1.22) and (1.27) with respect to arclength along the filament C , we find two constants of motion for filaments evolving according to equation (1.8),

$$\frac{1}{2}\frac{d}{dt}\int_C \kappa^2\, ds = 0\,, \tag{1.28}$$
$$\frac{d}{dt}\int_C \kappa^2\tau\, ds = 0\,.$$

Equations (1.28) are valid for a closed filament or for an infinite filament whose torsion and curvature tend to zero sufficiently rapidly as $|s| \to \infty$. Equations (1.28) would also be valid for a finite filament which doesn't close upon itself if we apply the correct boundary conditions to the endpoints of the filament ; for example, we could require that the terms in parentheses on the right sides of equations (1.22) and (1.27) vanish at the endpoints.

1.3 The Non-linear Schrödinger Equation

We now present a transformation due to Hasimoto [24], which transforms the self-induction equation into a nonlinear Schrödinger equation that describes the evolution of the curvature and torsion of the filament. We begin by writing the Frenet-Seret formulae for $\vec{n}$ and $\vec{b}$ in complex form as

$$\frac{d}{ds}(\vec{n} + i\vec{b}) = -i\,\tau(\vec{n} + i\vec{b}) - \kappa\vec{t}\,. \tag{1.29}$$

We introduce the new quantities $\vec{N}$ and ψ, where

$$\vec{N} = (\vec{n} + i\vec{b})\exp\left(i\int_0^s \tau(\xi,t)\, d\xi\right), \tag{1.30}$$

$$\psi = \kappa\exp\left(i\int_0^s \tau(\xi,t)\, d\xi\right). \tag{1.31}$$

Differentiating $\vec{N}$ with respect to s and using (1.29), we find that

$$\frac{\partial\vec{N}}{\partial s} = -i\,\tau\vec{N} - \psi\vec{t} + i\,\tau\vec{N} = -\psi\vec{t}\,. \tag{1.32}$$

We also see that

$$\frac{\partial\vec{t}}{\partial s} = \frac{1}{2}(\psi^*\vec{N} + \psi\vec{N}^*)\,, \tag{1.33}$$

where ψ^* and $\vec{N}^*$ denote the complex conjugate of ψ and $\vec{N}$, respectively. We wish to point out that equations (1.29) through (1.33) depend only on the Frenet-Seret formulae and are valid without any reference to a time dependence.

We now introduce equation (1.8) in order to determine the time evolution of the filament. Using (1.21) and (1.8), we find that

$$\frac{\partial \vec{t}}{\partial t} = \vec{t} \times \frac{\partial^2 \vec{t}}{\partial s^2} = \frac{\partial \kappa}{\partial s}\vec{b} - \kappa\tau\vec{n}$$
$$= \mathrm{Re}\left[\left(\frac{\partial \kappa}{\partial s} + i\,\kappa\tau\right)(\vec{b} + i\vec{n})\right],$$

where Re(·) denotes the real part of a number. Since $\frac{\partial \psi}{\partial s} = \left(\frac{\partial \ln\kappa}{\partial s} + i\,\tau\right)\psi$, we have that

$$\frac{\partial \vec{t}}{\partial t} = \mathrm{Re}\left(i\frac{\partial \psi}{\partial s}\vec{N}^*\right) = \frac{i}{2}\left(\frac{\partial \psi}{\partial s}\vec{N}^* - \frac{\partial \psi^*}{\partial s}\vec{N}\right). \tag{1.34}$$

We also note the orthogonality relations, which hold between $\vec{t}$, $\vec{N}$ and $\vec{N}^*$:

$$\vec{t}\cdot\vec{t} = 1, \quad \vec{N}\cdot\vec{N}^* = 2, \tag{1.35}$$
$$\vec{N}\cdot\vec{N} = \vec{N}^*\cdot\vec{N}^* = \vec{N}\cdot\vec{t} = \vec{N}^*\cdot\vec{t} = 0\,.$$

We now wish to find the equation governing the time evolution of $\vec{N}$. We write this equation in the general form,

$$\frac{\partial \vec{N}}{\partial t} = \alpha\vec{N} + \beta\vec{N}^* + \gamma\vec{t}\,, \tag{1.36}$$

where α, β and γ are complex functions of s and t, which are to be determined. Differentiating various orthogonality relations from (1.35), we find that

$$0 = \frac{1}{2}\frac{\partial(\vec{N}\cdot\vec{N}^*)}{\partial t} = \frac{1}{2}\left(\frac{\partial \vec{N}}{\partial t}\cdot\vec{N}^* + \vec{N}\cdot\frac{\partial \vec{N}^*}{\partial t}\right) = \alpha + \alpha^*\,,$$
$$0 = \frac{1}{4}\frac{\partial(\vec{N}\cdot\vec{N})}{\partial t} = \frac{1}{2}\vec{N}\cdot\frac{\partial \vec{N}}{\partial t} = \beta\,,$$
$$0 = \frac{\partial(\vec{N}\cdot\vec{t})}{\partial t} = \frac{\partial \vec{N}}{\partial t}\cdot\vec{t} + \vec{N}\cdot\frac{\partial \vec{t}}{\partial t} = \gamma + \vec{N}\cdot\frac{\partial \vec{t}}{\partial t}\,.$$

Thus we deduce three facts: (1) α is a purely imaginary function, which we denote by $\alpha = iR$, where R is a real function, (2) $\beta = 0$, and (3) $\gamma = -i\frac{\partial \psi}{\partial s}$, where we have used (1.34). Thus we write (1.36) as

$$\frac{\partial \vec{N}}{\partial t} = i\left(R\vec{N} - \frac{\partial \psi}{\partial s}\vec{t}\right). \tag{1.37}$$

Taking the time derivative of the terms of (1.32), we find that

$$\frac{\partial^2 \vec{N}}{\partial t\, \partial s} = -\frac{\partial \psi}{\partial t}\vec{t} - \psi\frac{\partial \vec{t}}{\partial t} \tag{1.38}$$

$$= -\frac{\partial \psi}{\partial t}\vec{t} - \frac{i}{2}\psi\left(\frac{\partial \psi}{\partial s}\vec{N}^* - \frac{\partial \psi^*}{\partial s}\vec{N}\right),$$

where we have used (1.34). Differentiating the terms of (1.37) with respect to s, we find that

$$\frac{\partial^2 \vec{N}}{\partial t\, \partial s} = i\left[\frac{\partial R}{\partial s}\vec{N} - R\,\psi\vec{t} - \frac{\partial^2 \psi}{\partial s^2}\vec{t} - \frac{1}{2}\frac{\partial \psi}{\partial s}\left(\psi^*\vec{N} + \psi\vec{N}^*\right)\right], \tag{1.39}$$

where we have used (1.32) and (1.33). Equating the coefficients of $\vec{t}$ and the coefficients of $i\vec{N}$ in equations (1.38) and (1.39), we find that

$$-\frac{\partial \psi}{\partial t} = -i\left(\frac{\partial^2 \psi}{\partial s^2} + R\,\psi\right), \tag{1.40}$$

$$\frac{1}{2}\psi\frac{\partial \psi^*}{\partial s} = \frac{\partial R}{\partial s} - \frac{1}{2}\frac{\partial \psi}{\partial s}\psi^*. \tag{1.41}$$

Integrating the members of equation (1.41) with respect to s, we obtain

$$R(s,t) = \frac{1}{2}\left(\psi(s,t)\psi^*(s,t) + A(t)\right), \tag{1.42}$$

where $A(t)$ is a function of t only. Using (1.42) in equation (1.40), we obtain:

$$\frac{1}{i}\frac{\partial \psi}{\partial t} = \frac{\partial^2 \psi}{\partial s^2} + \frac{1}{2}\psi\left(|\psi|^2 + A\right). \tag{1.43}$$

Equation (1.43) is a cubic non-linear Schrödinger equation. We can eliminate A from (1.43) by introducing the function Ψ,

$$\Psi = \Psi(s,t) = \psi(s,t)\exp\left(-\frac{i}{2}\int_0^t A(\xi)\,d\xi\right).$$

The equation governing the time evolution of Ψ is

$$\frac{1}{i}\frac{\partial \Psi}{\partial t} = \frac{\partial^2 \Psi}{\partial s^2} + \frac{1}{2}\Psi\,|\Psi|^2. \tag{1.44}$$

The function $A(t)$ appears in (1.43) because, in our definition of ψ, we have fixed $\psi(0,t)$ to be real for all times. A is not arbitrary, but can be determined from $\Psi(s,t)$. If we write $\Psi(s,t) = r(s,t)e^{i\theta(s,t)}$, then from the definition of Ψ we have

$$r(0,t)e^{i\theta(0,t)} = \psi(0,t)\exp\left(-\frac{i}{2}\int_0^t A(\xi)\,d\xi\right), \tag{1.45}$$

and since $\psi(0,t)$ is real we immediately see that

$$A(t) = -2\frac{d\,\theta(0,t)}{dt}\,. \tag{1.46}$$

If we were attempting to find $\psi(s,t)$, given $\psi(s,0)$, we could solve equation (1.44) to find $\Psi(s,t)$, since $\psi(s,0) = \Psi(s,0)$. We do not need $A(t)$ explicitly in this case to find $\psi(s,t)$, since from the argument given in the preceding paragraph, we can express $\psi(s,t)$ as

$$\psi(s,t) = \pm\frac{\Psi^*(0,t)}{|\,\Psi(0,t)\,|}\Psi(s,t)\,. \tag{1.47}$$

The correct sign in equation (1.47) is chosen by requiring that $\psi(0,t)$ and $\partial\psi(0,t)/\partial t$ be continuous functions of time.

Given $\psi(s,t)$ we know the shape of the filament as a function of time; however, we do not know the position or orientation of the filament. Thus in addition to ψ we must also determine the evolution of $\vec{r}$, $\vec{t}$ and $\vec{n}$ at one point on the filament. We have all of the necessary equations, we simply indicate which ones they are.

If we are given $\vec{r}$, $\vec{t}$ and $\vec{N}$ at one point on the filament C, we can determine the position of the rest of the filament by integrating the Frenet-Seret equations. We do not have to find κ and τ explicitly from ψ, since we can rewrite the Frenet-Seret equations using ψ. From (1.32) and (1.33) we have

$$\frac{d}{ds}\begin{pmatrix}\vec{r}\\ \vec{t}\\ \vec{N}\\ \vec{N}^*\end{pmatrix} = \begin{bmatrix}0 & 1 & 0 & 0\\ 0 & 0 & \psi^*/2 & \psi/2\\ 0 & -\psi & 0 & 0\\ 0 & -\psi^* & 0 & 0\end{bmatrix}\begin{pmatrix}\vec{r}\\ \vec{t}\\ \vec{N}\\ \vec{N}^*\end{pmatrix}. \tag{1.48}$$

Given $\vec{t}$ and $\vec{N}$ at $s=0$, we can integrate (1.48) to find $\vec{t}(s)$ and then integrate $\vec{t}(s)$ to find $\vec{r}(s)$, if we are given $\vec{r}(0)$.

In order to determine the necessary vectors at a point on the curve, we use equations (1.34) and (1.37). To be definite let us assume we are determining $\vec{t}$ and $\vec{N}$ at $s=0$. Written as a system of equations, (1.34) and (1.37) become

$$\frac{d}{dt}\begin{pmatrix}\vec{t}\\ \vec{N}\\ \vec{N}^*\end{pmatrix} = \begin{bmatrix}0 & -\frac{i}{2}\frac{\partial\psi^*}{\partial s} & \frac{i}{2}\frac{\partial\psi}{\partial s}\\ -i\frac{\partial\psi}{\partial s} & iR & 0\\ i\frac{\partial\psi^*}{\partial s} & 0 & -iR\end{bmatrix}\begin{pmatrix}\vec{t}\\ \vec{N}\\ \vec{N}^*\end{pmatrix}, \tag{1.49}$$

where all of the functions appearing in (1.49) are evaluated at $s=0$. All of the quantities in the matrix in equation (1.49) are assumed known as a function of t, since we assume we have solved (1.44) to determine $\psi(s,t)$.

The final equation we need determines the evolution of $\vec{r}$ at $s=0$. Using the definition of $\vec{N}$ and ψ along with (1.7) we find that

$$\frac{d\vec{r}}{dt} = \frac{i}{2}\left(\psi\vec{N}^* - \psi^*\vec{N}\right), \tag{1.50}$$

where once again all of the functions are evaluated at $s=0$.

In summary, in order to solve for $\vec{r}(s,t)$ using $\psi(s,t)$, we must do the following. First we solve (1.44) in order to determine $\Psi(s,t)$; then we use (1.47) in order to determine $\psi(s,t)$. Once we have $\psi(s,t)$ we solve (1.49) at the point $s=0$, using (1.46) and (1.42) to find $R(s,t)$, in order to find $\vec{t}(0,t)$ and $\vec{N}(0,t)$. We then solve (1.50) to find $\vec{r}(0,t)$ and using $\vec{r}(0,t)$, $\vec{t}(0,t)$ and $\vec{N}(0,t)$, we solve (1.48) to find $\vec{t}(s,t)$ and finally integrate $\vec{t}$ to find $\vec{r}(s,t)$. The analogous process could be carried out to solve for $\vec{r}(s,t)$, if we solve Betchov's equations for κ and τ.

1.4 Invariants

We now discuss some properties of the self-induction equation and its equivalent forms. The nonlinear Schrödinger equation is one of a family of soliton equations [32]. One of the properties of these equations is that they possess an infinite number of integral invariants. We present the first three of these invariants for equation (1.43) which we have taken from Newell [32] page 46:

$$\frac{1}{2}\frac{d}{dt}\int \psi^*\psi\, ds = 0,$$

$$\frac{i}{2}\frac{d}{dt}\int \left(\frac{\partial\psi^*}{\partial s}\psi - \frac{\partial\psi}{\partial s}\psi^*\right) ds = 0,$$

$$\frac{1}{2}\frac{d}{dt}\int \left(\frac{\partial\psi^*}{\partial s}\frac{\partial\psi}{\partial s} - \frac{1}{4}|\psi|^4\right) ds = 0.$$

If we write these same invariants in terms of the curvature and torsion, we find:

$$\frac{1}{2}\frac{d}{dt}\int \kappa^2\, ds = 0,$$

$$\frac{d}{dt}\int \kappa^2\tau\, ds = 0\,,$$

$$\frac{1}{2}\frac{d}{dt}\int \left((\kappa')^2 + \kappa^2\tau^2 - \frac{1}{4}\kappa^4\right) ds = 0.$$

We see that the first two invariants correspond to those given in (1.28). All three invariants can also be checked by direct substitution from (1.43) or the Betchov equations (1.22) and (1.27). We also note that these invariants can be written in terms of $\vec{t}$ and its derivatives with respect to s. We do not write these down explicitly, but derive an additional vector invariant directly from equations (1.7) and (1.8). We consider the quantity $\vec{A} = \int_0^L \vec{r}\times\vec{t}\; ds$, where we restrict our attention to a closed vortex filament of length L satisfying equation (1.7). For a planar filament, $|\vec{A}|$ is the area enclosed by the filament and the vector $\vec{A}$ points in the direction perpendicular to the plane of the filament; thus $\vec{A}$ defines a generalized area for a closed filament. Differentiating $\vec{A}$ with respect to time and recalling that $'$ denotes differentiation with respect to arclength we find:

$$\frac{d\vec{A}}{dt} = \int_0^L \left(\frac{\partial\vec{r}}{\partial t}\times\vec{t} + \vec{r}\times\frac{\partial\vec{t}}{\partial t}\right) ds \tag{1.51}$$

$$= \int_0^L \left((\vec{t}\times\vec{t}')\times\vec{t} + \vec{r}\times(\vec{t}\times\vec{t}'')\right) ds$$

$$= \int_0^L \left(2(\vec{t}\times\vec{t}')\times\vec{t} + [\vec{r}\times(\vec{t}\times\vec{t}')]'\right) ds$$

$$= \int_0^L 2(\vec{t}\times\vec{t}')\times\vec{t}\; ds = \int_0^L \vec{t}'\; ds = 0\,,$$

where we have used (1.7), (1.8) and the fact that functions of s are periodic with period L on closed filaments of length L. Equation (1.51) states that a closed filament maintains it orientation and its general shape as it propagates according to (1.7). In particular we see that circles are exact solutions of equation (1.7).

1.5 Exact Solutions

We now present some exact solutions to equation (1.7). The simplest solutions are those which have constant curvature and torsion. Curves with constant curvature and torsion are seen to be solutions of (1.7) by looking at the Betchov equations. The simplest solution is a straight line, which remains stationary for all times. Another solution is a circle of radius r, where r is independent of t. We write this solution down immediately as

$$\vec{r}(s,t) = \kappa_0 t\vec{b}_0 + \frac{1}{\kappa_0}\vec{t}_0\sin(\kappa_0 s) - \frac{1}{\kappa_0}\vec{n}_0\cos(\kappa_0 s)\,, \tag{1.52}$$

where $\kappa_0 = 1/r$ is the constant curvature of the circle. The vectors in (1.52) are constant in time and space; they are the tangent, normal and binormal vectors to the circle at $s=0$ and $t=0$. Solution (1.52) represents uniform translation of the circle in the $\vec{b}_0$ direction with speed equal to κ_0.

The third solution we present also has constant curvature and torsion. The first two solutions presented are limiting cases of this solution. This solution is the one where $\vec{r}(s,t)$ describes a helix. We write down the most general form of a helix with a fixed axis as

$$\vec{r}(s,t) = \frac{\kappa}{\kappa^2+\tau^2}\left(\vec{x}(t)\sin(\sqrt{\kappa^2+\tau^2}s) - \vec{y}(t)\cos(\sqrt{\kappa^2+\tau^2}s)\right) + \frac{\tau s}{\sqrt{\kappa^2+\tau^2}}\vec{z}_0 + \alpha(t)\vec{z}_0\,, \tag{1.53}$$

where κ and τ are the constant curvature and torsion, $\vec{z}_0$ is a unit vector in the direction of the axis of the helix, $\vec{x}(t)$ and $\vec{y}(t)$ are time dependent unit vectors forming an orthonormal basis with $\vec{z}_0$, and $\alpha(t)$ is a function of t as yet to be determined. Equation (1.53) allows for no translation of the helix in a direction perpendicular to $\vec{z}_0$, since by the cylindrical symmetry of the helix there can be none. We also do not allow for a rotation of the axis of the helix, since to have such a rotation would mean that some particles on the helix would move with an unbounded speed, whereas from equation (1.7) we know all particles move with speed κ. Using (1.7) and taking (1.53) as the definition of $\vec{r}(s,t)$, we find

$$\frac{d\alpha}{dt} = \frac{\kappa^2}{\sqrt{\kappa^2+\tau^2}}\,,$$

$$\frac{d\vec{x}}{dt} = -\tau\sqrt{\kappa^2+\tau^2}\,\vec{y}\ , \tag{1.54}$$
$$\frac{d\vec{y}}{dt} = \tau\sqrt{\kappa^2+\tau^2}\,\vec{x}\ .$$

Solving equations (1.54) we find that

$$\alpha(t) = \frac{\kappa^2 t}{\sqrt{\kappa^2+\tau^2}}\ ,$$
$$\vec{x}(t) = \vec{x}_0\cos(\tau\sqrt{\kappa^2+\tau^2}t) - \vec{y}_0\sin(\tau\sqrt{\kappa^2+\tau^2}t)\ ,$$
$$\vec{y}(t) = \vec{y}_0\cos(\tau\sqrt{\kappa^2+\tau^2}t) + \vec{x}_0\sin(\tau\sqrt{\kappa^2+\tau^2}t)\ .$$

Thus we see that the motion of the helix is made up of two parts. One part is a translation along its axis at a speed of $\frac{\kappa^2}{\sqrt{\kappa^2+\tau^2}}$ and the other is a negative rotation about its axis with an angular velocity of $\tau\sqrt{\kappa^2+\tau^2}$. Also we see that the limiting cases of $\tau\rightarrow\infty$ and $\tau\rightarrow 0$ correspond to the straight line and circle solutions which we mentioned in the previous paragraph. It is interesting to note that as $\tau\rightarrow\infty$ the angular speed of a particle becomes infinite, while the actual speed of a particle on the helix remains constant and equal to κ.

The next family of exact solutions is suggested by equation (1.22). If we consider curves which have constant torsion but not constant curvature, from (1.22) we see that κ^2 satisfies a wave equation. The quantity κ^2 moves along the curve with constant speed equal to 2τ. Thus we can write the curvature as a function of the quantity $\xi = s - 2\tau t$. If we sustitute $\kappa(s - 2\tau t)$ into equation (1.27), we find that $\kappa(\xi)$ satisfies equation (1.55).

$$\frac{d}{d\,\xi}\left(\frac{\kappa^4}{4} + \kappa^2\frac{d^2\ln\kappa}{d\,\xi^2}\right) = 0 \tag{1.55}$$

We find the solution of (1.55) satisfying the boundary conditions that $\kappa\rightarrow 0$ as $\xi\rightarrow\pm\infty$ is

$$\kappa(\xi) = 2\nu\,\mathrm{sech}(\nu\xi)\ , \tag{1.56}$$

where ν is an arbitrary constant.

Following the work of Hasimoto [24] we find the analytic expression for the actual shape of the curve which has constant torsion and which has its curvature specified by (1.56). In general $\vec{t}$, $\frac{d\vec{t}}{ds}$ and $\frac{d^2\vec{t}}{ds^2}$ are linearly independent vectors and thus, by expressing $\frac{d^3\vec{t}}{ds^3}$ in

terms of them, we can find a third order linear ordinary differential equation for $\vec{t}$. Clearly we can obtain analagous equations for $\vec{n}$ and $\vec{b}$. If we write the differential equation for $\vec{b}$ in the case where κ satisfies (1.56) and the torsion is constant, we find that

$$\frac{d^3\vec{b}}{d\eta^3} + \tanh\eta\frac{d^2\vec{b}}{d\eta^2} + (T^2 + 4\mathrm{sech}^2\eta)\frac{d\vec{b}}{d\eta} + T^2\tanh\eta\,\vec{b} = 0\,, \tag{1.57}$$

where $\eta = \nu(s - 2\tau t)$ and $T = \tau/\nu$. By defining $\vec{B}$ as

$$\vec{B} \equiv \frac{d\vec{b}}{d\eta} + \tanh\eta\,\vec{b}\,, \tag{1.58}$$

and using equation (1.57), we find that

$$\frac{d^2\vec{B}}{d\eta^2} + (T^2 + 2\mathrm{sech}^2\eta)\,\vec{B} = 0\,. \tag{1.59}$$

Two linearly independent solutions of (1.59) are

$$\vec{B} = \vec{x}_{\substack{+\\-}}(\tanh\eta \mp iT)e^{\pm iT\eta}\,,$$

where $\vec{x}_+$ and $\vec{x}_-$ are constant vectors. The corresponding solutions of (1.58) are

$$\vec{b} = \vec{x}_0\mathrm{sech}\eta\,,$$

$$\vec{b} = \vec{x}_{\substack{+\\-}}(1 - T^2 \mp 2iT\tanh\eta)e^{\pm iT\eta}\,,$$

where $\vec{x}_0$ is a constant vector.

We now apply boundary counditions to obtain a specific solution. Requiring that $|\vec{b}| = 1$ and choosing the solution where the tangent to the curve is parallel to the x axis as $\eta\to\infty$, we find that

$$b_x = 2\mu T\,\mathrm{sech}\eta\,,\quad b_y + ib_z = i\mu(1 - T^2 - 2iT\tanh\eta)\,e^{i\Theta}\,, \tag{1.60}$$

where $\mu = \dfrac{1}{1+T^2}$ and $\Theta = T\eta + \sigma(t)$. The function $\sigma(t)$ is a function of t, which is not determined by equation (1.57), since this equation determines the shape of the curve at a fixed time. The function σ allows for a rotation of the curve about the x axis. In order to obtain an expression for $\sigma(t)$, we must look at the original equation of motion, equation (1.7).

In order to find $\sigma(t)$, we write down the expressions for $\vec{t}$, $\vec{n}$ and $\vec{r}$. Using (1.17), (1.13) and (1.11) along with (1.60), we find that

$$\begin{aligned} n_x &= 2\mu \operatorname{sech}\eta \tanh\eta \ , \quad n_y + in_z = -\Big(1 - 2\mu(\tanh\eta - iT)\tanh\eta\Big)\, e^{i\Theta} \ , \\ t_x &= 1 - 2\mu \operatorname{sech}^2\eta \ , \quad t_y + it_z = -2\mu \operatorname{sech}\eta(\tanh\eta - iT)\, e^{i\Theta} \ , \\ x &= s - \frac{2\mu}{\nu}\tanh\eta \ , \quad y + iz = \frac{2\mu}{\nu}\operatorname{sech}\eta\, e^{i\Theta} \ , \end{aligned} \tag{1.61}$$

where x, y and z refer to the fixed coordinate system. Equation (1.7) is equivalent to

$$\frac{\partial \vec{r}}{\partial t} = \kappa \vec{b} \ , \tag{1.62}$$

where we have used the definitions of κ and $\vec{b}$ in order to obtain (1.62). We substitute the corresponding expressions from (1.56), (1.60) and (1.61) for the $x + iy$ component into equation (1.62) to obtain that

$$\frac{d\,\sigma(t)}{dt} = \nu^2 + \tau^2 \ . \tag{1.63}$$

Integrating (1.63) and defining $\sigma(0) = 0$, we find that

$$\sigma(t) = (\nu^2 + \tau^2)t \ . \tag{1.64}$$

Equation (1.61) is a two parameter family of exact solutions to equation (1.7). These solutions describe a disturbance moving along the filament with a velocity equal to 2τ. The filament itself is not moving along the axis of the filament, but remains stationary except for the portion where the disturbance is located. Looking at (1.61) we see that as the disturbance passes through a given point, that point undergoes a translation of $4\mu/\nu$ units along the axis of the filament in the direction of propagation of the disturbance.

Solution (1.61) is a soliton. In general the term soliton refers to a travelling wave solution of a nonlinear equation. There are N-soliton solutions to (1.7). These N-soliton solutions are approximately made up of N single soliton solutions placed along the filament. Exact N-soliton solutions are found by looking at equation (1.44). This set of exact solutions was found by Zakharov and Shabat [45]. We shall not discuss the N-soliton solutions in detail.

1.6 The Self-Similar Solution

The final exact solution which we discuss is one we discovered in which the filament is not smooth initially. In the calculations described in chapter six we must solve for the evolution of filaments which are not smooth, but contain discontinuities in the tangent field; thus this solution provides a means for checking the numerical method introduced in the next chapter. The initial conditions for the curvature are $\kappa(s,0) = \Theta_0\delta(s)$, where $\delta(s)$ is the Dirac delta function. These initial conditions describe a curve made of two semi-infinite lines, which intersect at their endpoints with an angle $\pi - \Theta_0$ between them. In terms of the tangent vector we describe this curve as

$$\vec{t}(s,0) = \begin{cases} \vec{t}_+ & \text{if } s > 0 \\ \vec{t}_- & \text{if } s < 0 \end{cases}, \tag{1.63}$$

where $\vec{t}_+$ and $\vec{t}_-$ are constant unit vectors such that $\vec{t}_+ \cdot \vec{t}_- = \cos\Theta_0$.

We proceed to solve (1.8) with (1.63) as initial conditions. Given a solution $\vec{t}(s,t)$ of equation (1.8), consider under what conditions the function $\vec{\tau}(s,t)$, defined as $\tau(s,t) = \vec{t}(s/\alpha, t/\beta)$, is also a solution of equation (1.8). By direct substitution, we find that $\tau(s,t)$ is a solution provided that $\beta/\alpha^2 = 1$. In order to emphasize the fact that each α defines a new solution of equation (1.8), that is, a solution with different initial conditions, we write $\vec{\tau} = \vec{\tau}(s,t,\alpha)$. If we look at initial conditions (1.63), we see that they remain invariant for all α under the scaling where $s \to s/\alpha$. If we consider the solution $\vec{t}(s,t)$ satisfying these initial conditions, then the function $\vec{\tau}(s,t,\alpha)$ associated with this $\vec{t}(s,t)$ is independent of α. If we let $\alpha = \sqrt{t}$, from the definition of $\vec{\tau}$ we find that $\vec{\tau}(s,t,\sqrt{t}) = \vec{t}(s/\sqrt{t},1)$. Thus the solution we are seeking is only a function of $\eta = s/\sqrt{t}$. Writing equation (1.8) in terms of η, we find that

$$\eta \frac{d\vec{t}}{d\eta} = 2\frac{d^2\vec{t}}{d\eta^2} \times \vec{t}\,. \tag{1.64}$$

Equation (1.64) can be solved by considering η to be a new parametrization of the

tangent field. The Frenet-Seret equations are valid if we replace the variable s by the variable η. The defining feature of arclength is the fact that differentiation of the filament with respect to this parameter gives a unit vector; in the derivation of equation (1.17) no use is made of this fact other then to guarantee that $\vec{t}$ is a unit vector. We must, however, remember that the quantities derived from $\vec{t}$ will differ, depending upon which parameter we use. The "curvature" derived using η as a parameter for $\vec{t}$ will be different from that obtained using s as a parameter for $\vec{t}$. We note this difference by denoting quantities obtained from $\vec{t}(\eta)$ with a $'$, while quantities without a $'$ denote quantities derived using $\vec{t}(s)$.

In view of the preceeding comments, we use equations (1.21) to replace the derivatives in (1.64) to find that

$$\eta\kappa' \ \vec{n}' \ = -2\frac{d\,\kappa'}{d\,\eta}\vec{b}' \ + 2\kappa' \ \tau' \ \vec{n}' \ . \tag{1.65}$$

Since the vectors in (1.65) are orthogonal we find that

$$\tau' \ = \frac{\eta}{2} \ , \ \text{and} \ \frac{d\,\kappa'}{d\,\eta} = 0 \ .$$

We now relate τ' and κ' to τ and κ. By noting that $\frac{\partial}{\partial s} = \frac{1}{\sqrt{t}}\frac{d}{d\,\eta}$, we find that

$$\kappa\vec{n} \ = \frac{\partial\vec{t}}{\partial s} = \frac{1}{\sqrt{t}}\frac{d\vec{t}}{d\,\eta} = \frac{\kappa'}{\sqrt{t}}\vec{n}' \ . \tag{1.66}$$

Equation (1.66) implies that $\vec{n}' \ = \vec{n}$, $\vec{b}' \ = \vec{b}$, and $\kappa' \ = \sqrt{t}\ \kappa$. From these observations and (1.21) we also see that $\tau' \ = \sqrt{t}\ \tau$.

The solution to (1.8) with initial conditions (1.63) is the filament that has curvature $\kappa = \frac{\kappa_0}{\sqrt{t}}$ and torsion $\tau = \frac{s}{2t}$. This solution illustrates the fact that disturbances can travel with infinite speed when they are governed by the self-induction equation. Initially the curvature is zero everywhere except at the origin; at later times the curvature is constant along the curve and equal to $\frac{\kappa_0}{\sqrt{t}}$. We use this solution in chapter 3 to investigate the convergence of the approximate solution obtained by our numerical scheme introduced in chapter 2.

1.7 Existence and Uniqueness of Solutions

In concluding this chapter we mention that global existence and uniqueness results for solutions of equation (1.44) have been proven by Ginibre and Velo [15]. Their results indicate that solutions of (1.44) are continuous functions of time with values in $\mathbf{H}^1(\mathbf{R}) \bigcap \mathbf{L}^\infty(\mathbf{R})$.

Chapter 2: Numerical Schemes for the Self-Induction Equations

In this chapter we discuss the numerical scheme to solve the self-induction equation. We present properties of this scheme, including stability and order of accuracy.

Delfour, Fortin and Payre [12] present a scheme to solve the non-linear Schrödinger equation (1.44). This is the method we originally used to solve the self-induction equation. We find that the method gives good results for curvatures and torsions which are bounded and obtained from smooth curves, but it is difficult to obtain good results for curves with singularities in their tangent fields. Another difficulty with using a scheme based on (1.44) is that physical boundary conditions on a vortex filament are difficult to use in terms of the curvature and torsion of the filament. As we showed in the first chapter it is an involved process to determine the position of a vortex filament from its curvature and torsion. We also want a method which can be generalized to include interactions which cause the vortex filament to stretch; this can not be done in a simple manner if we use the representation introduced by Hasimoto.

The above considerations led us to develop an alternate method for solving the self-induction equation and in the first section of this chapter we introduce a set of finite difference equations which approximate equation (1.8). As mentioned in chapter one, we chose to approximate (1.8) rather than (1.7) because of the simpler equation which results, and because it is easier to obtain invariants when considering the tangent field. The invariants obtained for our approximate solutions immediately imply stability of our method. (For a method based on equation (1.7) see Aref and Flinchem [2].) In order to find the position of the vortex filament from the tangent only a simple integration is required and most boundary conditions are easily written in terms of the tangent field. We also show in chapter five that we are able to generalize the method to include interactions which cause the vortex filament to stretch.

In the next section of this chapter we discuss methods for solving the finite difference equations. Since the method is nonlinear it is important to know under what conditions the finite difference equations can be solved. We present two methods for solving the finite difference equations of our method. We are able to show sufficient conditions for convergence of the methods and we are able to show existence and uniqueness of solutions of the finite difference equations for arbitrary initial conditions.

In the remainder of the chapter we further analyze our method. We first show that the method is stable and then also that it is linearly stable. We then carry out an analysis of the error of the method and conclude that the error is second order in space and time. Motivated by the error analysis we propose another method based on (1.8) which should be fourth order accurate, although we have done no calculations using this fourth order method.

2.1 The Finite Difference Equations

We develop the finite difference equations for solving the self-induction equation written in terms of the tangent field. We rewrite equation (1.8) here:

$$\frac{\partial \vec{t}}{\partial t} = \vec{t} \times \frac{\partial^2 \vec{t}}{\partial s^2} . \tag{2.1}$$

We chose equation (2.1) over equation (1.7) for the development of a scheme for the following reason: the linearized form of equation (1.7) contains one term, which is parabolic and one term which is hyperbolic. Thus a numerical scheme to solve (1.7) has to keep both terms stable. Equation (2.1) has only the parabolic term in its linearized form and this simplifies finding a stable scheme.

We denote by $\vec{t}_j^n$ the approximation to $\vec{t}(j\,\Delta s\,, n\,\Delta t\,)$. We define $\vec{t}_j^n$ by requiring that it satisfy the following difference equation.

$$\vec{t}_j^{\,n+1} - \vec{t}_j^{\,n} = \frac{\Delta t}{4(\Delta s\,)^2}\left(\vec{t}_j^{\,n+1} + \vec{t}_j^{\,n}\right) \times \left(\vec{t}_{j+1}^{\,n+1} + \vec{t}_{j+1}^{\,n} + \vec{t}_{j-1}^{\,n+1} + \vec{t}_{j-1}^{\,n}\right) \tag{2.2}$$

Scheme (2.2) is a Crank-Nicholson type scheme. The second member in the cross product in (2.2) is the formula for the second order difference equation for second order derivatives.

The term $(\vec{t}_j^{\,n+1} + \vec{t}_j^{\,n})$, of the difference formula has been cancelled by crossing it with the first member of the cross product.

Scheme (2.2) has three discrete invariants, which are that

$$|\vec{t}_j^{\,n+1}| = |\vec{t}_j^{\,n}| , \tag{2.3}$$

that

$$\sum_{j=1}^{N} \vec{t}_j^{\,n+1} = \sum_{j=1}^{N} \vec{t}_j^{\,n} , \tag{2.4}$$

and that

$$\sum_{j=1}^{N} |\vec{t}_{j+1}^{\,n+1} - \vec{t}_j^{\,n+1}|^2 = \sum_{j=1}^{N} |\vec{t}_{j+1}^{\,n} - \vec{t}_j^{\,n}|^2 . \tag{2.5}$$

The first invariant (2.3), corresponds to the fact that solutions to (2.1) do not stretch. $\vec{t}(s,t)$ has unit magnitude for all times; (2.3) guarantees that if the $\vec{t}_j^{\,0}$ have unit magnitude then the numerical solution $\vec{t}_j^{\,n}$ will also have unit magnitude for all n. The second invariant (2.4) guarantees that if the numerical curve is closed initially then it will remain closed for all times. This is also an invariant of equation (2.1), the fact that solutions to (2.1), which are closed curves initially remain closed curves for all future times. The third invariant (2.5), corresponds to the first invariant in (1.28), since the magnitude of the derivative of the tangent is equal to the curvature.

We verify (2.3) by multiplying both sides of equation (2.2) by the quantity $(\vec{t}_j^{\,n+1} + \vec{t}_j^{\,n})$. The right side of the resultant equation vanishes, since there are two identical terms in the triple product. The result is

$$\begin{aligned} &|\vec{t}_j^{\,n+1}|^2 - |\vec{t}_j^{\,n}|^2 \\ &= \lambda\left(\vec{t}_j^{\,n+1} + \vec{t}_j^{\,n}\right)\cdot\left(\vec{t}_j^{\,n+1} + \vec{t}_j^{\,n}\right)\times\left(\vec{t}_{j+1}^{\,n+1} + \vec{t}_{j+1}^{\,n} + \vec{t}_{j-1}^{\,n+1} + \vec{t}_{j-1}^{\,n}\right) = 0 , \end{aligned} \tag{2.6}$$

where

$$\lambda = \frac{\Delta t}{4(\Delta s)^2} .$$

Equation (2.3) then follows immediately from (2.6).

In order to verify equation (2.4), we sum both sides of equation (2.2) over j. Let $(\vec{t}_j^{\,n+1} + \vec{t}_j^{\,n}) \equiv \vec{t}_j$, then we have that

$$\sum_{j=1}^{N} \left(\vec{t}_j^{\,n+1} - \vec{t}_j^{\,n}\right) = \lambda \sum_{j=1}^{N} \left(\vec{t}_j \times \vec{t}_{j+1} - \vec{t}_{j-1} \times \vec{t}_j\right) \tag{2.7}$$
$$= \lambda \left(\vec{t}_N \times \vec{t}_{N+1} - \vec{t}_0 \times \vec{t}_1\right) .$$

If we assume periodic boundary conditions the second line in (2.7) vanishes and (2.4) follows directly.

The first step in verifying (2.5) is to write down equation (2.2) where the left side is evaluated at $j+1$. The result is that

$$\vec{t}_{j+1}^{\,n+1} - \vec{t}_{j+1}^{\,n} = \lambda \left(\vec{t}_{j+1} \times \vec{t}_{j+2} - \vec{t}_j \times \vec{t}_{j+1}\right) , \tag{2.8}$$

where we have used the notation introduced in the preceding paragraph. We then subtract the members of (2.2) from the corresponding members of (2.8) and multiply the members of the resultant equation by the quantity $(\vec{t}_{j+1} - \vec{t}_j)$. The result is that

$$|\, \vec{t}_{j+1}^{\,n+1} - \vec{t}_j^{\,n+1} \,|^2 - |\, \vec{t}_{j+1}^{\,n} - \vec{t}_j^{\,n} \,|^2 \tag{2.9}$$
$$= \lambda \left(\vec{t}_{j-1} \times \vec{t}_j \cdot \vec{t}_{j+1} - \vec{t}_j \cdot \vec{t}_{j+1} \times \vec{t}_{j+2}\right) .$$

Out of eight terms, which could appear on the right side of equation (2.9), only the triple products of the two terms, which actually do appear, are nonzero. Summing both sides of equation (2.9) over j, we find that

$$\sum_{j=1}^{N} \left(|\, \vec{t}_{j+1}^{\,n+1} - \vec{t}_j^{\,n+1} \,|^2 - |\, \vec{t}_{j+1}^{\,n} - \vec{t}_j^{\,n} \,|^2 \right) \tag{2.10}$$
$$= \lambda \left(\vec{t}_0 \times \vec{t}_1 \cdot \vec{t}_2 - \vec{t}_N \cdot \vec{t}_{N+1} \times \vec{t}_{N+2}\right) .$$

Once again if we assume periodic boundary conditions, the second line of (2.10) vanishes and we obtain (2.5).

Given an approximation to $\vec{t}(s,t)$, the procedure for finding an approximation to $\vec{r}(s,t)$ is simpler than that procedure required to find an approximation to $\vec{r}(s,t)$ from Ψ, the solution to the nonlinear Schrödinger equation. Our basis for finding an approximation to $\vec{r}(s,t)$ is equation (1.9).

In practice we use second order integration methods in evaluating the integrals in equation (1.9) to maintain second order accuracy. Let $\vec{v}$ be defined as

$$\vec{v}(0,t) \equiv \frac{\partial \vec{r}(0,t)}{\partial t} = \vec{t}(0,t) \times \frac{\partial \vec{t}(0,t)}{\partial s} ,$$

and let $\vec{v}_j^{\,n+1}$ denote the approximation of $\vec{v}(j\,\Delta s\,,(n+1/2)\Delta t)$ defined by

$$\vec{v}_j^{\,n+1} = \frac{1}{8\Delta s}\left(\vec{t}_j^{\,n+1} + \vec{t}_j^{\,n}\right) \times \left((\vec{t}_{j+1}^{\,n+1} + \vec{t}_{j+1}^{\,n}) - (\vec{t}_{j-1}^{\,n+1} + \vec{t}_{j-1}^{\,n})\right) . \tag{2.11}$$

Using definition (2.11) and equation (1.9) we obtain the following approximation to $\vec{r}(j\,\Delta s\,,n\,\Delta t)$.

$$\vec{r}_j^{\,n} = \vec{r}(0,0) + \Delta t \sum_{m=1}^{n}\left(\vec{v}_0^{\,m}\right) + \frac{\Delta s}{2}\sum_{i=1}^{j}\left(\vec{t}_i^{\,n} + \vec{t}_{i-1}^{\,n}\right) \tag{2.12}$$

Using approximation (2.11) for the velocity gives us a self-consistency property for the motion of a point on the filament. This consistency property is the fact that the calculated position in 3-space of a particle on the filament is independent of where on the filament we calculate the velocity numerically, provided we use (2.11). In order to verify this consistency property, we show that the motion of a particle at time step $n+1$ is given by

$$\vec{r}_j^{\,n+1} - \vec{r}_j^{\,n} = \Delta t\ \vec{v}_j^{\,n+1} ,$$

for all j and n. We rewrite (2.12) at time step $n+1$ and obtain that

$$\vec{r}_j^{\,n+1} = \vec{r}(0,0) + \Delta t \sum_{m=1}^{n+1}\left(\vec{v}_0^{\,m}\right) + \frac{\Delta s}{2}\sum_{i=1}^{j}\left(\vec{t}_i^{\,n+1} + \vec{t}_{i-1}^{\,n+1}\right) . \tag{2.13}$$

Subtracting the corresponding terms of (2.12) from (2.13) and using the notation previously introduced, that $\vec{t}_j = (\vec{t}_j^{\,n+1} + \vec{t}_j^{\,n})$ we find that

$$\begin{aligned}
\vec{r}_j^{\,n+1} - \vec{r}_j^{\,n} &= \Delta t\ \vec{v}_0^{\,n+1} + \frac{\Delta s}{2}\sum_{i=1}^{j}\left(\vec{t}_i^{\,n+1} - \vec{t}_i^{\,n} + \vec{t}_{i-1}^{\,n+1} - \vec{t}_{i-1}^{\,n}\right) \\
&= \Delta t\ \vec{v}_0^{\,n+1} + \frac{\Delta t}{8\Delta s}\sum_{i=1}^{j}\left(\vec{t}_i \times (\vec{t}_{i+1} + \vec{t}_{i-1}) + \vec{t}_{i-1} \times (\vec{t}_i + \vec{t}_{i-2})\right) \\
&= \Delta t\ \vec{v}_0^{\,n+1} + \frac{\Delta t}{8\Delta s}\sum_{i=1}^{j}\left(\vec{t}_i \times (\vec{t}_{i+1} - \vec{t}_{i-1}) - \vec{t}_{i-1} \times (\vec{t}_i - \vec{t}_{i-2})\right) \\
&= \Delta t\ \vec{v}_0^{\,n+1} + \Delta t \sum_{i=1}^{j}\left(\vec{v}_i^{\,n+1} - \vec{v}_{i-1}^{\,n+1}\right) \\
&= \Delta t\ \vec{v}_j^{\,n+1} ,
\end{aligned}$$

where we have used (2.2) and (2.11).

2.2 Methods for Solving the Finite Difference Equations

We present two methods for solving equation (2.2). Both methods are iterative. We define a sequence of approximate solutions $\vec{x}_j^k$, and if they converge to some $\vec{x}_j^\infty$, we define $\vec{t}_j^{n+1} = \vec{x}_j^\infty$.

The first method is obtained in the following manner. Assume we know $\vec{t}_j^n$ and that we are seeking $\vec{t}_j^{n+1}$. The approximating sequence $\vec{x}_j^{k+1}$ is then defined in the following manner. First define $\vec{y}_j^{k+1}$, by requiring that

$$\vec{y}_j^{k+1} - \vec{t}_j^n = \lambda\left(\vec{t}_j^n + \vec{x}_j^k\right) \times \left(\vec{t}_{j-1}^n + \vec{t}_{j+1}^n + \vec{x}_{j-1}^k + \vec{x}_{j+1}^k\right), \tag{2.14}$$

where

$$\lambda = \frac{\Delta t}{4(\Delta s)^2}.$$

By picking λ small enough we can guarantee that $|\vec{y}_j^{k+1}| \neq 0$; using the triangle inequality from equation (2.14) we see that

$$1 - 8\lambda \leq |\vec{y}_j^{k+1}| \leq 1 + 8\lambda,$$

where we have used the fact that all of the vectors on the right side of equation (2.14) have unit magnitude. We define $\vec{x}_j^{k+1}$ by requiring that

$$\vec{x}_j^{k+1} = \frac{\vec{y}_j^{k+1}}{|\vec{y}_j^{k+1}|}. \tag{2.15}$$

In this way we define a sequence, in which all of the vectors are of unit magnitude. Recall that solutions of equation (2.2) are required to have unit magnitude.

We now derive conditions under which the sequence defined by (2.14) and (2.15) converges. To begin let us write equation (2.14) explicitly for two iterations.

$$\begin{aligned} \vec{y}_j^{k+1} - \vec{t}_j^n &= \lambda\left(\vec{t}_j^n + \vec{x}_j^k\right) \times \left(\vec{t}_{j-1}^n + \vec{t}_{j+1}^n + \vec{x}_{j-1}^k + \vec{x}_{j+1}^k\right) \\ \vec{y}_j^k - \vec{t}_j^n &= \lambda\left(\vec{t}_j^n + \vec{x}_j^{k-1}\right) \times \left(\vec{t}_{j-1}^n + \vec{t}_{j+1}^n + \vec{x}_{j-1}^{k-1} + \vec{x}_{j+1}^{k-1}\right) \end{aligned} \tag{2.16}$$

Subtracting the terms of the second equation from the terms of the first equation in (2.16),

and adding and subtracting a term from the right side of the result, we find that

$$\begin{aligned}
\vec{y}_j^{\,k+1} - \vec{y}_j^{\,k} = \lambda\Big\{ & \left(\vec{t}_j^{\,n} + \vec{x}_j^{\,k}\right)\times\left(\vec{t}_{j-1}^{\,n} + \vec{t}_{j+1}^{\,n} + \vec{x}_{j-1}^{\,k} + \vec{x}_{j+1}^{\,k}\right) \\
& - \left(\vec{t}_j^{\,n} + \vec{x}_j^{\,k-1}\right)\times\left(\vec{t}_{j-1}^{\,n} + \vec{t}_{j+1}^{\,n} + \vec{x}_{j-1}^{\,k} + \vec{x}_{j+1}^{\,k}\right) \\
& + \left(\vec{t}_j^{\,n} + \vec{x}_j^{\,k-1}\right)\times\left(\vec{t}_{j-1}^{\,n} + \vec{t}_{j+1}^{\,n} + \vec{x}_{j-1}^{\,k} + \vec{x}_{j+1}^{\,k}\right) \\
& - \left(\vec{t}_j^{\,n} + \vec{x}_j^{\,k-1}\right)\times\left(\vec{t}_{j-1}^{\,n} + \vec{t}_{j+1}^{\,n} + \vec{x}_{j-1}^{\,k-1} + \vec{x}_{j+1}^{\,k-1}\right)\Big\} \\
= \lambda\Big\{ & \left(\vec{x}_j^{\,k} - \vec{x}_j^{\,k-1}\right)\times\left(\vec{t}_{j-1}^{\,n} + \vec{t}_{j+1}^{\,n} + \vec{x}_{j-1}^{\,k} + \vec{x}_{j+1}^{\,k}\right) \\
& + \left(\vec{t}_j^{\,n} + \vec{x}_j^{\,k-1}\right)\times\left(\vec{x}_{j-1}^{\,k} - \vec{x}_{j-1}^{\,k-1} + \vec{x}_{j+1}^{\,k} - \vec{x}_{j+1}^{\,k-1}\right)\Big\}.
\end{aligned} \tag{2.17}$$

Maximizing both sides of equation (2.17) over j and using the triangle inequality, we obtain that

$$\max_j \mid \vec{y}_j^{\,k+1} - \vec{y}_j^{\,k} \mid \;\leq 8\lambda \max_j \mid \vec{x}_j^{\,k} - \vec{x}_j^{\,k-1} \mid \;. \tag{2.18}$$

Observe that if $\vec{x}$ and $\vec{y}$ are two nonzero vectors then

$$\left(\mid \vec{x} \mid \mid \vec{y} \mid \right)^{1/2} \left| \frac{\vec{x}}{\mid \vec{x} \mid} - \frac{\vec{y}}{\mid \vec{y} \mid} \right| \leq \mid \vec{x} - \vec{y} \mid \;. \tag{2.19}$$

We verify equation (2.19) by noting that $(x + 1/x) \geq 2$, provided that $x > 0$, and then by observing that

$$\begin{aligned}
\mid \vec{x} - \vec{y} \mid^2 &= \mid \vec{x} \mid \mid \vec{y} \mid \left(\frac{\mid \vec{x} \mid}{\mid \vec{y} \mid} + \frac{\mid \vec{y} \mid}{\mid \vec{x} \mid} \right) - 2(\vec{x}\cdot\vec{y}) \\
&\geq 2 \mid \vec{x} \mid \mid \vec{y} \mid \left(1 - \frac{\vec{x}\cdot\vec{y}}{\mid \vec{x} \mid \mid \vec{y} \mid} \right) \\
&= \mid \vec{x} \mid \mid \vec{y} \mid \left| \frac{\vec{x}}{\mid \vec{x} \mid} - \frac{\vec{y}}{\mid \vec{y} \mid} \right|^2 .
\end{aligned}$$

Thus if we combine equations (2.19) and (2.18) and use the fact that $\mid \vec{y}_j^{\,k} \mid \;\geq 1 - 8\lambda$ for all k, we obtain that

$$
\begin{aligned}
&(1-8\lambda)\max_j \ |\vec{x}_j^{\,k+1}-\vec{x}_j^{\,k}| \\
&\le \min_j \left(|\vec{y}_j^{\,k+1}| \ \ |\vec{y}_j^{\,k}| \right)^{1/2} \max_j \ |\vec{x}_j^{\,k+1}-\vec{x}_j^{\,k}| \\
&\le \max_j \left((|\vec{y}_j^{\,k+1}| \ \ |\vec{y}_j^{\,k}|)^{1/2} \ |\vec{x}_j^{\,k+1}-\vec{x}_j^{\,k}| \right) \\
&\le \max_j \ |\vec{y}_j^{\,k+1}-\vec{y}_j^{\,k}| \\
&\le 8\lambda \max_j \ |\vec{x}_j^{\,k}-\vec{x}_j^{\,k-1}| \ .
\end{aligned}
\tag{2.20}
$$

We view (2.14) and (2.15) as a general mapping of the compact manifold, formed by taking N copies of the unit sphere, into itself. If we pick $\lambda < 1/16$, then by a well known theorem [37], inequality (2.20) shows that (2.14) defines a contraction mapping. Consequently the $\vec{x}_j^{\,k}$ converge to the unique fixed point of the manifold and the fixed point satisfies equation (2.2).

We now present a second method for finding a solution to equation (2.2). This method is also iterative. In order to define the sequence of approximate solutions $\vec{x}_j^{\,k}$, we must first solve the following equation for $\vec{x}$.

$$
\vec{x} + \vec{b}\times\vec{x} = \vec{t} + \vec{t}\times\vec{b} \tag{2.21}
$$

If we cross the terms of (2.21) with the vector $\vec{b}$, we find that

$$
\vec{b}\times\vec{x} + \vec{b}(\vec{b}\cdot\vec{x}) - \vec{x}\,|\,\vec{b}\,|^2 = \vec{b}\times\vec{t} + \vec{t}\,|\,\vec{b}\,|^2 - \vec{b}(\vec{b}\cdot\vec{t}) \ . \tag{2.22}
$$

By dotting the members of (2.21) with the vector $\vec{b}$, we observe that

$$
(\vec{b}\cdot\vec{x}) = (\vec{b}\cdot\vec{t}) \ . \tag{2.23}
$$

Subtracting the terms of (2.22) from the corresponding terms of (2.21) and substituting (2.23), we see that

$$
\vec{x}(1 + |\,\vec{b}\,|^2) = \vec{t}(1 - |\,\vec{b}\,|^2) + 2(\vec{t}\times\vec{b}) + 2\vec{b}(\vec{t}\cdot\vec{b}) \ . \tag{2.24}
$$

Equation (2.24) uniquely defines $\vec{x}$ in terms of the vectors $\vec{t}$ and $\vec{b}$. It should also be noted that $\vec{x}$ has the same magnitude as $\vec{t}$, if $\vec{x}$ is defined by (2.24).

We now define the sequence of approximate solutions to (2.2), by requiring that $\vec{x}_j^{\,k+1}$ satisfy

$$
\vec{x}_j^{\,k+1} - \vec{t}_j^{\,n} = \lambda\left(\vec{x}_j^{\,k+1} + \vec{t}_j^{\,n}\right)\times\left(\vec{t}_{j-1}^{\,n} + \vec{t}_{j+1}^{\,n} + \vec{x}_{j-1}^{\,k} + \vec{x}_{j+1}^{\,k}\right) , \tag{2.25}
$$

where once again

$$\lambda = \frac{\Delta t}{4(\Delta s)^2} .$$

Equation (2.25) can be written in the form of equation (2.21), and thus we can solve equation (2.25) for $\vec{x}_j^{k+1}$ by using equation (2.24). The $\vec{x}_j^k$ obtained in this manner are of unit magnitude, if the vectors $\vec{t}_j^n$ are of unit magnitude.

We show that the sequence $\vec{x}_j^k$ defined by (2.25) converges provided that $\lambda < 1/4$. We view (2.25) as a general mapping from $\mathbf{R}^{3N}$ to $\mathbf{R}^{3N}$, where N is defined so that $1 \leq j \leq N$. We show that (2.25) is a contraction mapping. We begin by writing down the mapping by (2.25) of two arbitrary points in $\mathbf{R}^{3N}$.

$$\begin{aligned} \vec{x}_j - \vec{t}_j^n &= \lambda\left(\vec{x}_j + \vec{t}_j^n\right) \times \left(\vec{t}_{j-1}^n + \vec{t}_{j+1}^n + \vec{u}_{j-1} + \vec{u}_{j+1}\right) \\ \vec{y}_j - \vec{t}_j^n &= \lambda\left(\vec{y}_j + \vec{t}_j^n\right) \times \left(\vec{t}_{j-1}^n + \vec{t}_{j+1}^n + \vec{v}_{j-1} + \vec{v}_{j+1}\right) \end{aligned} \tag{2.26}$$

Subtracting the terms of the second equation in (2.26), from those of the first we obtain that

$$\begin{aligned} \vec{x}_j - \vec{y}_j &= \lambda\Big\{ \left(\vec{x}_j + \vec{t}_j^n\right) \times \left(\vec{t}_{j-1}^n + \vec{t}_{j+1}^n + \vec{u}_{j-1} + \vec{u}_{j+1}\right) \\ &\quad - \left(\vec{y}_j + \vec{t}_j^n\right) \times \left(\vec{t}_{j-1}^n + \vec{t}_{j+1}^n + \vec{u}_{j-1} + \vec{u}_{j+1}\right) \\ &\quad + \left(\vec{y}_j + \vec{t}_j^n\right) \times \left(\vec{t}_{j-1}^n + \vec{t}_{j+1}^n + \vec{u}_{j-1} + \vec{u}_{j+1}\right) \\ &\quad - \left(\vec{y}_j + \vec{t}_j^n\right) \times \left(\vec{t}_{j-1}^n + \vec{t}_{j+1}^n + \vec{v}_{j-1} + \vec{v}_{j+1}\right) \Big\} \\ &= \lambda\Big\{ \left(\vec{x}_j - \vec{y}_j\right) \times \left(\vec{t}_{j-1}^n + \vec{t}_{j+1}^n + \vec{u}_{j-1} + \vec{u}_{j+1}\right) \\ &\quad + \left(\vec{y}_j + \vec{t}_j^n\right) \times \left(\vec{u}_{j-1} - \vec{v}_{j-1} + \vec{u}_{j+1} - \vec{v}_{j+1}\right) \Big\} . \end{aligned} \tag{2.27}$$

We dot the members of (2.27) by the quantity $(\vec{x}_j - \vec{y}_j)$, and find that

$$\begin{aligned} |\vec{x}_j - \vec{y}_j|^2 &= \\ = \lambda\left(\vec{x}_j - \vec{y}_j\right) \cdot \left(\vec{t}_j^n + \vec{y}_j\right) &\times \left(\vec{u}_{j-1} - \vec{v}_{j-1} + \vec{u}_{j+1} - \vec{v}_{j+1}\right) . \end{aligned} \tag{2.28}$$

We apply the triangle inequality to the right side of (2.28) and maximize both sides over j, in order to obtain that

$$\max_j |\vec{x}_j - \vec{y}_j|^2 \leq 4\lambda \left(\max_j |\vec{x}_j - \vec{y}_j|\right)\left(\max_j |\vec{u}_j - \vec{v}_j|\right) . \tag{2.29}$$

Dividing both sides of equation (2.29) by $\max_j |\vec{x}_j - \vec{y}_j|$, we see the final result, that

$$\max_j \ | \vec{x}_j - \vec{y}_j | \ \leq 4\lambda \max_j \ | \vec{u}_j - \vec{v}_j | \ . \tag{2.30}$$

Inequality (2.30) shows that (2.25) defines a contraction map, provided that $\lambda < 1/4$. We have assumed in obtaining (2.29) that the mapping (2.25) is defined on the compact sub-manifold of $\mathbf{R}^{3N}$, defined by taking N copies of the unit 2-sphere. Viewed in this way, (2.25) defines a contraction mapping on a compact metric space and thus, by a well known theorem [37], the $\vec{x}_j^k$ converge to the unique fixed point of the sub-manifold. Also by looking at (2.25), we see that the fixed point satisfies equation (2.2). Thus we have the following existence and uniqueness result for (2.2).

Given $\vec{t}_j^n$ such that $| \vec{t}_j^n | = 1$ for $1 \leq j \leq N$, if $\left| \frac{\Delta t}{(\Delta s)^2} \right| < 1$, there exists a unique $\vec{t}_j^{n+1}$ satisfying equation (2.2). Thus we have shown that there exists a unique solution to equation (2.2) for any initial conditions for all future and past times.

Equation (2.25) also suggests a family of predictor-corrector type schemes for finding approximate solutions to equation (1.8). Instead of using (2.25) to find the solution to (2.2), (2.25) would be used for a fixed number of iterations and the final iterate would be taken as the approximate solution. In practice if the fixed number of iterates taken is large, the method would produce the same solution as that obtained from (2.2). For a small number of iterations, however, the scheme would be different. The interesting thing to note is that all solutions obtained from any of these schemes satisfy equation (2.3), and as is discussed in the next paragraphs, this means the schemes are stable.

2.3 Stability

We now discuss the stability of (2.2). A scheme is stable if the approximate solutions obtained from the scheme are bounded in some norm. Scheme (2.2) is stable in the $\mathbf{H}_0^0$ norm, where the norm is defined as

$$|| \tilde{t}^n ||_0^2 = \Delta s \sum_{j=1}^{j=N} | \vec{t}_j^n |^2 , \tag{2.31}$$

where $\tilde{t}^n$ denotes the solution vector to (2.2), composed of the N 3-vectors $\vec{t}_j^n$. This is also

the norm in which the predictor-corrector schemes based on (2.25) are stable. From (2.3) we obtain the result that

$$||\tilde{t}^{\,n}||_0 = ||\tilde{t}^{\,0}||_0 ,$$

which shows stability in the $\mathbf{H}_0^0$ norm. Equation (2.2) is also stable in the $\mathbf{H}_0^1$ norm, defined as

$$||\tilde{t}^{\,n}||_1^{\,2} = \Delta s \sum_{j=1}^{j=N} |\vec{t}_j^{\,n}|^2 + \Delta s \sum_{j=1}^{j=N} \frac{|\vec{t}_j^{\,n} - \vec{t}_{j-1}^{\,n}|^2}{(\Delta s)^2} .$$

From (2.3) and (2.5) we have that

$$||\tilde{t}^{\,n}||_1 = ||\tilde{t}^{\,0}||_1 ,$$

which shows stabilty in the $\mathbf{H}_0^1$ norm.

We now analyze the local linear stability of (2.4). A scheme is linearly stable if the linearization of the nonlinear scheme is linearly stable [35]. The idea behind local linear stability analysis is that if a scheme is unstable to small perturbations about an exact solution, then the full nonlinear scheme is also probably unstable. Kreiss [27], however, showed that this is not necessarily true for equations of the Schrödinger type. He showed that for Schrödinger type equations, a scheme may be linearly stable and still not be stable, and also that a stable scheme may be linearly unstable.

Let $\vec{\tau}_j^{\,n}$ denote the perturbation to the exact solution $\vec{t}_j^{\,n}$. In order to determine the linear scheme we substitute a solution of the form $\vec{t}_j^{\,n} + \vec{\tau}_j^{\,n}$ into equation (2.12) and consider the linear equation which results by dropping all terms of higher order in $\vec{\tau}$. The equation we obtain is that

$$\begin{aligned} \vec{\tau}_j^{\,n+1} - \vec{\tau}_j^{\,n} = \lambda \Big\{ & \left(\vec{t}_j^{\,n} + \vec{t}_j^{\,n+1}\right) \times \left(\vec{\tau}_{j-1}^{\,n} + \vec{\tau}_{j+1}^{\,n} + \vec{\tau}_{j-1}^{\,n+1} + \vec{\tau}_{j+1}^{\,n+1}\right) \\ & + \left(\vec{\tau}_j^{\,n} + \vec{\tau}_j^{\,n+1}\right) \times \left(\vec{t}_{j-1}^{\,n} + \vec{t}_{j+1}^{\,n} + \vec{t}_{j-1}^{\,n+1} + \vec{t}_{j+1}^{\,n+1}\right) \Big\} . \end{aligned} \tag{2.32}$$

Equation (2.32) is a linear evolution equation for the $\vec{\tau}_j^{\,n+1}$ since the $\vec{t}_j^{\,n}$ are assumed known. We now proceed with the standard Fourier method of stability analysis [6,17]. We assume that $\vec{\tau}_j^{\,n} = \vec{\tau}^{\,n}\, e^{ij\xi}$ and substitute this form into equation (2.32). We find that

$$\vec{\tau}^{n+1} - \vec{\omega}\times\vec{\tau}^{n+1} = \vec{\tau}^{n} + \vec{\omega}\times\vec{\tau}^{n} \ ,$$

where

$$\vec{\omega} = \lambda\left(2\cos(\xi)(\vec{t}_j^{\,n} + \vec{t}_j^{\,n+1}) - (\vec{t}_{j-1}^{\,n} + \vec{t}_{j+1}^{\,n} + \vec{t}_{j-1}^{\,n+1} + \vec{t}_{j+1}^{\,n+1})\right) .$$

Let C be the matrix defined by $C\vec{\tau} = \vec{\omega}\times\vec{\tau}$, then we have that

$$\vec{\tau}^{n+1} = (I - C)^{-1}(I + C)\vec{\tau}^{n} = A\vec{\tau}^{n} \ , \qquad (2.33).$$

where I is the identity matrix, and $A = (I - C)^{-1}(I + C)$. It can be shown that the Euclidean norm of any matrix B is

$$|B|^2 = \max_i \lambda_i (B^* B) \ ,$$

where the maximum is over the eigenvalues λ_i of the matrix $B^* B$ and where B^* denotes the hermitean conjugate of B. Thus we see that in order to find the norm of the matrix A, we must find the eigenvalues of the matrix $[(I - C)^{-1}(I + C)]^T [(I - C)^{-1}(I + C)]$, where the superscript T denotes the transpose. Since C is antisymmetric, $C^T = -C$, and since the transpose operation commutes with the inverse operation, we have that

$$\begin{aligned} &[(I - C)^{-1}(I + C)]^T [(I - C)^{-1}(I + C)] \\ &= (I - C)(I + C)^{-1}(I - C)^{-1}(I + C) = I \end{aligned} \qquad (2.34)$$

The second equality in (2.34) is true since all of the matrices in parentheses commute with each other. Thus we find that $|A| = 1$ and this fact along with equation (2.33) implies that

$$|\vec{\tau}^{n+1}| \leq |\vec{\tau}^{n}| \ . \qquad (2.35)$$

Equation (2.35) implies that

$$|\vec{\tau}^{n}| \leq |\vec{\tau}^{0}| \ ,$$

and thus we find that (2.2) is locally linearly stable.

2.4 Accuracy

We present an error analysis of the approximate solution obtained from equation (2.2). We assume that we have an exact smooth solution $\vec{t}(s,t)$ of equation (2.1). and substitute it into the finite difference equations (2.2). If we carry out a Taylor expansion about the

point $s = j\Delta s$, $t = n\Delta t$, we find

$$\vec{t}(j\Delta s,(n+1)\Delta t) - \vec{t} \tag{2.36}$$
$$- \frac{\Delta t}{4\Delta s^2}\Big(\vec{t}(j\Delta s,(n+1)\Delta t) + \vec{t}\Big)\times\Big(\vec{t}((j+1)\Delta s,(n+1)\Delta t) + \vec{t}((j+1)\Delta s,n\Delta t)$$
$$+ \vec{t}((j-1)\Delta s,(n+1)\Delta t) + \vec{t}((j-1)\Delta s,n\Delta t)\Big)$$
$$= \frac{\Delta t\ \Delta s^2}{4!}\vec{t}_{ssss} - \frac{\Delta t^3}{3!}\vec{t}_{ttt}$$
$$+ \frac{\Delta t^3}{4}\Big(\vec{t}\times\vec{t}_{ttss} + \vec{t}_t\times\vec{t}_{ss} + \vec{t}_t\times\vec{t}_{tss}\Big) + \cdots,$$

where the subscripts denote partial derivatives and all quantities without an explicit argument in (2.36) are evaluated at $s = j\Delta s$ and $t = n\Delta t$. We see that the exact solution satisfies equation (2.2) up to $O(\Delta t^3) + O(\Delta t\,\Delta s^2)$ locally and that the global error is $O(\Delta t^2) + O(\Delta s^2)$. If E is the error, which we define precisely in the next chapter, we should have

$$E \le k_0(\Delta s)^2 + k_1(\Delta t)^2, \tag{2.37}$$

where k_0 and k_1 depend only on the initial conditions. In the next chapter we see that for smooth solutions inequality (2.37) is valid.

We now discuss a higher order method for solving equation (2.1). In practice when solving equation (2.2) we use the method represented by equation (2.25). We have shown that the sequence produced by this method converges to the unique solution provided that the condition $\Delta t/(\Delta s)^2 < 1$ is satisfied. If we assume that $\Delta t = \gamma(\Delta s)^2$, with $\gamma < 1$, from (2.37) we have that the error takes the form:

$$E \le k_0\Delta s^2 + \gamma^2 k_1\Delta s^4.$$

With this restriction on Δt, the error due to the approximation of the spatial derivative dominates the total error. By making the approximation of the spatial derivative fourth-order accurate, we obtain a scheme which is fourth order accurate. This leads us to define the following finite difference equation for solving equation (2.1).

$$\vec{t}_j^{\,n+1} - \vec{t}_j^{\,n} = \frac{\Delta t}{4(\Delta s)^2}\,\vec{t}_j \times \left(\frac{4}{3}(\vec{t}_{j-1} + \vec{t}_{j+1}) - \frac{1}{12}(\vec{t}_{j-2} + \vec{t}_{j+2})\right), \tag{2.38}$$

where on the righthand side of (2.38) we define $\vec{t}_j = (\vec{t}_j^{\,n} + \vec{t}_j^{\,n+1})$. Equation (2.38) is obtained by replacing the second order approximation of the second derivative in (2.2) by the fourth order approximation.

We solve equation (2.38) by using a modified version of (2.25); the modification being that we replace the second term in the cross product of (2.25) by the second term in the cross product of equation (2.38). This replacement results only in a redefinition of the vector $\vec{b}$ in equation (2.21). The method for solving (2.38) is then identical to that for solving (2.2), once these replacements have been made. Similarly the proof contained in equations (2.26)-(2.30) can be carried over to the present case with the previously mentioned modification. We obtain an existence and uniqueness result for the solution to (2.38) provided that

$$\frac{\Delta t}{\Delta s^2} < \frac{12}{17} \,. \tag{2.39}$$

Condition (2.39) is only slightly more restrictive than that one obtained for the solution to (2.2).

Solutions of (2.38) share two important properties with solutions of (2.2) Solutions of equation (2.38) satisfy equations (2.3) and (2.4), and thus we have immediately that scheme (2.38) is stable in the $\mathbf{H}_0^0$ norm, defined in equation (2.31). Equation (2.5) is not satisfied a priori by solutions of (2.38), however, and thus (2.38) is not a priori $\mathbf{H}_0^1$ stable.

We have done no calculations using (2.38), but foresee no problems in using the scheme. The important advantage of using (2.38) over (2.2) is that the overall error of solutions obtained from (2.38) should be fourth order, that is

$$E \leq k\,(\Delta s\,)^4 \,.$$

and furthermore for a given Δs the computational effort required to solve (2.38) is approximately the same as that required to solve (2.2).

2.5 Summary of the Method

We conclude this chapter by summarizing the method used to solve the self-induction

equation. We approximate equation (2.1) with the finite difference equations (2.2). We then solve (2.2) by using the sequence defined in equation (2.25). Once we have solved equation (2.2) to give us an approximate tangent field, we use equations (2.11) and (2.12) to give us an approximation to the position of the vortex filament.

Chapter 3: Numerical Results for the Self-Induction Equation

In this chapter we discuss the accuracy of equation (3.1) by comparing some exact soliton solutions (1.61) with the approximate solutions. We also discuss the numerical solution of the self-similar problem given in (1.63). In chapter five we introduce an approximation which causes singularities in the vortex filaments. Locally these singularities look like the initial conditions of the self-similar problem and thus a thorough understanding of the convergence properties for this particular problem is especially important. The soliton solutions are smooth and the order of convergence is second order in time and space. The self-similar solution is singular initially and the rate of convergence is generally of lower order.

We now exhibit numerically the accuracy of scheme (3.1):

$$\vec{t}_j^{\,n+1} - \vec{t}_j^{\,n} = \frac{\Delta t}{4(\Delta s)^2}\left(\vec{t}_j^{\,n} + \vec{t}_j^{\,n+1}\right) \times \left(\vec{t}_{j-1}^{\,n} + \vec{t}_{j-1}^{\,n+1} + \vec{t}_{j+1}^{\,n} + \vec{t}_{j+1}^{\,n+1}\right) . \tag{3.1}$$

From equation (2.37), if we assume that the error, $E(\Delta s, \Delta t)$, is of the form, $E(\Delta s, \Delta t) = d(\Delta s)^2 + b(\Delta t)^2$, then following Hald and Del Prete [18] we have

$$\frac{E(\Delta s, 4\Delta t) - E(\Delta s, 2\Delta t)}{E(\Delta s, 2\Delta t) - E(\Delta s, \Delta t)} = 4 . \tag{3.2}$$

The coefficients d and b are assumed constants independent of Δs and Δt, but are a function of the particular solution under consideration.

We compare the exact solutions given by equation (1.61) to the approximate solutions calculated using equation (3.1). Our initial conditions are chosen to be exact at $t = 0$; within roundoff error there is no error due to the initial conditions. We calculate two types of error: the L_2 error, defined as

$$E_{L_2} = \left(\Delta s \sum_{j=1}^{j=N} | \vec{t}(j\,\Delta s, n\,\Delta t) - \vec{t}_j^{\,n} |^2 \right)^{1/2} ,$$

and the max error, defined as

$$E_{\max} = \max_j \; | \vec{t}(j\,\Delta s, n\,\Delta t) - \vec{t}_j^{\,n} | \; .$$

In table 3.1 we show the L_2 error and the ratio given in equation (3.2). The parameters ν and τ in the table refer to the corresponding parameters of the exact solution given by (1.61).

We see that for a fixed Δs and for small Δt, equation (3.2) is satisfied. When we calculate the error for other values of Δs, ν, and τ, we find similar results to those given in table 3.1, for the max norm as well as the L_2 norm. Thus we conclude that the error has the form:

$$E = a + b(\Delta t)^2 , \tag{3.3}$$

where a and b are functions of Δs.

In order to determine the dependence of the error on Δs, we assume that the error has the form given by equation (3.3) and calculate the corresponding values of a and b. Table 3.2 shows the values of the parameters a and b calculated for the L_2 error, while table 3.3 shows the corresponding data for the max error. Both errors are calculated for three different values of ν and τ. If a is proportional to $(\Delta s)^2$, then the ratio given in the last columns of tables 3.2 and 3.3 should equal 4. We see that this is the case as $\Delta s \rightarrow 0$. This can also be seen in figures 3.1 and 3.2, where we plot a versus Δs. The plotted points are those given in tables 3.2 and 3.3. The curves on the plots are straight lines corresponding to a function of the form $f(\Delta s) = k_0(\Delta s)^2$, where k_0 is a constant independent of Δs.

Th· parameter b is not independent of Δs, but is a decreasing function of Δs. Thus if we define $k_1 = b(0)$, that is take k_1 to be the value of b at $\Delta s = 0$, we find that the error E, can be written as

$$E \approx k_0(\Delta s)^2 + k_1(\Delta t)^2 , \tag{3.4}$$

where the error in (3.4) can be either the L_2 or the max error.

We now investigate the order of convergence for the self-similar problem which we discuss in chapter one. The analytical expression obtained there is written in terms of the curvature and torsion as:

$$\kappa = \frac{\kappa_0}{\sqrt{t}} , \quad \tau = \frac{s}{2t} . \tag{3.5}$$

The initial conditions for this solution are given by

$$\vec{t}(s,0) = \begin{cases} \vec{t}_+ \text{ if } s > 0 \\ \vec{t}_- \text{ if } s < 0 \end{cases} \tag{3.6}$$

where $\vec{t}_+$ and $\vec{t}_-$ are constant unit vectors. We define the angle Θ_0, between $\vec{t}_+$ and $\vec{t}_-$ by setting $\cos\Theta_0 = \vec{t}_+ \cdot \vec{t}_-$.

The parameter κ_0 is a function of Θ_0. In figure 3.3 we show calculated values of κ_0 as a function of Θ_0. The calculated values are obtained by solving equation (1.17) for the tangent field determined by the curvature and torsion given in equation (3.5). We fix κ_0 for a particular calculation and determine Θ_0 by calculating the angle between $\vec{t}(-s,t)$ and $\vec{t}(s,t)$ as s increases; since we calculate the tangent field only to a finite value of s, the tangent is still oscillating about its asymptotic value and we calculate an upper and lower bound on Θ_0. An upper and lower bound on κ_0 are plotted in figure 3.3 while the average of the two bounds is plotted in figure 3.4. The curves drawn in figures 3.3 and 3.4 are linear interpolants to the data points, which are represented by the open circles on the plots. We see that for small values of Θ_0, κ_0 is close to a linear function of Θ_0, but as $\Theta_0 \to \pi$, $\kappa_0 \to \infty$.

We now make a detailed comparison of the exact solution with $\Theta_0 = \pi/2$, which corresponds to $\kappa \approx 0.4697$, to the approximate solution obtained from equation (3.1). It should be remembered that equation (3.5) represents a self-similar solution to equation (1.8), and thus for a fixed ratio $\lambda = \Delta t / \Delta s^2$ we obtain a single sequence of approximate solutions independent of Δt. This sequence can be viewed as approximating the curve at a fixed time, T, by scaling Δt and Δs so that after n time steps we have $T = n\,\Delta t$, and $\Delta s = (\Delta t / \lambda)^{1/2}$; or the sequence can be viewed as approximating the curve for times $T = n\,\Delta t$ by keeping Δt fixed. We discuss the solution in both ways at different times, but it should be emphasized that the approximate solution is only a function of the number of time steps n, and the ratio $\lambda = \Delta t / \Delta s^2$.

In chapter one we noted that curvature along the curve given by equation (3.6) is propagated instantaneously to $s = \infty$. Since equation (3.1) is implicit it is not apparent a priori at what rate the numerical solution will be propagated. If the numerical solution were

propagated instantaneously to the boundary, it would be difficult to specify boundary conditions. It turns out, however, that the numerical data travel with a finite speed and thus it is sufficient to specify the fixed boundary conditions of $\vec{t}_+$ or $\vec{t}_-$ at the corresponding ends of the approximate solution.

In figures 3.5, 3.6, and 3.7 we project the $s < 0$ part of the calculated solution onto the $y-z$ plane. Initially the curve coincides with the positive parts of the x and y axes. In figure 3.5 the number of time steps n, is 400, in figure 3.6 $n = 800$, and in figure 3.7 $n = 1200$. In these figures the finite propagation speed is apparent in that the oscillations stop at a finite distance from the origin rather than continuing to $s = \infty$.

The finite propagation speed is even more apparent when we look at the curvature and the torsion of the approximate solution as a function of arclength s. In figure 3.8 we plot the curvature of the approximate solution versus the arclength of the curve; note that the origin has been translated so that it is located at $s = 1000.0$. The straight line represents what the exact value of the curvature should be. The shaded portion of the plot is produced by the rapid oscillation of the curvature about the exact value; the same phenomena is observed in figure 3.9 where we plot the torsion as a function of the arclength. Once again the straight line in 3.9 represents the exact solution. We note that the curvature and the torsion represent derivatives of the tangent and thus for a singular solution we do not find it surprising that they do not converge to the exact answer in the L_2 or max norm. The data seems to indicate that they are converging in a weaker topology.

In figures 3.10 and 3.11 we again plot the curvature for the same initial conditions as those of figure 3.8; the difference is that in figure 3.8, $\lambda = 1/8$ whereas in figures 3.10 and 3.11, $\lambda = 1/2$. We see that the speed of propagation of the data is not significantly different between the two although λ changes by a factor of 4. We also see from figures 3.10 and 3.11 that the rate is constant in time.

In figures 3.8 through 3.10 the boundary vectors are kept fixed at their initial values, however, because of the finite propagation speed of the data along the curve, the approximate solutions are no different than if the boundary conditions had been kept fixed at $|s| = \infty$. The boundary condition at $-\infty$ is $\vec{t}(-\infty) = (0,-1,0)$ and the boundary condition at $+\infty$ is $\vec{t}(\infty) = (1,0,0)$. An inefficient way of maintaining the boundary at infinity is to start with a large number of vectors initially and continue the calculation until the data reach the boundary. A more efficient method is to start with a small number of vectors initially, say 400, and at each time step add an additional vector to each boundary. This method works well since the calculation propagates outward at an constant rate.

We now compare the exact with the approximate self-similar solution. In figure 3.12 we show the projection of the exact and approximate solutions onto the $y-z$ plane. We see the two curves coincide near the origin, but the approximate solution becomes inaccurate as s increases.

We calculate the L_2 and the max error over several finite intervals of the curve in order to ascertain the rate of convergence to the exact solution. We calculate the errors at time $t = 1.0$. First we calculate the L_2 difference between the initial curve and the curve at time $t = 1.0$; this value gives an upper bound to the L_2 error of the approximate solution. Numerically integrating the self-similar solution, we find that

$$\int_0^\infty |\vec{t}(s,1) - \vec{t}_+|^2 ds \approx 1.00 ,$$

where $\vec{t}(s,1)$ is the self-similar solution with $\Theta_0 = \pi/2$, $\kappa_0 \approx 0.4697$. In figure 3.13 we plot $|\vec{t}(s,1) - \vec{t}_+|$ versus arclength for the exact solution. This plot indicates the behaviour of the exact solution as $s \to \infty$. From figure 3.13 we see that $|\vec{t}(s,1) - \vec{t}_+|$ is proportional to s^{-2} for $s > 10$.

In figures 3.14 to 3.17, we show the L_2 error calculated over four intervals. The error is a symmetric function of the arclength and so we only consider the error in the $s > 0$ por-

tion of the curve. The plots are obtained by scaling Δt after each n so that $n\,\Delta t = 1$ and $\Delta s = (\Delta t/\lambda)^{1/2}$; then the errors are calculated and plotted as a function of Δs. The jagged line results from connecting the data points by straight lines. As n becomes larger, the data points become more closely spaced.

The curves in figures 3.14 to 3.17 are characterized by a slowly decreasing portion for larger Δs and a more rapidly decreasing portion as Δs decreases. The shoulder in the plots is the point at which the calculated oscillations have filled the interval of concern. Extrapolating from the calculated errors, it appears that if we were to calculate the L_2 error over the whole interval $0 \leq s \leq \infty$, the error would be proportional to a power of Δs less than one. From figure 3.17 the power would be approximately 1/2. That is for the error calculated over the whole curve we would have that $E_{L_2} \leq c\,\Delta s^{1/2}$. For a finite interval, the error is proportional to a higher power of Δs. From figures 3.14, 3.15 and 3.16 it appears that the error is proportional to Δs as $\Delta s \to 0$.

In figure 3.18 we show the maximum error in the interval $0 \leq s \leq 20$. The interesting thing to notice about the maximum error is that there are intervals over which the error increases as Δs decreases. This is due to the fact that both the exact and approximate solutions spiral about the y-axis and at certain points the spirals in the approximate solution are out of phase with those of the exact solution. For an example of this see figure 3.12, remembering that the plot is a projection of a curve in three dimensions.

Table 3.1

L2 Error in the Soliton Solution

Time $= 1.0 \quad \nu = 0.1 \quad \tau = 1.0 \quad \Delta s = 1.0$

Δt	Error, $E(\Delta t)$	$\frac{E(4\Delta t) - E(2\Delta t)}{E(2\Delta t) - E(\Delta t)}$
1.0	0.1302003073	-
0.5	0.0906754398	-
0.25	0.0795215364	3.54
0.125	0.0766410320	3.87
0.0625	0.0759149562	3.97
0.03125	0.0757331126	3.99
0.015625	0.0756875571	3.99
0.0078125	0.0756761792	4.00

Table 3.2

L2 Error in the Soliton Solution

$$E(\Delta t) = a + b(\Delta t)^2$$

Time = 1.0 $\nu = 0.1$ $\tau = 1.0$

Δs	a	b	$\frac{a(2\Delta s)}{a(\Delta s)}$
1.0	7.567×10^{-2}	0.0621	-
0.5	1.944×10^{-2}	0.0764	3.89
0.25	4.892×10^{-3}	0.0804	3.97
0.125	1.225×10^{-3}	0.0801	3.99
Time = 0.125 $\nu = 0.2$ $\tau = 4.0$			
0.5	1.838×10^{-1}	4.58	-
0.25	5.155×10^{-2}	10.61	3.57
0.125	1.323×10^{-2}	12.92	3.90
0.0625	3.330×10^{-3}	13.56	3.97
Time = 0.125 $\nu = 0.1$ $\tau = 4.0$			
0.5	1.290×10^{-1}	3.24	-
0.25	3.612×10^{-2}	7.41	3.57
0.125	9.269×10^{-3}	8.98	3.90
0.0625	2.332×10^{-3}	9.42	3.97

Table 3.3

Max Error in the Soliton Solution

$E(\Delta t) = \mathrm{a} + \mathrm{b}(\Delta t)^2$

Time $= 1.0 \quad \nu = 0.1 \quad \tau = 1.0$

Δs	a	b	$\frac{a(2\Delta s)}{a(\Delta s)}$
1.0	1.717×10^{-2}	0.0142	-
0.5	4.417×10^{-3}	0.0177	3.89
0.25	1.112×10^{-3}	0.0187	3.97
0.125	2.785×10^{-4}	0.0199	3.99
Time $= 0.125 \quad \nu = 0.2 \quad \tau = 4.0$			
0.5	5.818×10^{-2}	1.44	-
0.25	1.637×10^{-2}	3.38	3.55
0.125	4.203×10^{-3}	4.12	3.89
0.0625	1.058×10^{-3}	4.34	3.97
Time $= 0.125 \quad \nu = 0.1 \quad \tau = 4.0$			
0.5	2.886×10^{-2}	0.72	-
0.25	8.085×10^{-3}	1.66	3.57
0.125	2.075×10^{-3}	2.01	3.90
0.0625	5.220×10^{-4}	2.12	3.98

figure 3.1

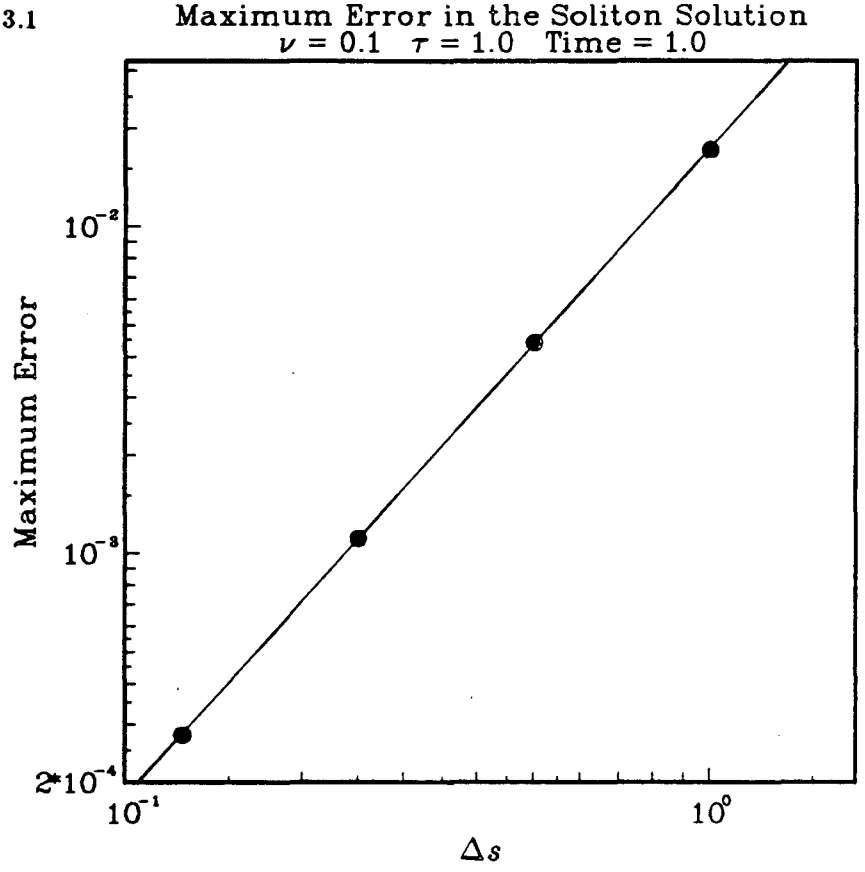
Maximum Error in the Soliton Solution
ν = 0.1 τ = 1.0 Time = 1.0
Maximum Error
10^{-2}
10^{-3}
$2*10^{-4}$
10^{-1}
10^{0}
Δs

figure 3.2

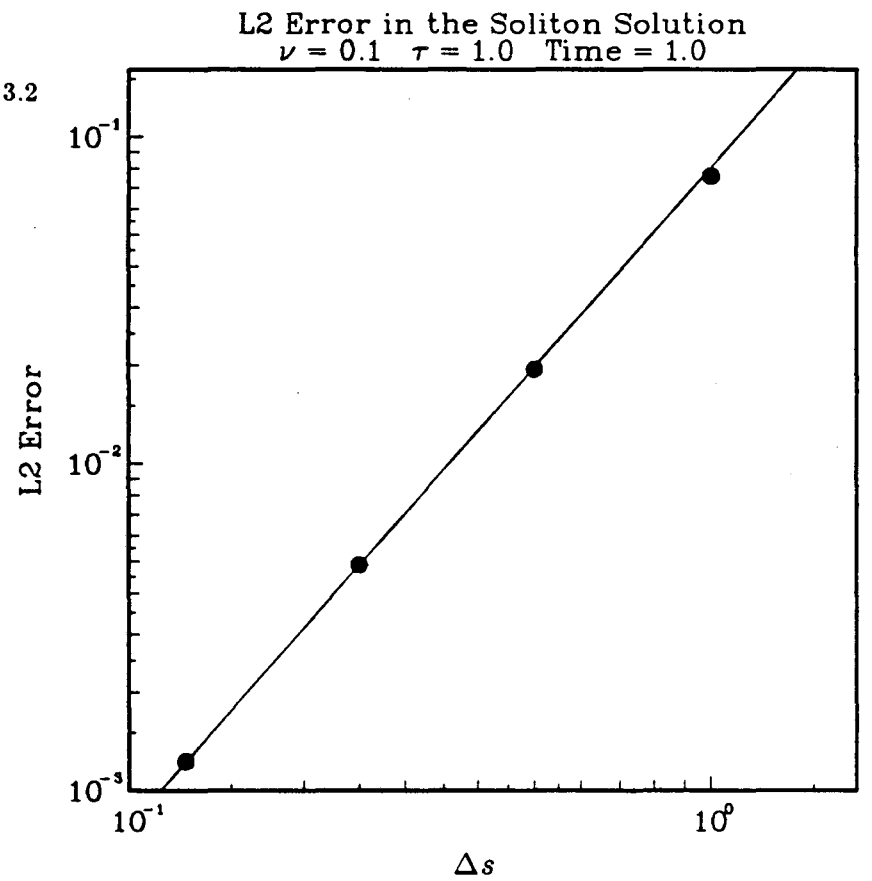
L2 Error in the Soliton Solution
$\nu = 0.1 \quad \tau = 1.0 \quad$ Time = 1.0
L2 Error
10^{-1}
10^{-2}
10^{-3}
10^{-1}
10^{0}
Δs

figure 3.3

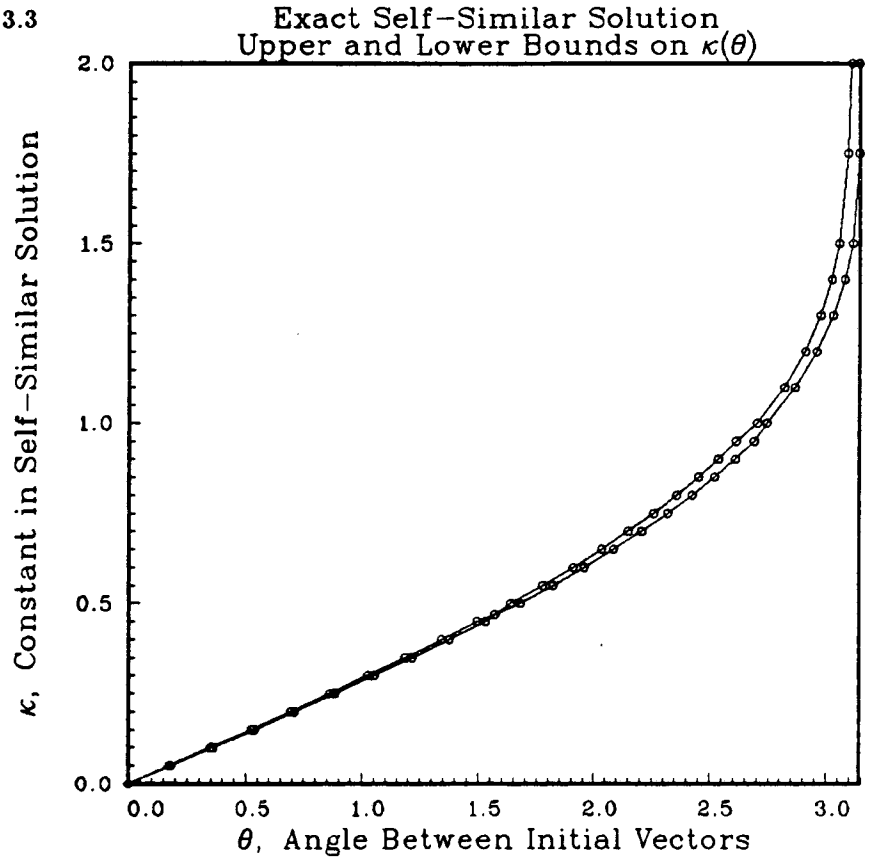
Exact Self−Similar Solution
Upper and Lower Bounds on $\kappa(\theta)$
2.0
1.5
1.0
0.5
0.0
κ, Constant in Self−Similar Solution
0.0
0.5
1.0
1.5
2.0
2.5
3.0
θ, Angle Between Initial Vectors

figure 3.4

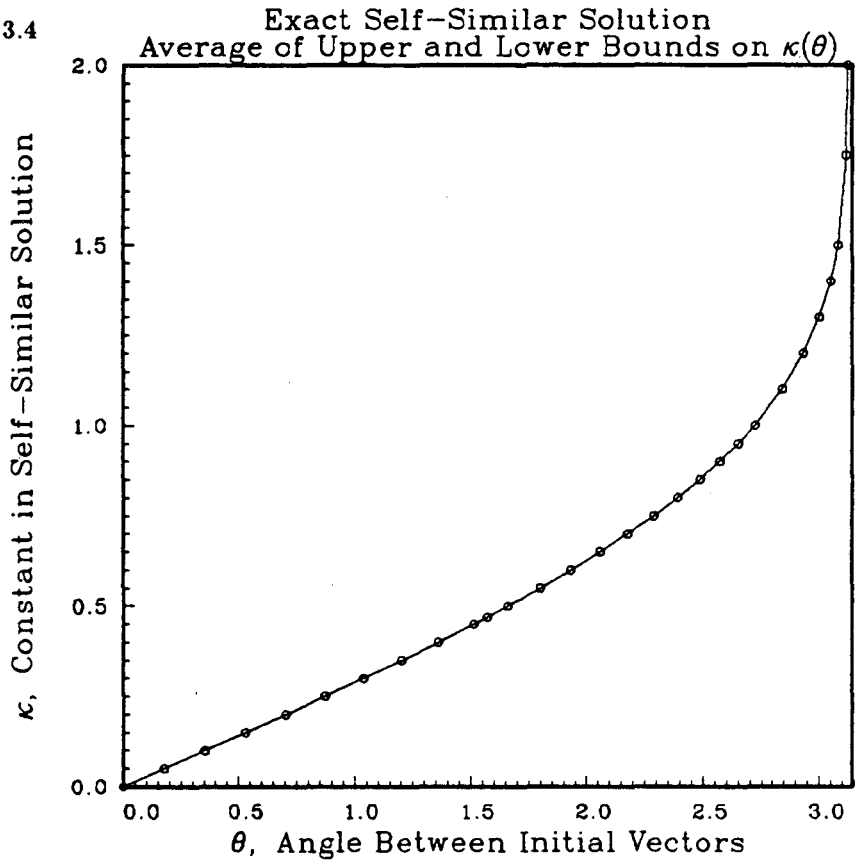
Exact Self−Similar Solution
Average of Upper and Lower Bounds on $\kappa(\theta)$
κ, Constant in Self−Similar Solution
2.0
1.5
1.0
0.5
0.0
0.0
0.5
1.0
1.5
2.0
2.5
3.0
θ, Angle Between Initial Vectors

figure 3.5

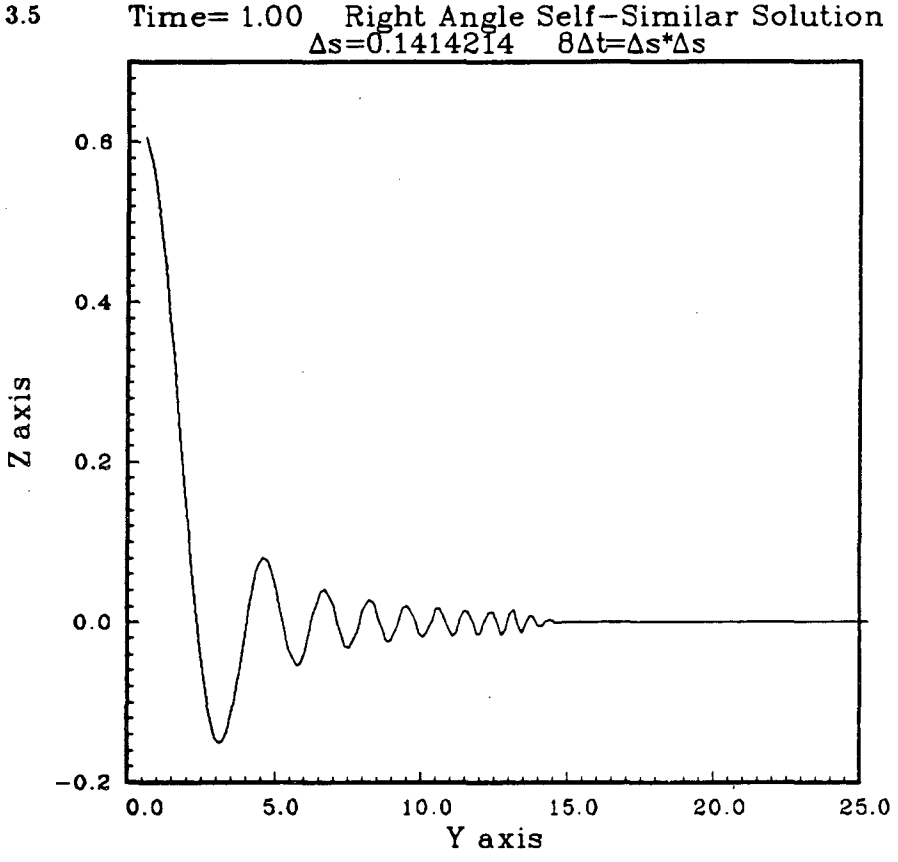
Time= 1.00 Right Angle Self-Similar Solution
Δs=0.1414214 8Δt=Δs*Δs
0.6
0.4
0.2
0.0
-0.2
Z axis
0.0
5.0
10.0
15.0
20.0
25.0
Y axis

figure 3.6

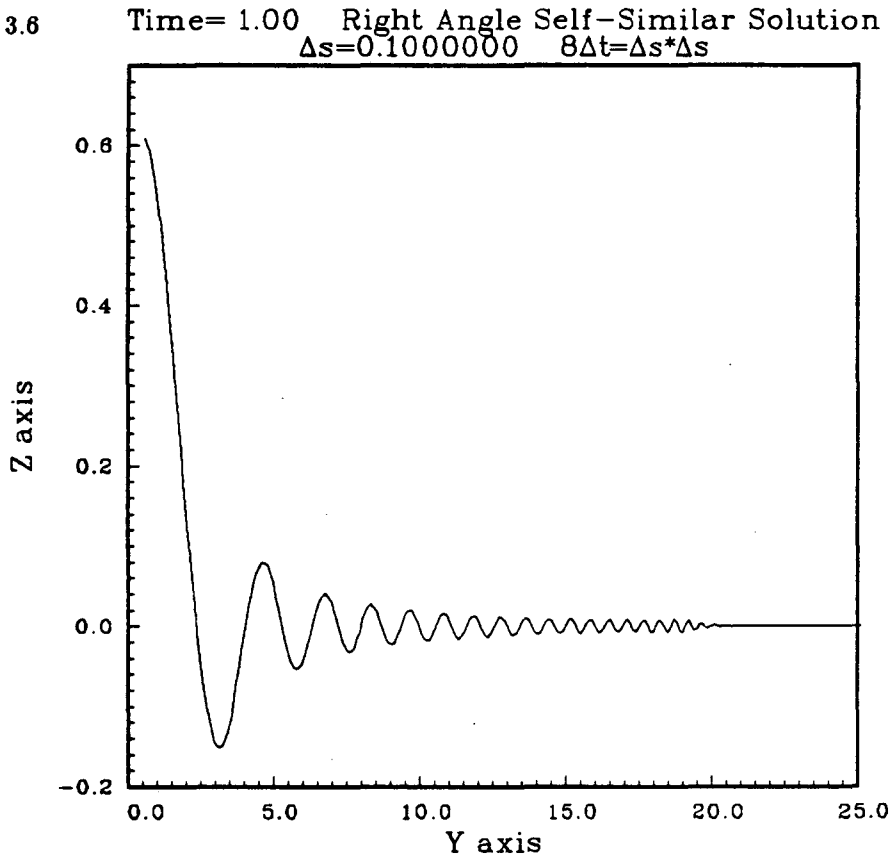
Time= 1.00 Right Angle Self-Similar Solution
Δs=0.1000000 8Δt=Δs*Δs
0.6
0.4
0.2
0.0
-0.2
Z axis
0.0
5.0
10.0
15.0
20.0
25.0
Y axis

figure 3.7

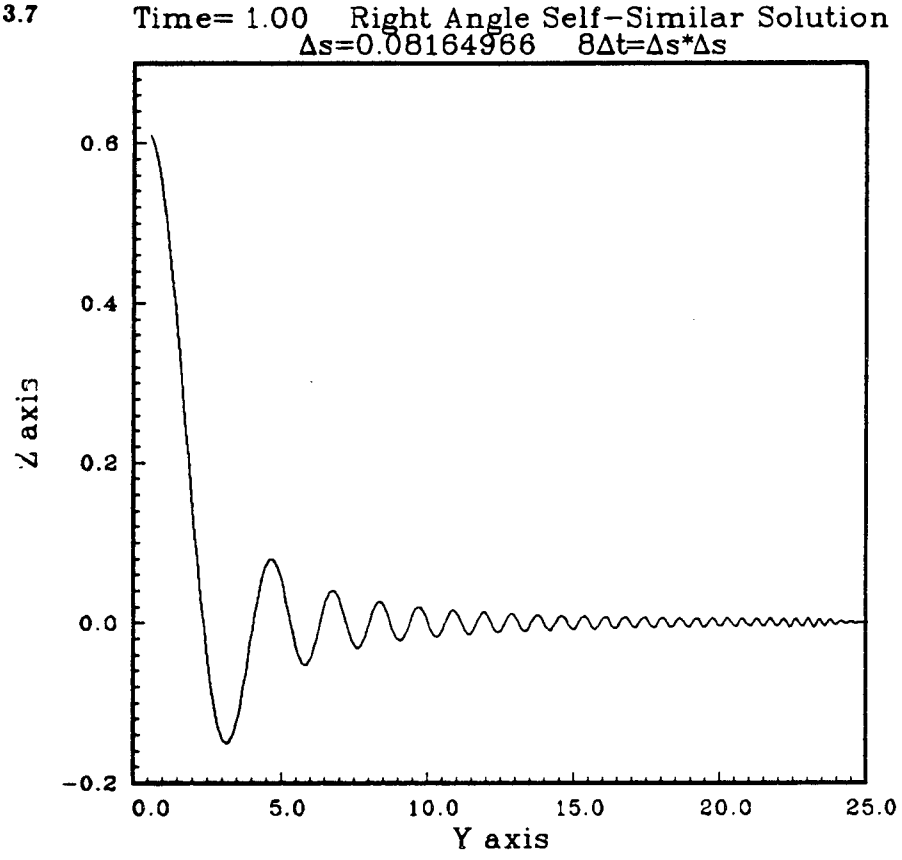
Time= 1.00 Right Angle Self-Similar Solution
Δs=0.08164966 8Δt=Δs*Δs
0.6
0.4
0.2
0.0
-0.2
Z axis
0.0
5.0
10.0
15.0
20.0
25.0
Y axis

figure 3.8

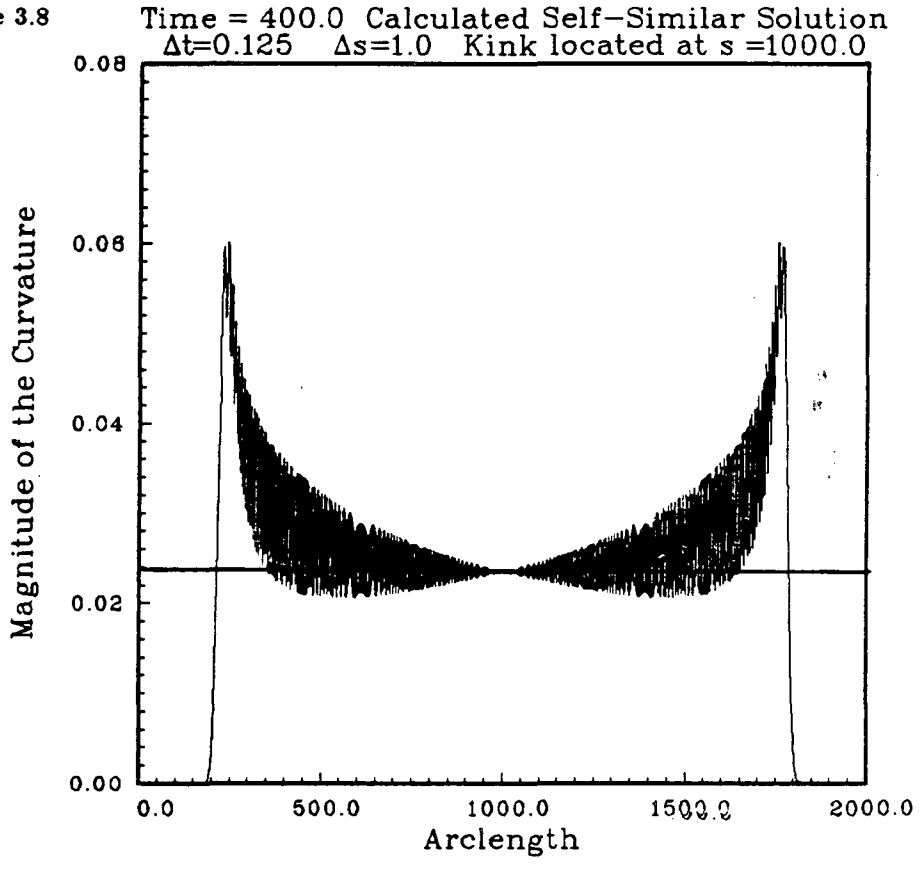
Time = 400.0 Calculated Self−Similar Solution
Δt=0.125 Δs=1.0 Kink located at s =1000.0
Magnitude of the Curvature
0.08
0.06
0.04
0.02
0.00
0.0
500.0
1000.0
1500.0
2000.0
Arclength

figure 3.9

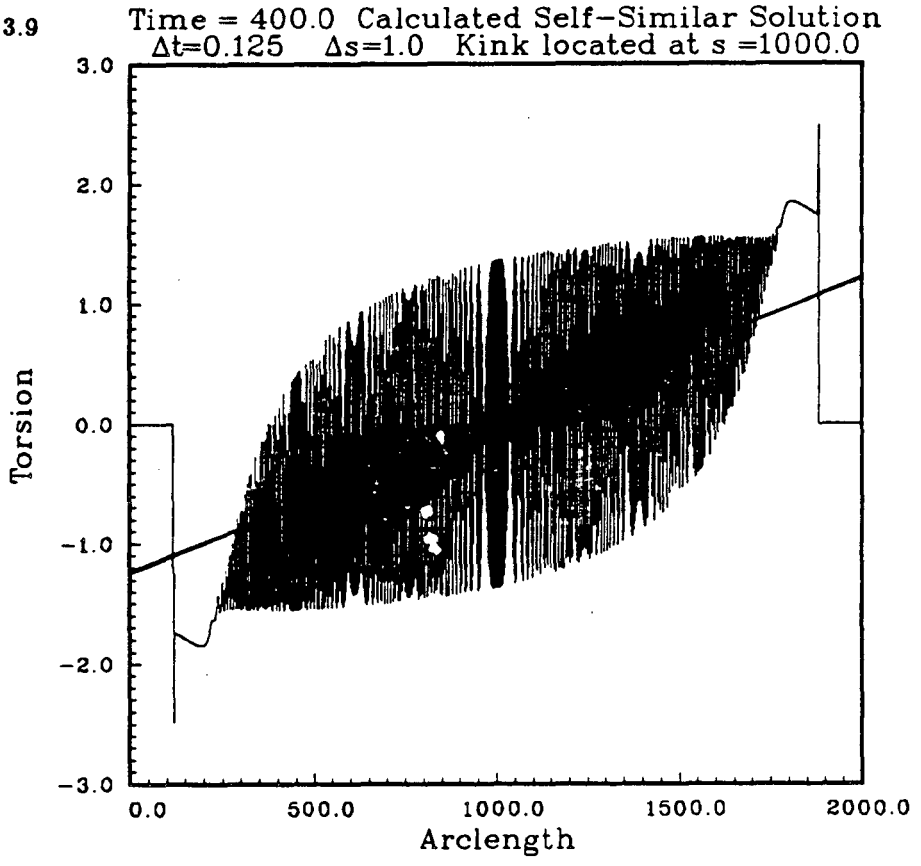
Time = 400.0 Calculated Self−Similar Solution
Δt=0.125 Δs=1.0 Kink located at s =1000.0
3.0
2.0
1.0
0.0
−1.0
−2.0
−3.0
Torsion
0.0
500.0
1000.0
1500.0
2000.0
Arclength

figure 3.10

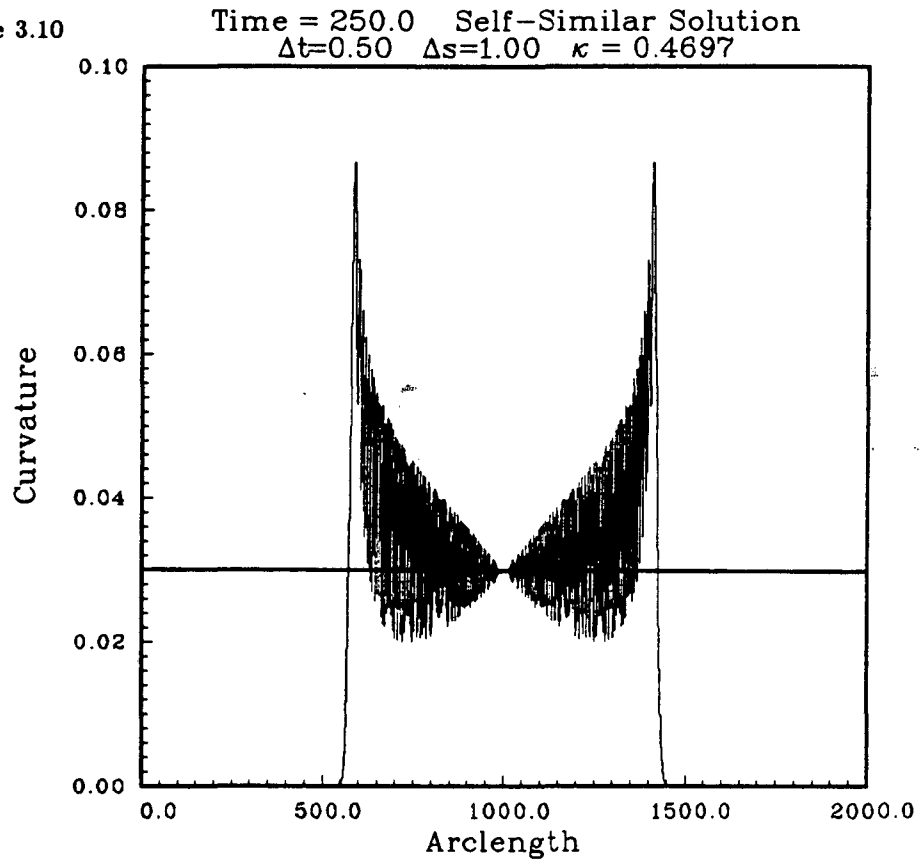
Time = 250.0 Self-Similar Solution
Δt=0.50 Δs=1.00 κ = 0.4697
0.10
0.08
0.06
0.04
0.02
0.00
Curvature
0.0
500.0
1000.0
1500.0
2000.0
Arclength

figure 3.11

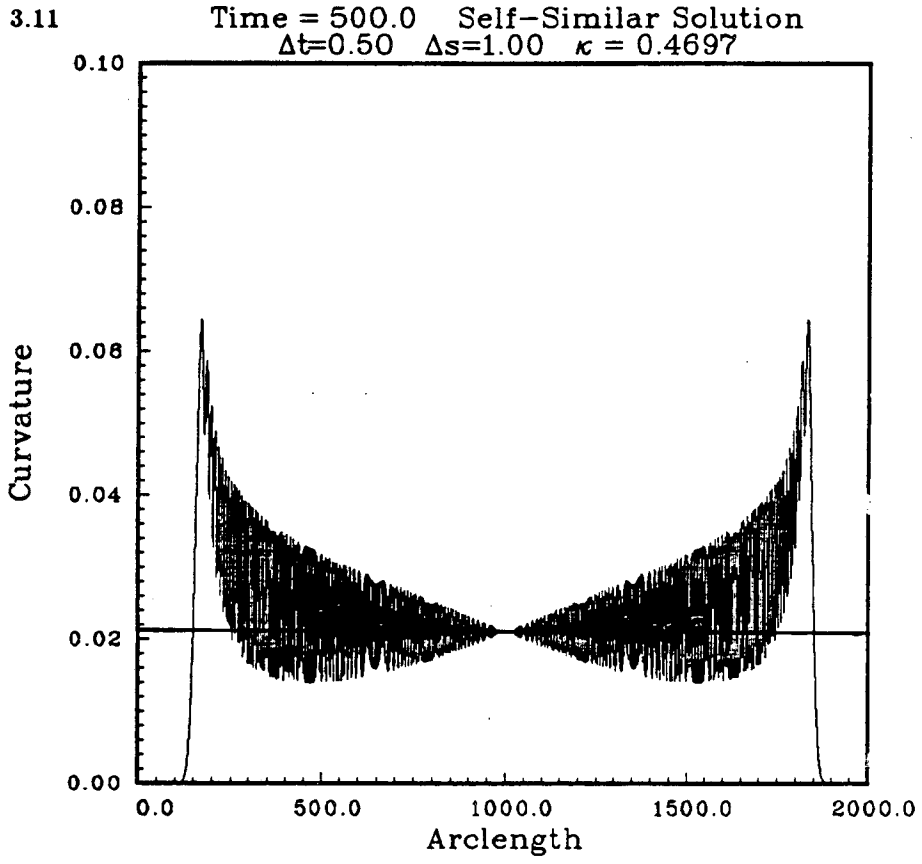
Time = 500.0 Self−Similar Solution
Δt=0.50 Δs=1.00 κ = 0.4697
0.10
0.08
0.06
0.04
0.02
0.00
Curvature
0.0
500.0
1000.0
1500.0
2000.0
Arclength

figure 3.12

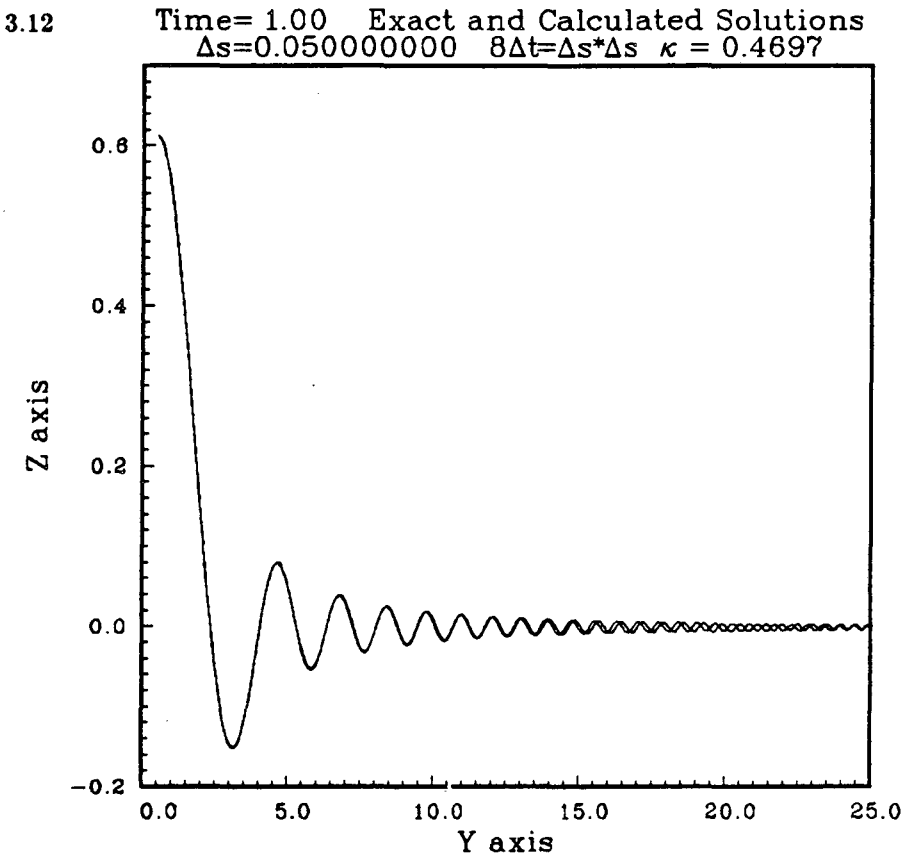
Time= 1.00 Exact and Calculated Solutions
Δs=0.050000000 8Δt=Δs*Δs κ = 0.4697
0.6
0.4
0.2
0.0
−0.2
Z axis
0.0
5.0
10.0
15.0
20.0
25.0
Y axis

figure 3.13

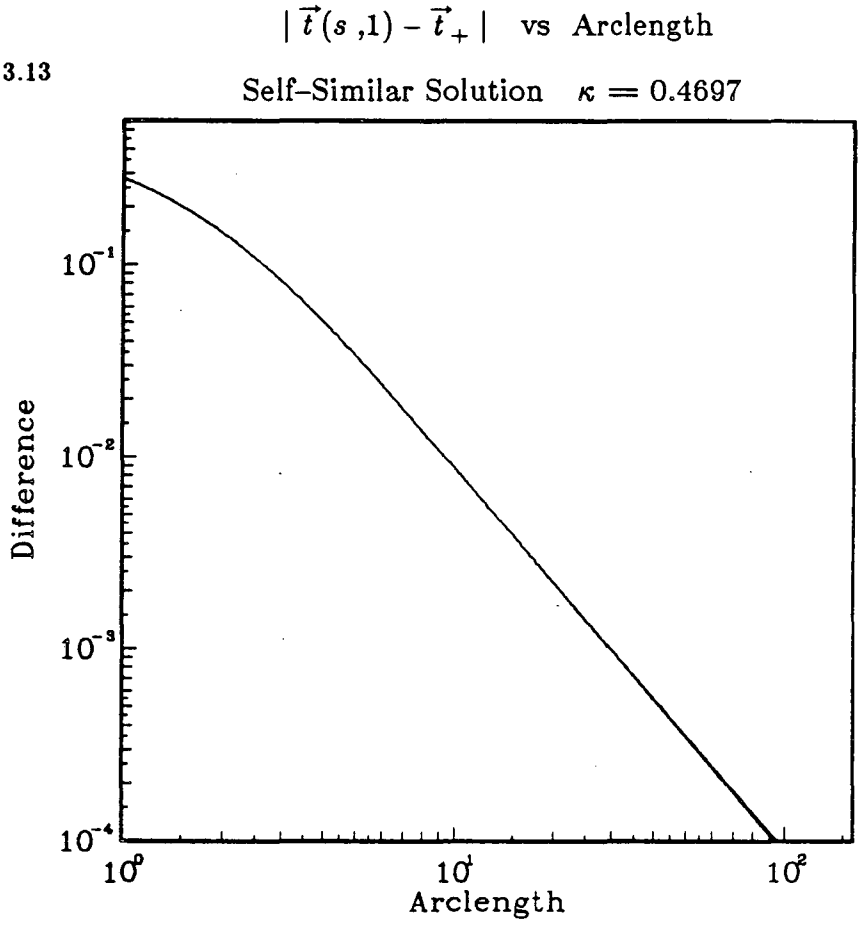
$|\vec{t}(s,1) - \vec{t}_+|$ vs Arclength
Self–Similar Solution $\kappa = 0.4697$
Difference
10^{-1}
10^{-2}
10^{-3}
10^{-4}
10^{0}
10^{1}
10^{2}
Arclength

figure 3.14

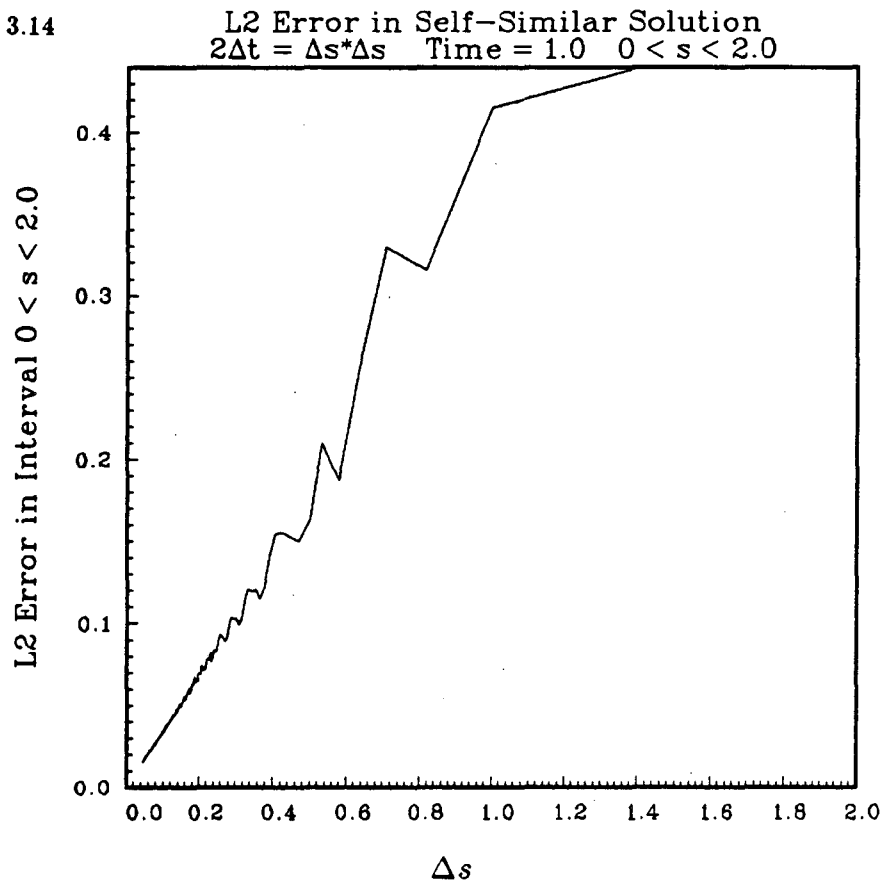
L2 Error in Self−Similar Solution
2Δt = Δs*Δs Time = 1.0 0 < s < 2.0
L2 Error in Interval 0 < s < 2.0
0.0
0.1
0.2
0.3
0.4
0.0 0.2 0.4 0.6 0.8 1.0 1.2 1.4 1.6 1.8 2.0
Δs

figure 3.15

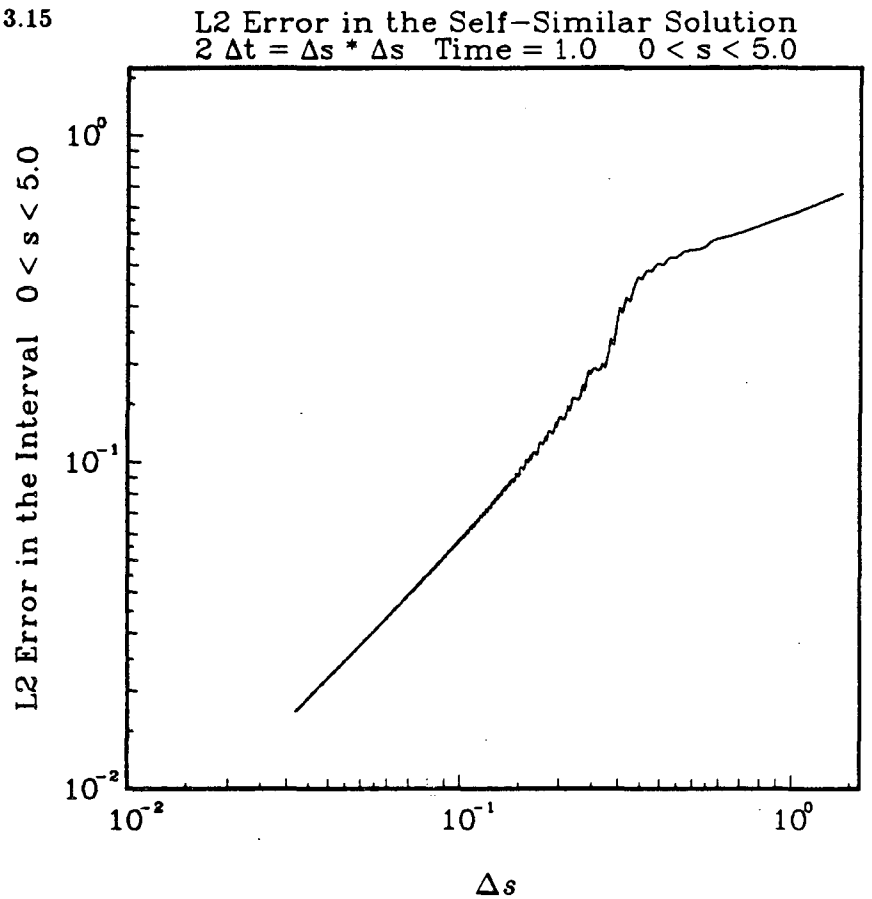
L2 Error in the Self−Similar Solution
2 Δt = Δs * Δs Time = 1.0 0 < s < 5.0
L2 Error in the Interval 0 < s < 5.0
10^0
10^-1
10^-2
10^-2
10^-1
10^0
Δs

figure 3.16

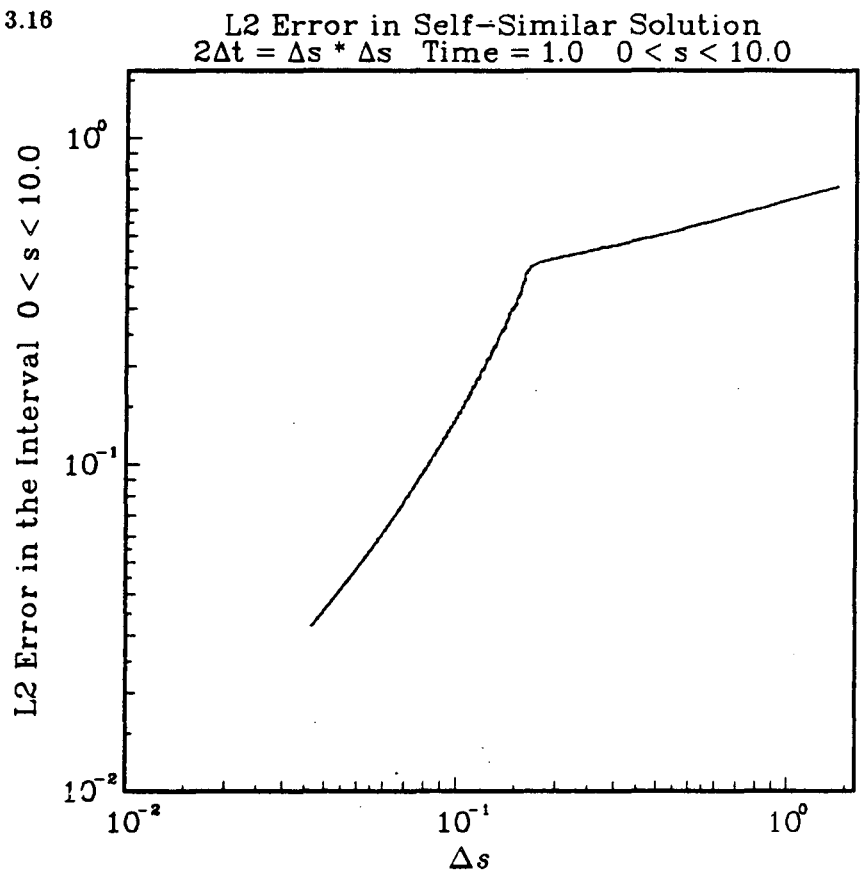
L2 Error in Self-Similar Solution
2Δt = Δs * Δs Time = 1.0 0 < s < 10.0
L2 Error in the Interval 0 < s < 10.0
10^0
10^-1
10^-2
10^-2
10^-1
10^0
Δs

figure 3.17

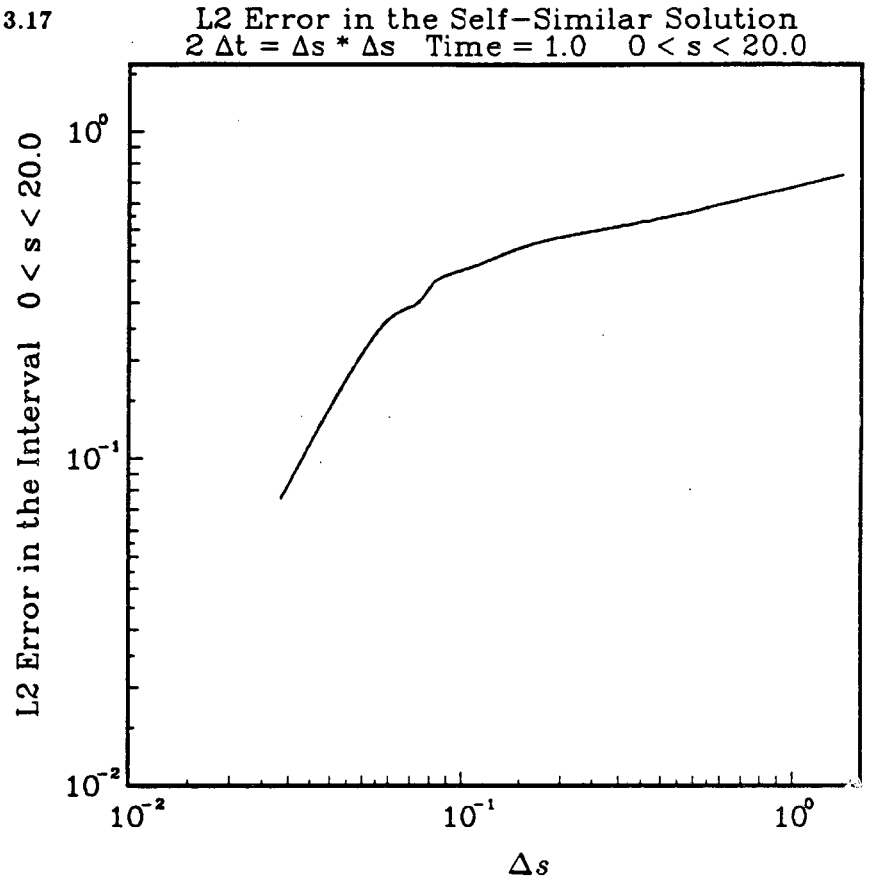
L2 Error in the Self−Similar Solution
2 Δt = Δs * Δs Time = 1.0 0 < s < 20.0
L2 Error in the Interval 0 < s < 20.0
10^0
10^-1
10^-2
10^-2
10^-1
10^0
Δs

figure 3.18

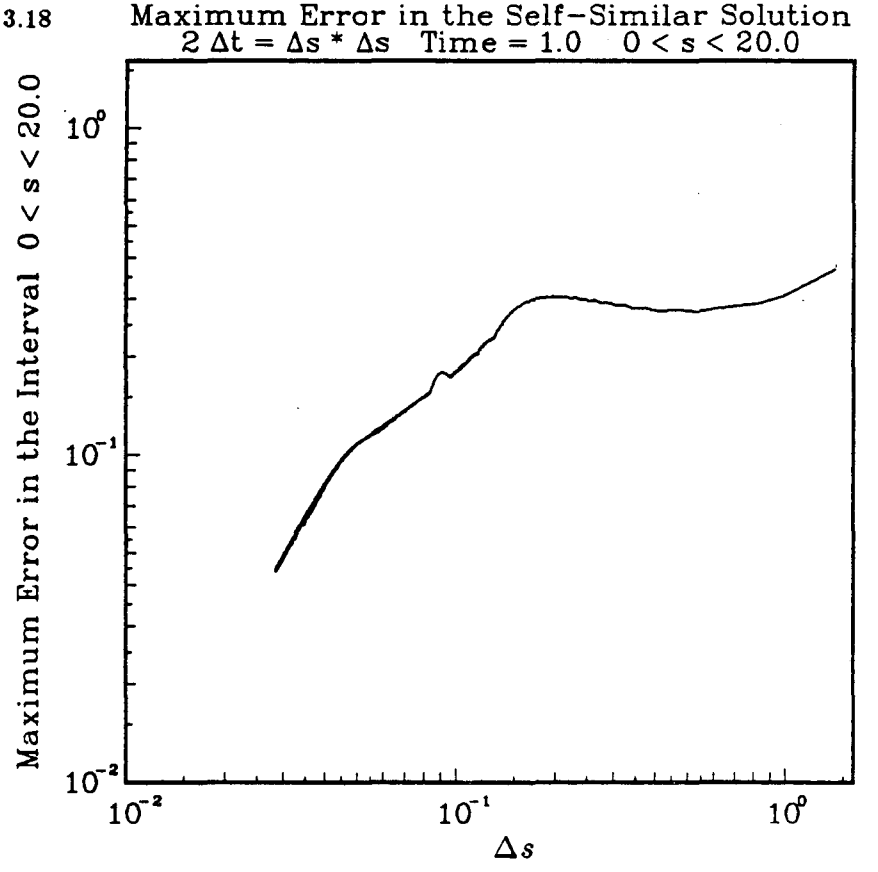
Maximum Error in the Self-Similar Solution
2 Δt = Δs * Δs Time = 1.0 0 < s < 20.0
Maximum Error in the Interval 0 < s < 20.0
10^0
10^-1
10^-2
10^-2
10^-1
10^0
Δs

Chapter 4: Self-Induction Plus Stretching for Superfluid Helium

In this chapter we present a brief introduction to superfluid Helium and to the two fluid model used to describe the fluid dynamics of the liquid. We then present a set of equations which approximate the evolution of a superfluid vortex. We present some properties of the evolution equation and some exact solutions of the equation.

Helium becomes liquid at a temperature of 4.2 °K under one atmosphere of pressure. Liquid Helium becomes superfluid at a temperature of 2.17 °K. Above 2.17 °K liquid Helium behaves like an ordinary fluid; below 2.17 °K it exhibits extraordinary properties which an ordinary fluid does not.

One of the many remarkable properties of the superfluid is that it can flow with no apparent viscosity; it can flow through small capillaries (10^{-4} cm) with no observable energy dissipation. Another property unique to superfluids is that the liquid responds to gradients in the chemical potential and not simply gradients in the pressure; thus both temperature and pressure drive the superfluid. An interesting consequence of this is the fact that heat does not diffuse through the fluid, but propagates through the fluid as a wave with a definite speed.

The many remarkable properties of superfluid Helium led people to realize that the fluid was more than just a fluid with no viscosity. It was clear that a new fluid dynamics was necessary to describe this fluid. In 1941 Landau [28] developed such a theory; it is called the two fluid model. The motivation for the theory was the fact that experiments showed that part of the fluid flowed as if it carried no entropy. Thus Landau's idea was to introduce a second velocity field in order to describe the fluid. One velocity field describes that part of the fluid which carries entropy and the other field describes that part which carries no entropy. These two velocity fields are usually denoted as $\vec{v}_n$ and $\vec{v}_s$. The n subscript denotes the normal component and the s subscript denotes the superfluid component. The other information necessary for the development of the theory is the experimental observa-

tion that the superfluid velocity $\vec{v}_s$ is driven by a gradient in the chemical potential rather than simply by a gradient in the pressure [25]. These observations, along with the usual conservation laws, (mass, momentum, and energy) allow for the development of the two fluid model of superfluids. For an introduction to the two fluid model of superfluids see [26,29,34]. We follow closely the presentation given in Putterman [34].

4.1 The Two Fluid Equations

We give a brief presentation of the two fluid model with no dissipation taken into account; that is, we present the two fluid equations which are analgous to the Euler equation. The first equation is obtained by requiring that mass be conserved. It is the same continuity equation as that obtained for an ordinary fluid:

$$\frac{\partial \rho}{\partial t} + \nabla\cdot(\rho\vec{v}) = 0 \ . \tag{4.1}$$

In equation (4.1) ρ is the density of the fluid and $\vec{v}$ is the real velocity of the fluid, that is the velocity giving the rate of particle motion. The second equation results from the requirement that entropy be conserved and that it be transported with velocity $\vec{v}_n$. We have

$$\frac{\partial \rho s}{\partial t} + \nabla\cdot(\rho s\vec{v}_n) = 0 \ , \tag{4.2}$$

where s is the entropy per unit mass. The velocities $\vec{v}$ and $\vec{v}_n$ are independent; the first specifies the motion of the total mass and the second specifies the motion of the part of the mass carrying the entropy. Associated with this velocity $\vec{v}_n$, is the density of fluid ρ_n, moving with this velocity. From these quantities we define the corresponding quantities ρ_s and $\vec{v}_s$, associated with the superfluid component by requiring that

$$\rho = \rho_n + \rho_s \ ,$$

and

$$\vec{J} \equiv \rho\vec{v} = \rho_n \vec{v}_n + \rho_s \vec{v}_s \ . \tag{4.3}$$

The next equation is a statement of the fact that the chemical potential drives the superfluid:

$$\frac{\partial \vec{v}_s}{\partial t} + (\vec{v}_s \cdot \nabla)\vec{v}_s = -\nabla\mu \ , \tag{4.4}$$

where μ is the chemical potential. In an ordinary material the chemical potential is related to the temperature T and pressure p by the expression:

$$d\,\mu = \frac{1}{\rho} dp - s dT \ . \tag{4.5}$$

The final equation is a statement of the conservation of momentum:

$$\frac{\partial \vec{J}}{\partial t} + \nabla \cdot \mathbf{P} = 0 \ . \tag{4.6}$$

The momentum flux $\vec{J}$, is defined in equation (4.3). The stress tensor $\mathbf{P}$, is defined in the same way as it is for an ordinary fluid. Taking into account the fact that we have two independent velocity fields, we have

$$(\mathbf{P})_{ij} = p\,\delta_{ij} + \rho_n\, v_{n,i}\, v_{n,j} + \rho_s\, v_{s,i}\, v_{s,j} \ ,$$

where δ_{ij} is the Kronecker delta.

Equations (4.1), (4.2), (4.4), and (4.6) are the Landau two fluid equations. They are eight independent scalar equations for the eight independent quantities ρ, s, $\vec{v}_n$ and $\vec{v}_s$ which describe the flow of the superfluid. We also need thermodynamic relations for determining ρ_n, p, and μ in terms of the eight independent quantities. These thermodynamic quantities are not only functions of the entropy s, and density ρ, but also are functions of the quantity $(\vec{v}_n - \vec{v}_s)^2$. The quantity $(\vec{v}_n - \vec{v}_s)^2$ is chosen as an independent variable since it is a scalar which is invariant under rotations and Galilean transformations. It can be shown that the expression analagous to equation (4.5), but correct for superfluids takes the form:

$$d\,\mu = \frac{1}{\rho} dp - s dT - \frac{1}{2}\frac{\rho_n}{\rho} d\,(\vec{v}_n - \vec{v}_s)^2 \ . \tag{4.7}$$

We now make some simplifying assumptions about the two fluid equations in order to obtain a simpler set of equations. The first assumption that we make is that the quantity $\rho s / \rho_n$ is a constant. This assumption states that entropy per unit volume is proportional to the normal fluid density. Between the temperatures of 2.17 °K and 1.7 °K $\frac{\rho s}{\rho_n}$ changes by

less than 10 percent, whereas s changes by a factor of 4 . Applying this assumption to equation (4.2) implies:

$$\frac{\partial \rho_n}{\partial t} + \nabla\cdot(\rho_n \vec{v}_n) = 0 \ . \tag{4.8}$$

Equations (4.8) and (4.1) then imply that

$$\frac{\partial \rho_s}{\partial t} + \nabla\cdot(\rho_s \vec{v}_s) = 0 \ . \tag{4.9}$$

Thus we have that each component of the superfluid satisfies its own continuity equation. If we use some basic calculus vector identities we obtain:

$$\begin{aligned} &\frac{\partial \rho \vec{v}}{\partial t} + \nabla\cdot(\rho \vec{v}\vec{v}) \\ &= \vec{v}\left(\frac{\partial \rho}{\partial t} + \nabla\cdot(\rho \vec{v})\right) + \rho\frac{\partial \vec{v}}{\partial t} + \rho(\vec{v}\cdot\nabla)\vec{v} \ . \end{aligned} \tag{4.10}$$

Note that the first term in parentheses on the right side of (4.10) is in the form of the continuity equation (4.1). Thus if we substitute equation (4.10) along with equations (4.8) and (4.9), into equation (4.6) we obtain:

$$\rho_n \frac{D_n \vec{v}_n}{Dt} + \rho_s \frac{D_s \vec{v}_s}{Dt} + \nabla p = 0 \ , \tag{4.11}$$

where $\frac{D_n}{Dt} \equiv \frac{\partial}{\partial t} + \vec{v}_n \cdot \nabla$ and $\frac{D_s}{Dt} \equiv \frac{\partial}{\partial t} + \vec{v}_s \cdot \nabla$. Substituting equation (4.4) into (4.11) we find:

$$\rho_n \frac{D_n \vec{v}_n}{Dt} = -\nabla p + \rho_s \nabla \mu \ .$$

If we use equation (4.7) we find:

$$\rho_n \frac{D_n \vec{v}_n}{Dt} = -\frac{\rho_n}{\rho}\nabla p - \rho_s s \nabla T - \frac{1}{2}\frac{\rho_s \rho_n}{\rho}\nabla(\vec{v}_n - \vec{v}_s)^2 \ . \tag{4.12}$$

We also rewrite equation (4.4), substituting equation (4.7), as:

$$\rho_s \frac{D_s \vec{v}_s}{Dt} = -\frac{\rho_s}{\rho}\nabla p + \rho_s s \nabla T + \frac{1}{2}\frac{\rho_s \rho_n}{\rho}\nabla(\vec{v}_n - \vec{v}_s)^2 \ . \tag{4.13}$$

Equations (4.8), (4.9), (4.12), and (4.13) are an alternate version of the two fluid equations, provided that $\rho s / \rho_n$ is constant.

If we generalize equations (4.8), (4.9), (4.12), and (4.13) to include dissipation, there are five dissipation coefficients in the linear theory. In most work the only coefficient which is explicitly included is the first viscosity coefficient η, for the normal component. If we include this single dissipation term, then equations (4.12) and (4.13) can be rewritten as [19,36]:

$$\rho_s \frac{D_s \vec{v}_s}{Dt} = -\frac{\rho_s}{\rho}\nabla p + \rho_s s \nabla T - \vec{F}_{ns} ,$$

$$\rho_n \frac{D_n \vec{v}_n}{Dt} = -\frac{\rho_n}{\rho}\nabla p - \rho_s s \nabla T + \vec{F}_{ns} + \eta \Delta \vec{v}_n .$$

The term $\vec{F}_{ns}$ is to be interpreted as being the mutual friction force per unit volume between the normal and superfluid components and it can include terms which cause dissipation. $\vec{F}_{ns}$ is the force exerted on the normal fluid by the superfluid.

4.2 Quantized Vortices

Another condition is put on the velocity $\vec{v}_s$; it is assumed that $\nabla \times \vec{v}_s = 0$ almost everywhere in the fluid. The velocity $\vec{v}_s$ is not curl free everywhere in the fluid. It was first postulated by Onsager [33], and later verified experimentally, that vortices occur in the superfluid. The circulation of the vortices in the superfluid component is quantized:

$$\int_C \vec{v}_s \cdot d\vec{l} = \frac{nh}{m} , \quad n = 1,2,3, \cdots ,$$

where the integral is a line integral taken along a closed curve C, h is Planck's constant, and m is the mass of a helium atom. The constant h/m has a value of $9.967 \times 10^{-4} \mathrm{cm}^2/\mathrm{s}$. The core diameter of these vortices has been inferred to be on the order of 10^{-8}cm. This points out another reason that equation (4.4) is chosen as it is: any velocity field which satisfies equation (4.4) satisfies the conditions necessary for Helmhotz' Theorem to hold [10]. The strength of the superfluid vortex is conserved as it evolves with the flow of the superfluid.

Because of the presence of quantized vortices in superfluid helium, the force $\vec{F}_{ns}$ is interpretted as being a drag force exerted on the quantized vortices. In order to study this force expermentally, Hall and Vinen [20] performed an experiment on a sample of uniformly

rotating helium. In their experiment they assumed that the quantized vortices were straight and parallel to the axis of rotation of the superfluid. With this assumption we can calculate a vortex line density L_0, which gives the number of quantized vortices per unit area. If we consider a cylinder of radius r, rotating with an angular velocity ω, then the circulation of the fluid just inside the cylinder is equal to $2\pi\omega r^2$. Since each quantized vortex has circulation equal to h/m, we find that there are $2\omega m/h$ quantized vortices per unit area, thus we have that $L_0 = 2\omega m/h$. If we assume that each vortex stretches the height of the cylinder, then L_0 also gives the line density, that is the total length of vortices present per unit volume. In performing the experiment it is assumed that the total length of vortices present in the system is proportional to the angular rotation rate of the bulk fluid. We see that for a rotation rate of 1 radian per second $L_0 = 2 \times 10^3 \mathrm{cm}^{-2}$.

Under the conditions of their experiment, Hall and Vinen [21] found that $\vec{F}_{ns}$ could be expressed as:

$$\vec{F}_{ns} = -\frac{B\rho_s\rho_n}{\rho\omega}\vec{\omega}\times\left(\vec{\omega}\times(\vec{v}_s - \vec{v}_n)\right) - \frac{B'\rho_s\rho_n}{\rho\omega}\vec{\omega}\times(\vec{v}_s - \vec{v}_n), \tag{4.14}$$

where B and B' are constants determined from the experiment, and $\vec{\omega}$ is the angular velocity of the rotating liquid. Equation (4.14) is obtained by considering the quantized vortex to be a solid cylinder with a circulation about the cylinder equal to h/m. (It should be noted that this interpretation of a vortex is not consistent with the fluid dynamics equations.) The cylinder is then assumed to be acted on by the Magnus force. The Magnus force per unit length $\vec{F}$, is given by [10]:

$$\vec{F} = \rho\Gamma\vec{U}\times\vec{t}, \tag{4.15}$$

where $\vec{U}$ is the velocity of the fluid relative to the cylinder, ρ is the density of the fluid, Γ is the circulation around the cylinder, and $\vec{t}$ is a unit vector parallel to the axis of the cylinder. Equation (4.15) is only valid in two dimensions or for an infinitely long cylinder, but the result is often used in three dimensions. The Magnus force is then balanced by the drag force from the normal component of the superfluid, in order to obtain the final velocity of

the cylinder. The total velocity $\vec{v}_t$, of the cylinder is defined as:

$$\vec{v}_t = \vec{v}_l + \vec{v}_{nc} \ . \tag{4.16}$$

The term $\vec{v}_l$ is the velocity the vortex would have if no drag force were present and the term $\vec{v}_{nc}$, the non-conservative velocity, is the correction to the total velocity due to the drag on the vortex. The result is [38]:

$$\vec{v}_{nc} = \frac{\rho_n B}{2\rho\omega}\vec{\omega}\times(\vec{v}_n - \vec{v}_s - \vec{v}_l) - \frac{\rho_n B'}{2\rho\omega^2}\vec{\omega}\times\left(\vec{\omega}\times(\vec{v}_n - \vec{v}_s - \vec{v}_l)\right) . \tag{4.17}$$

In equations (4.14) and (4.17), $\vec{v}_s$ and $\vec{v}_n$ are interpreted to be spatial averages of the actual local velocities.

In order to use equation (4.16) to obtain an equation which describes the motion of a quantized vortex, we must find an expression for $\vec{v}_l$. $\vec{v}_l$ is the velocity of the vortex if it satisfies equation (4.4). If we assume that the superfluid is incompressible then from chapter one we know then that $\vec{v}_l$ is given by equation (1.2) evaluated at the location of the vortex. Rather than use equation (1.4), Schwarz [38] suggested using the self-induction approximation, equation (1.7). Thus it is assumed that:

$$\vec{v}_l = \beta\vec{t}\times\vec{t}' \ , \tag{4.18}$$

where β is the constant given in equation (1.6), $\vec{t}$ denotes the tangent along the vortex and $\vec{t}'$ denotes the derivative of the tangent with respect to arclength measured along the vortex. The ratio $\vec{\omega}/\omega$ is assumed to be equal to the tangent along the vortex. Combining equations (4.17) and (4.18) we find:

$$\vec{v}_t = \beta\vec{t}\times\vec{t}' + \alpha\vec{t}\times(\vec{v}_n - \vec{v}_s - \beta\vec{t}\times\vec{t}') - \alpha'\ \vec{t}\times\left(\vec{t}\times(\vec{v}_n - \vec{v}_s - \beta\vec{t}\times\vec{t}')\right) , \tag{4.19}$$

where α and α' are the coefficients from (4.17). Following the approximation of Schwarz, we neglect the α', since it is generally ten times smaller than α. For values of α and α' see [3]. We obtain:

$$\vec{v}_t = \beta\vec{t}\times\vec{t}' + \alpha\vec{t}\times(\vec{v}_n - \vec{v}_s) + \alpha\beta\vec{t}' \ . \tag{4.20}$$

At this point we wish to recapitulate and emphasize some important differences between superfluid vortices and ordinary fluid vortices. Throughout our discussion of the

two fluid equations we have emphasized the similarity between the equations describing the superfluid component and the Euler equation describing an isentropic fluid; in fact equation (4.5) is Euler's equation. The paradoxical fact is that vortices described by the same equation behave so differently. Ordinary fluid vortices stretch and fold as they evolve in an Eulerian fluid in such a complicated manner that it is difficult to calculate their evolution for even short periods of time [7,8,9,42,43]. Superfluid vortices on the other hand, appear to remain relatively ordered. Although equation (4.20) causes the vortices to stretch, the equation smooths kinks rather than producing more of them. The fact then is that superfluid vortices are much better behaved than their ordinary fluid counterparts, and this can only be reconciled by concluding that much information is lacking from the two fluid equations. The quantum mechanics of the superfluid vortices cannot be ignored.

4.3 The Model Equation

We now end our discussion of the general fluid dynamics of superfluids and focus our attention on the application of equation (4.20) to a particular flow situation. We wish to consider equation (4.20) for the case of uniform counterflow. This situation is approximately realized when superfluid helium flows through a small tube. For this case we assume that $\vec{v}_n - \vec{v}_s$ is a constant. We denote this constant by: $\vec{v}_n - \vec{v}_s = \beta\vec{v}_0$. We also denote that $\vec{v}_t = \partial\vec{r}/\partial t$, where $\vec{r}$ is the position of a particle on the quantized vortex. Our result for the motion of the vortex is:

$$\frac{\partial\vec{r}}{\partial t} = \vec{t}\times\vec{t}' + \alpha\vec{t}\times\vec{v}_0 + \alpha\vec{t}' \quad , \tag{4.21}$$

where we have redefined the time t in equation (4.21) in order to eliminate the constant β. Equation (4.21) is identical to the one given by Schwarz [39].

We are interested in using equation (4.21) to model a system of turbulent superfluid vortices. We wish to give a dimensional argument due to Schwarz [39] based on (4.20) and (4.21) in order to determine the scaling of the line length density L_0 in terms of the magni-

tude of $\vec{v}_0$ which we denote as $\gamma = |\vec{v}_0|$. The line length density L_0 has units of inverse length squared, α is dimensionless, β has units of length squared per unit time, and γ has units of inverse length. Thus we find that γ^2 is the only combination of β and γ which has the same dimensions as the line length density L_0. Thus from this argument we would conjecture

$$L_0 = \epsilon(\alpha)\gamma^2 , \tag{4.22}$$

where $\epsilon(\alpha)$ is a function of α.

We now proceed to analyze equation (4.21). In the paragraph following equation (1.7) we discuss the choice of independent variable for equation (1.7); that discussion is valid for equation (4.21) as well. The partial derivative on the left side of equation (4.21) is taken with respect to a fixed particle on the vortex. Thus we consider $\vec{r}$ to be a function of time t and ξ, where ξ is a variable which labels the fluid particles located along the filament.

Our approach to analyze equation (4.21) is to consider it as a perturbation of the self-induction equation (1.7); thus we parallel as closely as possible the analysis given in chapter one for the self-induction equation. We wish to write equation (4.21) in terms of the tangent field; when doing this for equation (1.7), it is sufficient to differentiate with respect to arclength. The arclength of a vortex evolving according to equation (4.21) is not constant, however, and we must differentiate both sides of (4.21) with respect to ξ. We reintroduce the notation used in chapter one:

$$\vec{r}' \equiv \frac{\partial \vec{r}(\xi,t)}{\partial \xi} , \quad g \equiv |\vec{r}'| = \frac{\partial s}{\partial \xi} , \quad \text{and} \quad h \equiv \frac{1}{g} .$$

With this notation we note that: $\frac{\partial}{\partial s} = h\frac{\partial}{\partial \xi}$, since $\frac{\partial \vec{r}}{\partial s} = \vec{t} = h\,\vec{r}' = h\frac{\partial \vec{r}}{\partial \xi}$. Differentiating the terms of equation (4.21), we obtain:

$$\begin{aligned} \frac{\partial \vec{r}}{\partial t} &= \frac{\partial}{\partial \xi}\Big(\vec{t}\times\vec{t}' + \alpha\vec{t}\times\vec{v}_0 + \alpha\vec{t}'\Big) \\ &= g\Big(\vec{t}\times\vec{t}'' + \alpha\vec{t}'\times\vec{v}_0 + \alpha\vec{t}''\Big) , \end{aligned} \tag{4.23}$$

where $' \equiv \partial/\partial s$. We note that equation (4.23) reduces to equation (1.8) for the case $\alpha = 0$.

Next we wish to investigate the local stretching of the vortex evolving according to (4.23). The local stretching is given by the function g. Multiplying the members of (4.23) by $\vec{r}$, we see:

$$g\frac{\partial g}{\partial t} = \vec{r}\cdot\frac{\partial \vec{r}}{\partial t} = \alpha g\left(\vec{r}\cdot\vec{t}' \times\vec{v}_0 + \vec{r}\cdot\vec{t}''\right)$$
$$= \alpha g^2\kappa\left(\vec{b}\cdot\vec{v}_0 - \kappa\right),$$

where we have used equation (1.21). Thus we have:

$$\frac{\partial g}{\partial t} = \alpha g\,\kappa\left(\vec{b}\cdot\vec{v}_0 - \kappa\right); \tag{4.24}$$

the vortex stretches if $\kappa < \vec{b}\cdot\vec{v}_0$ and it contracts if $\kappa > \vec{b}\cdot\vec{v}_0$.

If we note that $\frac{\partial \vec{r}}{\partial t} = g\frac{\partial \vec{t}}{\partial t} + \vec{t}\frac{\partial g}{\partial t}$, then using equations (4.23) and (4.24) we find:

$$\frac{\partial \vec{t}}{\partial t} = \vec{t}\times\vec{t}'' + \alpha\vec{t}'\times\vec{v}_0 + \alpha\vec{t}'' - \alpha\kappa(\vec{b}\cdot\vec{v}_0 - \kappa)\vec{t}\,. \tag{4.25}$$

Since $\frac{\partial}{\partial t}(h\frac{\partial}{\partial \xi}\vec{t}) = \frac{\partial h}{\partial t}\frac{\partial \vec{t}}{\partial \xi} + h\frac{\partial^2\vec{t}}{\partial\xi\partial t}$, and since $\frac{\partial h}{\partial t} = -h^2\frac{\partial g}{\partial t}$, we see that

$$\frac{\partial \vec{t}'}{\partial t} = [tv\times\vec{t}'']' + \alpha\vec{t}''\times\vec{v}_0 + \alpha\vec{t}''' \tag{4.26}$$
$$- [\alpha\kappa(\vec{b}\cdot\vec{v}_0 - \kappa)\vec{t}]' - \alpha\kappa(\vec{b}\cdot\vec{v}_0 - \kappa)\vec{t}'\,.$$

Multiplying the terms of (4.26) by $\vec{t}'$, we have that

$$\kappa\frac{\partial\kappa}{\partial t} = \vec{t}'\cdot\frac{\partial \vec{t}'}{\partial t} \tag{4.27}$$
$$= -2\alpha\kappa^3(\vec{b}\cdot\vec{v}_0 - \kappa) - [\vec{t}\cdot\vec{t}'\times\vec{t}'']' + \alpha\vec{t}'\cdot\vec{t}''' + \alpha\vec{t}'\cdot\vec{t}''\times\vec{v}_0\,.$$

If we observe that $\frac{\partial\kappa\vec{b}}{\partial t} = \frac{\partial\vec{t}\times\vec{t}'}{\partial t} = \vec{t}\times\frac{\partial\vec{t}'}{\partial t} + \frac{\partial\vec{t}}{\partial t}\times\vec{t}'$, we find:

$$\frac{\partial\kappa\vec{b}}{\partial t} = \vec{t}\times[\vec{t}\times\vec{t}'']' + \alpha\vec{t}\times(\vec{t}''\times\vec{v}_0) + \alpha\vec{t}\times\vec{t}''' \tag{4.28}$$
$$+ (\vec{t}\times\vec{t}'')\times\vec{t}' + \alpha(\vec{t}'\times\vec{v}_0)\times\vec{t}' + \alpha\vec{t}''\times\vec{t}' - 3\alpha\kappa^3(\vec{b}\cdot\vec{v}_0 - \kappa)\vec{b}\,,$$

where we have used (4.25) and (4.26). Equations (4.27) and (4.28) are analagous to the Betchov equations presented in chapter one.

In analogy to equation (1.9), we write down a formal expression, which allows us to obtain $\vec{r}(\xi,t)$ once we have found $\vec{t}(\xi,t)$:

$$\vec{r}(\xi,t) = \vec{r}(0,0) + \int_0^t \vec{v}(0,\eta)\, d\eta + \int_0^\xi \vec{\tau}(\varsigma,t)\, d\varsigma\,, \tag{4.29}$$

where $\vec{v}(\cdot,\cdot)$ is defined by the right side of equation (4.21). In order to show that $\vec{r}$ as defined by equation (4.29) satisfies equation (4.21) we differentiate equation (4.29) to obtain:

$$\begin{aligned}
\frac{\partial \vec{r}}{\partial t} &= \vec{v}(0,t) + \int_0^\xi \frac{\partial \vec{\tau}}{\partial t}\, d\varsigma \\
&= \vec{v}(0,t) + \int_0^\xi \left(\vec{t}\times\vec{t}'' + \alpha\vec{t}' \times\vec{v}_0 + \alpha\vec{t}''\right) g\, d\varsigma \\
&= \vec{v}(0,t) + \int_0^\xi \left(\vec{t}\times\vec{t}'' + \alpha\vec{t}' \times\vec{v}_0 + \alpha\vec{t}''\right) ds \\
&= \vec{v}(0,t) + \vec{v}(\xi,t) - \vec{v}(0,t) = \vec{v}(\xi,t)\,,
\end{aligned}$$

where we have used equation (4.23). We use equation (4.29) as our basis for determining $\vec{r}$ after we have solved equation (4.23) to determine $\vec{\tau}$.

4.4 Exact Solutions of the Model Equation

We now look for particular solutions of equation (4.23). We examine the class of solutions which can be described by circles. We note that solutions which are circles satisfy the following differential equation:

$$\vec{t}'' = -\kappa^2\vec{t}\,. \tag{4.30}$$

If we substitute equation (4.30) into (4.27) we obtain:

$$\begin{aligned}
\frac{\partial \kappa}{\partial t} &= -2\alpha\kappa^2(\vec{b}\cdot\vec{v}_0 - \kappa) - \alpha\kappa^3 + \alpha\kappa^2(\vec{b}\cdot\vec{v}_0) \\
&= -\alpha\kappa^2(\vec{b}\cdot\vec{v}_0) + \alpha\kappa^3\,,
\end{aligned} \tag{4.31}$$

where we have used equation (1.21). If we substitute equation (4.30) into (4.28) we find:

$$\begin{aligned}
\frac{\partial \kappa\vec{b}}{\partial t} &= \alpha\kappa^2\vec{v}_0 + \alpha\kappa^2\vec{b}(\vec{b}\cdot\vec{v}_0) - 2\alpha\kappa^3\vec{b} - 3\alpha\kappa^2\vec{b}(bv\cdot\vec{v}_0 - \kappa) \\
&= \alpha\kappa^2\vec{v}_0 - 2\alpha\kappa^2\vec{b}(\vec{b}\cdot\vec{v}_0) + \alpha\kappa^3\vec{b}\,.
\end{aligned} \tag{4.32}$$

Multiplying the members of (4.32) by $\vec{v}_0$ we obtain:

$$\frac{\partial \vec{b}\cdot\vec{v}_0}{\partial t} = \alpha\kappa^2\,|\,\vec{v}_0\,|^2 - \alpha\kappa^2(\vec{b}\cdot\vec{v}_0)^2\,, \tag{4.33}$$

where we have used equation (4.31) to eliminate some of the terms from equation (4.32). If

we note that for circles of radius r, $\kappa = 1/r$, we rewrite (4.31) and (4.33) as:

$$\frac{1}{\alpha \mid \vec{v}_0 \mid^2} \frac{d \mid \vec{v}_0 \mid r}{dt} = \cos\theta - \frac{1}{\mid \vec{v}_0 \mid r} , \tag{4.34}$$

and

$$\frac{1}{\alpha \mid \vec{v}_0 \mid^2} \frac{d \cos\theta}{dt} = \frac{1 - \cos^2\theta}{\mid \vec{v}_0 \mid r} , \tag{4.35}$$

where $\cos\theta \equiv \vec{b} \cdot \frac{\vec{v}_0}{\mid \vec{v}_0 \mid}$. Thus we have shown that vortices in the shape of circles satisfy equation (4.23). The evolution of the radius and binormal of the circles are given by equations (4.34) and (4.35).

Equation (4.35) has stationary solutions at $\cos\theta = \pm 1$. The point $\cos\theta = -1$ is an unstable equilibrium point while the point $\cos\theta = 1$ is a stable equilibrium point; all circular solutions tend to align their binormal with $\vec{v}_0$. We solve (4.34) and (4.35) explicitly for the points $\cos\theta = \pm 1$. We find for the point $\cos\theta = 1$:

$$r - r_0 + \ln\left(\frac{r - 1}{r_0 - 1}\right) = t ,$$

where r_0 is the initial value of r, and r and t have been redefined so that $r \mid \vec{v}_0 \mid$ becomes r and $\alpha \mid \vec{v}_0 \mid^2 t$ becomes t. For $r_0 < 1$, r decreases to zero in a finite time t_0, where

$$t_0 = -\ln(1 - r_0) - r_0 .$$

For $r_0 > 1$,r increases unboundedly. For the case $\cos\theta = -1$, we find:

$$-(r - r_0) + \ln\left(\frac{r + 1}{r_0 + 1}\right) = t .$$

r goes to zero in time t_0 for all r_0, where

$$t_0 = r_0 - \ln(1 + r_0) .$$

If we consider the solutions of (4.34) and (4.35) as a function of the initial conditions, $\cos\theta_0$ and r_0, we find that if we fix $\cos\theta_0$ for small r_0, r goes to zero in a finite time; for large r_0, r increases unboundedly. The radius, at which the solution stops decaying to zero, increases as $\cos\theta_0$ decreases, until at $\cos\theta_0 = -1$ all solutions go to zero in a finite time.

Figures 4.1, 4.2, 4.3, and 4.4 show the radius as a function of time for fixed values of $\cos\theta_0$. The $\cos\theta$ given in the captions of these four figures is the initial value $\cos\theta_0$; it should be emphasized that $\cos\theta$ is also varying along the pictured curves, except for the $\cos\theta_0 = \pm 1$ cases. Figures 4.5 and 4.6 show $\cos\theta$ as a function of time for a given fixed initial radius r_0. Once again we emphasize that the radius is not fixed in figures 4.5 and 4.6.

We know of no exact solutions of equation 4.28 other than the solutions presented above.

figure 4.1

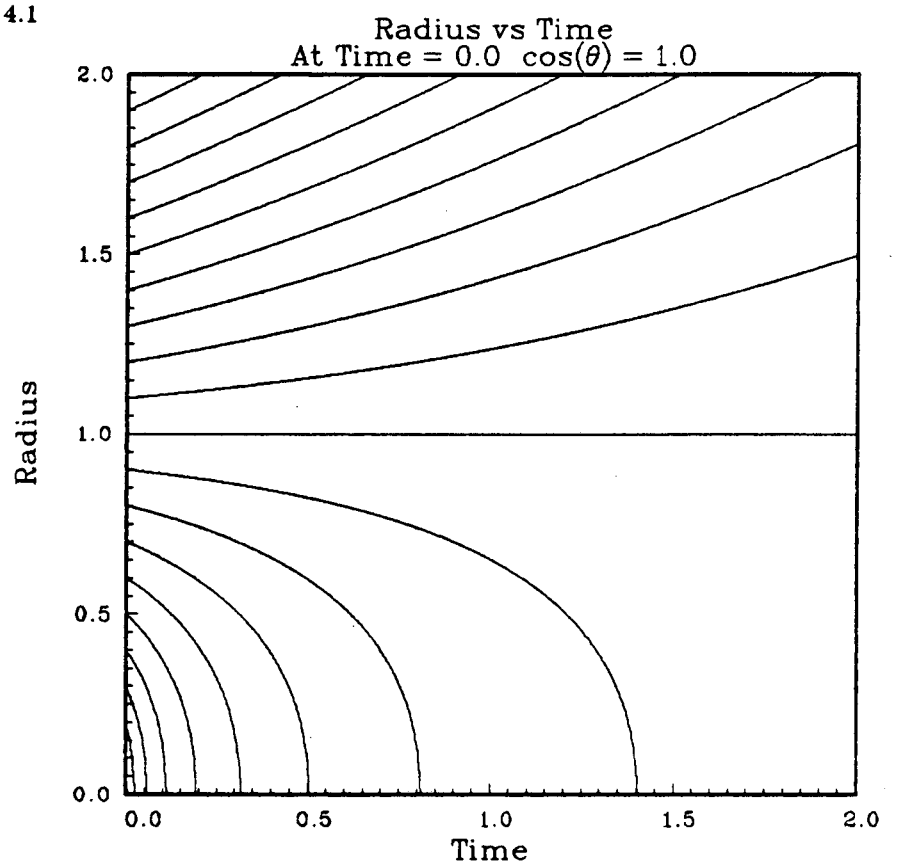
Radius vs Time
At Time = 0.0 cos(θ) = 1.0
2.0
1.5
1.0
0.5
0.0
Radius
0.0
0.5
1.0
1.5
2.0
Time

figure 4.2

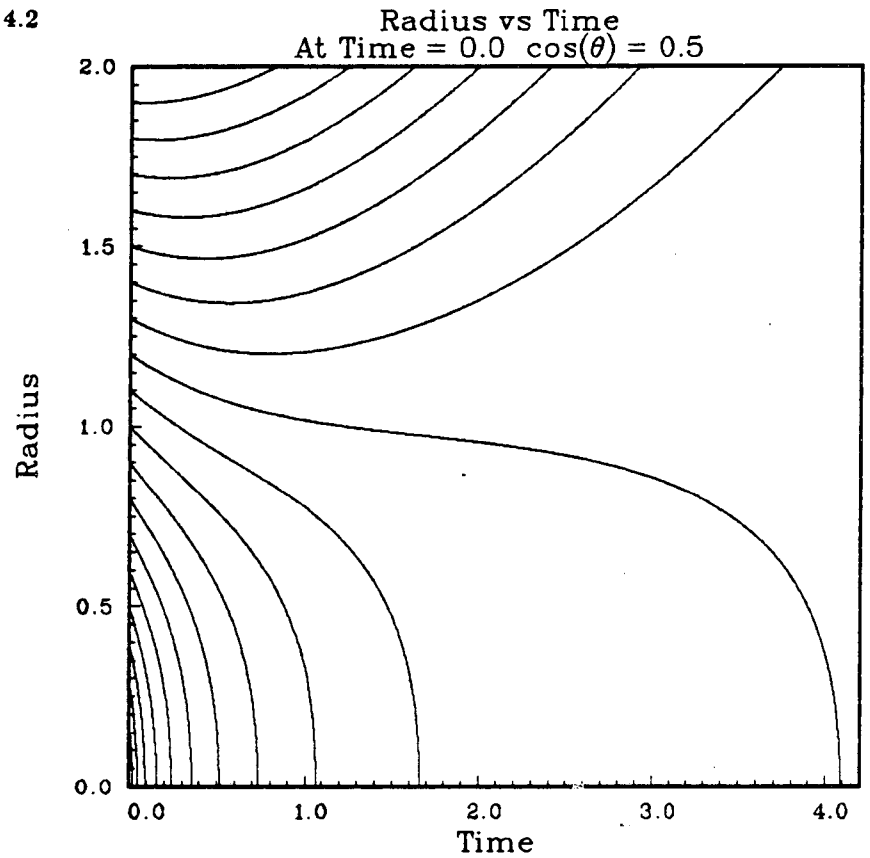
Radius vs Time
At Time = 0.0 cos(θ) = 0.5
2.0
1.5
1.0
0.5
0.0
Radius
0.0
1.0
2.0
3.0
4.0
Time

figure 4.3

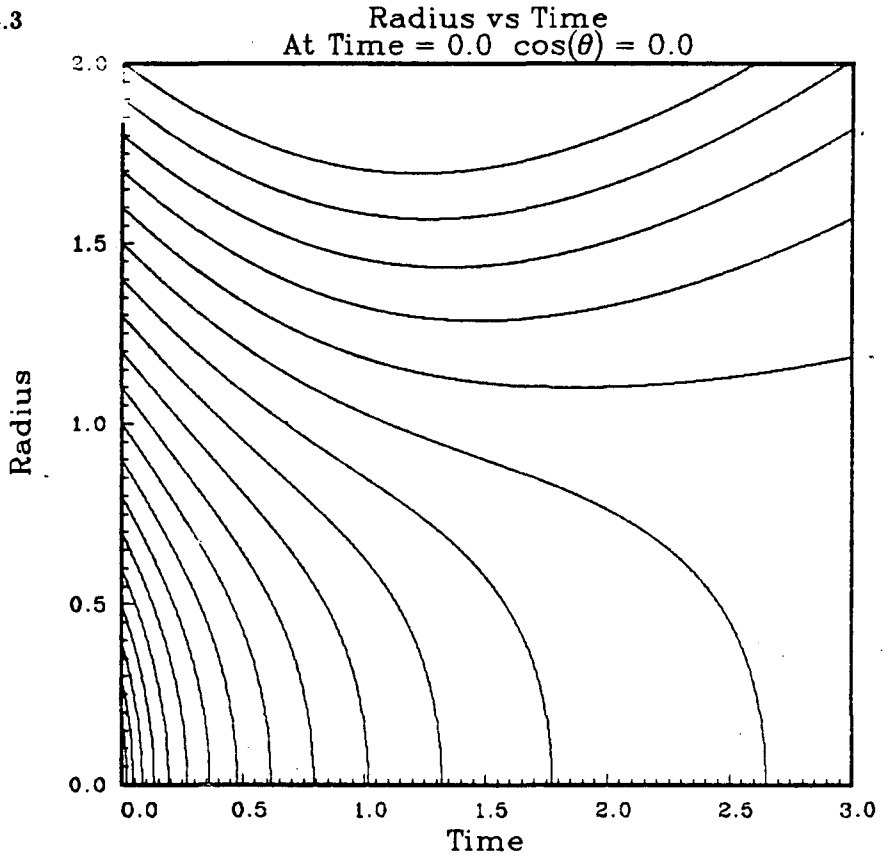
Radius vs Time
At Time = 0.0 cos(θ) = 0.0
2.0
1.5
1.0
0.5
0.0
Radius
0.0
0.5
1.0
1.5
2.0
2.5
3.0
Time

figure 4.4

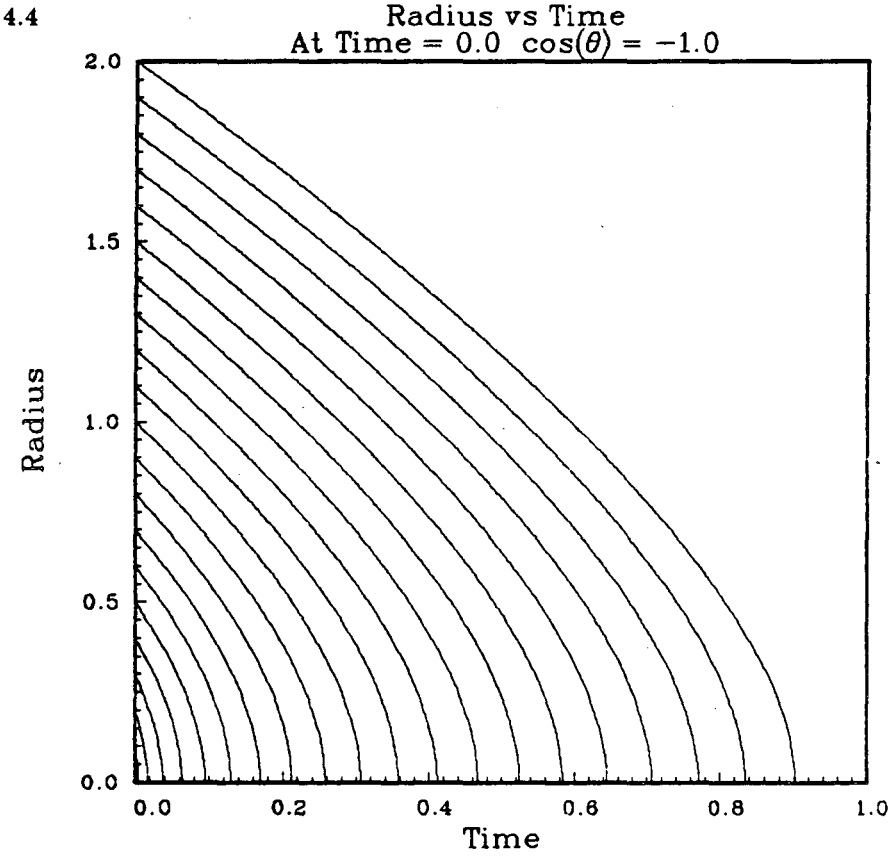
Radius vs Time
At Time = 0.0 cos(θ) = −1.0
2.0
1.5
1.0
0.5
0.0
Radius
0.0
0.2
0.4
0.6
0.8
1.0
Time

figure 4.5

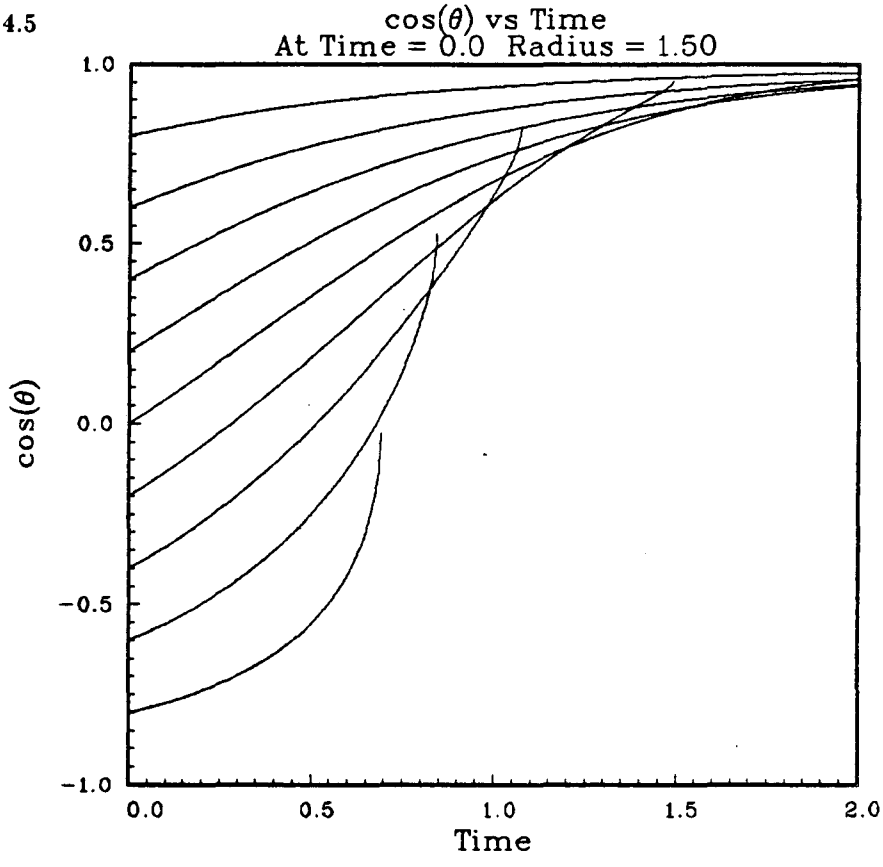
cos(θ) vs Time
At Time = 0.0 Radius = 1.50
1.0
0.5
0.0
−0.5
−1.0
cos(θ)
0.0
0.5
1.0
1.5
2.0
Time

figure 4.6

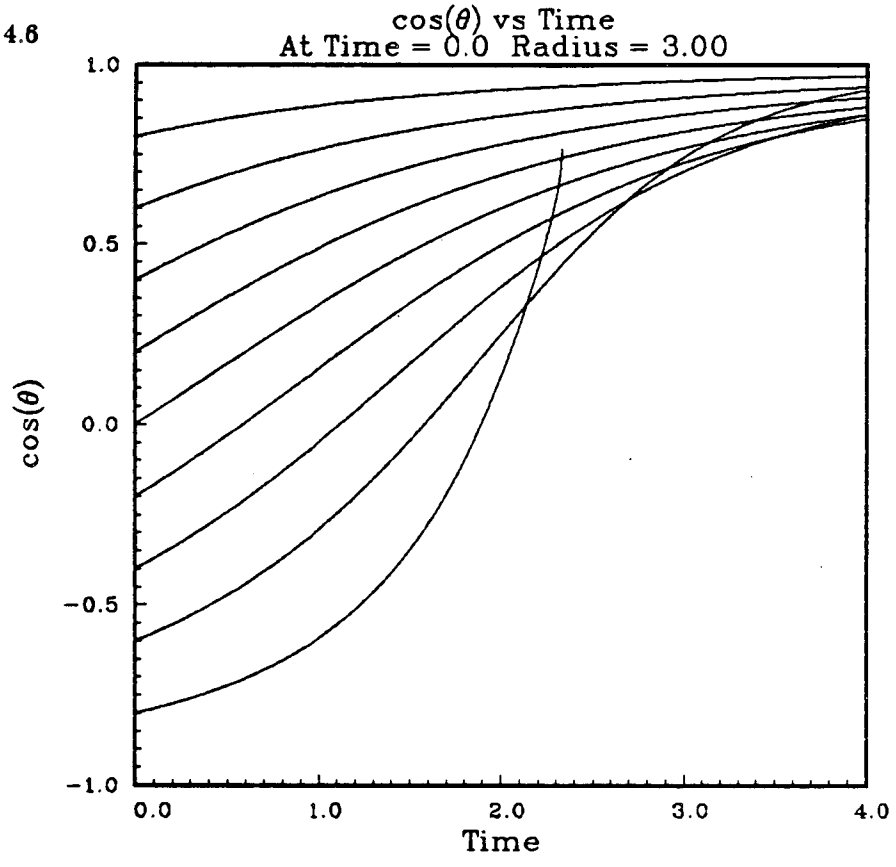
cos(θ) vs Time
At Time = 0.0 Radius = 3.00
1.0
0.5
0.0
−0.5
−1.0
cos(θ)
0.0
1.0
2.0
3.0
4.0
Time

Chapter 5: Numerical Methods That Account for Stretching

In this chapter we present a finite difference scheme for solving equation 5.1:

$$\frac{\partial \vec{r}}{\partial t} = g\left(\vec{t}\times\vec{t}'' + \alpha\vec{t}' \times\vec{v}_0 + \alpha\vec{t}''\right), \tag{5.1}$$

where $' \equiv \frac{\partial}{\partial s}$ is the derivative with respect to arclength. We present the scheme as a perturbation of the method used for the self-induction equation. We then discuss the stability of the scheme and a method for solving the finite difference equations. We then introduce a nonlocal interaction which consists of reconnecting vortices which cross one another. We discuss the use of the nonlocal interaction in conjunction with equation (5.1) to model turbulence in superfluid helium. We then discuss a numerical inaccuracy which is present in the method if the spatial step is chosen too large. Finally we discuss some details of the implementation of the reconnection interaction.

5.1 The Finite Difference Equations

While developing the method for solving equation (5.1), we keep in mind the results obtained in the first three chapters for solving the self-induction equation (1.8). We view equation (5.1) as a perturbation of equation (1.8); equation (5.1) reduces to (1.8) when $\alpha = 0$. We begin by presenting a stable method for solving the self-induction part of equation (5.1) which accommodates stretching of the vortex. Once the self-induction part of the scheme is presented, we add the other terms present in equation (5.1). We solve only equation (5.1), however, other terms than those present could be added, for instance those terms omitted from equation (4.19), or a non-uniform flow field specified.

We wish to write all of the terms on the right side of equation (5.1) in terms of the variable ξ. Using the definitions given in chapters one and four that $' = \frac{\partial}{\partial s} = h\frac{\partial}{\partial \xi}$, we find:

$$\vec{t}'' = h\frac{\partial}{\partial \xi}\left(h\frac{\partial \vec{t}}{\partial \xi}\right); \tag{5.2}$$

thus we rewrite (5.1) as:

$$\frac{\partial \vec{r}}{\partial t} = \vec{t} \times \frac{\partial}{\partial \xi}\left(h \frac{\partial \vec{t}}{\partial \xi}\right) + \alpha \frac{\partial \vec{t}}{\partial \xi} \times \vec{v}_0 + \alpha \frac{\partial}{\partial \xi}\left(h \frac{\partial \vec{t}}{\partial \xi}\right) . \tag{5.3}$$

Equation (5.2) leads us to use a second order finite difference formula for approximating $\frac{d}{dx}\left(u \frac{dw}{dx}\right)$. We approximate $\frac{d}{dx}\left(u \frac{dw}{dx}\right)$ by:

$$\frac{d}{dx}\left(u \frac{dw}{dx}\right) = \Delta_0(u\, \Delta_0 w) + O(\Delta x^2) , \tag{5.4}$$

where Δ_0 is the central difference operator defined by:

$$\Delta_0 w \equiv \frac{1}{2\Delta x}(w_{j+1} - w_{j-1}) ,$$

where Δx is the grid spacing and $w_j = w(j\,\Delta x)$. We expand equation (5.4) and find:

$$\Delta_0(u\, \Delta_0 w) = \frac{1}{4\Delta x^2}\left(u_{j+1} w_{j+2} - w_j (u_{j+1} + u_{j-1}) + u_{j-1} w_{j-2}\right) . \tag{5.5}$$

We want to apply equation (5.5) to the self-induction equation, which from equation (5.3) is:

$$\frac{\partial \vec{r}}{\partial t} = \vec{t} \times \frac{\partial}{\partial \xi}\left(h \frac{\partial \vec{t}}{\partial \xi}\right) . \tag{5.6}$$

If we approximate equation (5.6) by (5.5), we obtain:

$$\frac{\partial \vec{r}_j}{\partial t} = \frac{1}{4\Delta \xi^2} \vec{t}_j \times (h_{j+1} \vec{t}_{j+2} + h_{j-1} \vec{t}_{j-2}) , \tag{5.7}$$

where equation (5.7) is valid to second order in $\Delta\xi$. Recall that a vortex evolving according to the self-induction equation does not stretch; this is one of the three properties which is preserved by solutions of equation (3.1). We want to approximate equation (5.7) by a finite difference equation which also preserves the arclength conservation property. We see this can be accomplished by using the same second order Crank-Nicholson method used to discretize time in equation (2.2); the resultant finite difference equation is:

$$\vec{r}_j^{\,n+1} - \vec{r}_j^{\,n} = \frac{\Delta t}{4\Delta \xi^2} h_j \vec{r}_j \times \left(h_{j+1} h_{j+2} \vec{r}_{j+2} + h_{j-1} h_{j-2} \vec{r}_{j-2}\right) , \tag{5.8}$$

where we define $\vec{r}_j^{\,n} \equiv \vec{r}(j\,\Delta\xi, n\,\Delta t)$, $\vec{r}_j \equiv \frac{1}{2}\left(\vec{r}_j^{\,n} + \vec{r}_j^{\,n+1}\right)$ and $h_j \equiv \frac{1}{|\vec{r}_j|}$. If we multi-

ply the members of equation 5.9 by $\vec{r}_j$, we see:

$$\frac{1}{2}(\vec{r}_j^{\,n+1} + \vec{r}_j^{\,n})\cdot(\vec{r}_j^{\,n+1} - \vec{r}_j^{\,n}) = \frac{1}{2}(\,|\,\vec{r}_j^{\,n+1}\,|^2 - \,|\,\vec{r}_j^{\,n}\,|^2) = 0\,. \tag{5.9}$$

Equation (5.9) implies that the method is $\mathbf{H}_0^0$ stable, as defined in equation (2.61).

Solutions of equation (5.8) also have the property:

$$\sum_{j=1}^{j=N} \vec{r}_j^{\,n+1} = \sum_{j=1}^{j=N} \vec{r}_j^{\,n}\,. \tag{5.10}$$

If we sum the terms of equation (5.8) we find:

$$\sum_{j=1}^{j=N}\left(\vec{r}_j^{\,n+1} - \vec{r}_j^{\,n}\right) = \frac{\Delta t}{4\Delta\xi^2}\Big(h_2 h_1 h_0\,\vec{r}_2\times\vec{r}_0 + h_1 h_0 h_{-1}\,\vec{r}_1\times\vec{r}_{-1}$$
$$+\, h_N\, h_{N+1} h_{N+2}\,\vec{r}_N\times\vec{r}_{N+2} + h_{N-1} h_N\, h_{N+1}\,\vec{r}_{N-1}\times\vec{r}_{N+1}\Big) = 0\,,$$

where we have assumed $\vec{r}_j = \vec{r}_{j+N}$. Thus we have a generalized scheme for solving the self-induction equation, which has two invariants and is stable in the $\mathbf{H}_0^0$ norm.

We use equation (5.8) as a basis for solving equations which are perturbations of the self-induction equation when the perturbation terms cause the vortex filament to stretch. As an example, we write down the following finite difference scheme for solving equation (5.3):

$$\vec{r}_j^{\,n+1} - \vec{r}_j^{\,n} = \frac{\Delta t}{4\Delta\xi^2} h_j\,\vec{r}_j \times \Big(h_{j+1} h_{j+2}\vec{r}_{j+2} + h_{j-1} h_{j-2}\vec{r}_{j-2}\Big) \tag{5.11}$$
$$+\, \alpha\frac{\Delta t}{2\Delta\xi}\Big(h_{j+1}\vec{r}_{j+1} - h_{j-1}\vec{r}_{j-1}\Big)\times\vec{v}_0$$
$$+\, \alpha\frac{\Delta t}{4\Delta\xi^2}\Big(h_{j+1} h_{j+2}\vec{r}_{j+2} - (h_{j+1} + h_{j-1})h_j\,\vec{r}_j + h_{j-1} h_{j-2}\vec{r}_{j-2}\Big)\,;$$

where we have used the central difference operator and equation (5.5). We note that solutions of equation (5.11) satisfy equation (5.10).

Once we have found the solution to equation (5.11), in order to find the position of the approximation points, we carry out the integrations numerically in equation (4.29) in order to obtain an approximation for $\vec{r}(j\,\Delta\xi, n+1\Delta t)$, which we denote $\vec{r}_j^{\,n+1}$. We obtain:

$$\vec{r}_j^{\,n+1} = \vec{r}_0^{\,0} + \Delta t \sum_{m=1}^{m=n} \vec{v}_0^{\,m} + \frac{\Delta\xi}{2}\sum_{i=1}^{i=j}(\vec{r}_{i-1}^{\,n+1} + \vec{r}_i^{\,n+1})\,.$$

We define $\vec{v}_j^{\,m}$ as:

$$\vec{v}_j^m = \frac{h_j}{2\Delta\xi}\,\vec{t}_j \times (\vec{t}_{j+1} - \vec{t}_{j-1}) + \alpha\vec{t}_j \times \vec{v}_0 + \frac{\alpha h_j}{2\Delta\xi}\,(\vec{t}_{j+1} - \vec{t}_{j-1})\,, \tag{5.12}$$

where $\vec{\tau}_j \equiv \dfrac{\vec{\tau}_j^m + \vec{\tau}_j^{m+1}}{2}$, $h_j \equiv \dfrac{1}{|\vec{\tau}_j|}$ and $\vec{t}_j \equiv h_j\vec{\tau}_j$. With these definitions the method is formally second order in space and time.

We wish to discuss the implementation of equation (5.11) and the choice of the parameter ξ. As briefly discussed in chapter 4, ξ is a parameter which labels the particles along the vortex. The vector $\vec{\tau}_j^n$ approximates the tangent to the vortex at the $j\,\Delta\xi$ position on the vortex. We need to know the position $\vec{r}$, of the point $j\,\Delta\xi$ on the vortex; from equation (4.10), given the position of a particle on the vortex, we can find the position of any other point on the vortex: $\vec{r}(j\,\Delta\xi) = \vec{r}(0) + \int_0^{\xi} \vec{\tau} d\,\xi$. If we use the trapezoidal method to approximate the integral, we find $\vec{r}(j\,\Delta\xi) \equiv \vec{r}(0) + \frac{\Delta\xi}{2}\sum_{i=1}^{i=j}(\vec{\tau}_{i-1} + \vec{\tau}_i)$; in this method the vortex curve is approximated by placing the vectors $\vec{\tau}_j^n$ end to end, and the $j\,\Delta\xi$ particle on the vortex is located at the center of the vector $\vec{\tau}_j^n$. A convenient choice for ξ is to take ξ to be the arclength along the curve initially. With the choice of ξ as the initial arclength, we have that $|\vec{\tau}_j^0| = 1$ for all j, and the approximation points are evenly spaced along the vortex initially. As the vortex evolves, the vectors $\vec{\tau}_j^n$ stretch and contract. If $|\vec{\tau}_j^n|$ becomes large, the spacing of the approximation points also becomes large. At some point it becomes reasonable to introduce more approximation points, so that the spacing of the points remains relatively constant throughout the calculation . There are a number of ways of introducing more approximation points, for instance see Greengard [16] and Anderson and Greengard [1]; we choose a method due to Chorin [8] for spacing the points as explained below.

If a vector $\vec{\tau}_j^n$ is greater than a certain length $l_{\max}^0$, we divide the vector in half and track the two vectors individually. The vector $\vec{\tau}_j^n$ is replaced by two vectors $\vec{\tau}_{j-1/2}^n$ and $\vec{\tau}_{j+1/2}^n$, where $\vec{\tau}_j^n = 2\vec{\tau}_{j-1/2}^n = 2\vec{\tau}_{j+1/2}^n$. This process of replacing a vector by two vectors corresponds to a local redefinition of the parameter ξ. We let $\xi' = \xi$ except at the j-th

vector where we set $\xi' = 2\xi$, and as a result the old approximation is equal to the new, except at the j-th vector where $\frac{\partial \vec{r}}{\partial \xi'} = \frac{1}{2}\frac{\partial \vec{r}}{\partial \xi} = \frac{\vec{r}}{2}$. If we then let $\Delta\xi' = \Delta\xi$, we find that we have two consecutive vectors equal to $\vec{r}/2$ where we previously had one equal to $\vec{r}$. At any time step n, the curve can be reparametrized and the reparametrization is valid, for fixed $\Delta\xi$, provided that $\Delta\vec{r}_j = \Delta\xi\vec{r}_j^n$, where $\Delta\vec{r}_j$ is the difference in positions between the $j-1$ and j particles on the vortex.

The technical redefinition of ξ is more confusing than the actual application. In the numerical application, if the magnitude of the vector $\vec{r}_j^n$ is greater than $l^0_{\max}$, the vector is simply replaced by two vectors which are equal to half the original vector. It may also happen that $|\vec{r}_j^n|$ becomes small; in this case we replace the vectors $\vec{r}_j^n$ and $\vec{r}_{j+1}^n$, by the vector $\vec{r}_j^n + \vec{r}_{j+1}^n$. In order to maintain an approximation in which the physical spacing of the approximation points doesn't become too large or too small, we place the following constraint on the lengths of $\vec{r}_j^n$:

$$l^0_{\min} \leq |\vec{r}_j^n| \leq l^0_{\max} \ . \tag{5.13}$$

In order to maintain condition (5.13), after each time step we redefine the vectors which do not satisfy this condition as described above. Some care should be taken when chosing the values of $l^0_{\min}$ and $l^0_{\max}$ so that they are self consistent. A sufficient condition is that $2l^0_{\min} < l^0_{\max}$.

5.2 Stability

We now discuss the stablility of equation (5.11). We can not prove rigorously that equation (5.11) is stable, but give a plausible argument supprted by numerical experiments. If we multiply the members of (5.11) by $h_j\vec{r}_j$, we find:

$$h_j\left(|\vec{r}_j^{n+1}|^2 - |\vec{r}_j^n|^2\right) = \frac{\alpha\Delta t}{2(\Delta\xi)}\vec{t}_j\cdot(\vec{t}_{j+1} - \vec{t}_{j-1})\times\vec{v}_0 \tag{5.14}$$
$$+ \frac{\alpha\Delta t}{4(\Delta\xi)^2}\left(h_{j+1}(\vec{t}_j\cdot\vec{t}_{j+2} - 1) + h_{j-1}(\vec{t}_j\cdot\vec{t}_{j-2} - 1)\right),$$

where we define $\vec{t}_j \equiv h_j\vec{r}_j$. Since $|\vec{t}_j| = 1$, the second term on the right side of (5.14) is

negative, and therefore we have:

$$h_j \mid \vec{r}_j^{\,n+1} \mid^2 \leq h_j \mid \vec{r}_j^{\,n} \mid^2 + \frac{\alpha \Delta t \mid \vec{v}_0 \mid}{\Delta \xi} , \tag{5.15}$$

where we have used the triangle inequality. From the definition of h_j, we know that it is strictly positive and furthermore if $\mid \vec{r}_j^{\,n+1} \mid \leq l^1_{\max}$ we obtain the lower bound on h_j:

$$h_j \geq \frac{2}{(l^0_{\max} + l^1_{\max})} .$$

We divide the members of (5.15) by h_j and take the maximum of the resultant inequality over j to obtain:

$$(l^1_{\max})^2 \leq (l^0_{\max})^2 + \frac{\alpha \Delta t \mid \vec{v}_0 \mid (l^1_{\max} + l^0_{\max})}{2 \Delta \xi} . \tag{5.16}$$

Dividing the members of inequality (5.16) by $(l^1_{\max} + l^0_{\max})$, we find

$$l^1_{\max} \leq l^0_{\max} + \frac{\alpha \Delta t \mid \vec{v}_0 \mid}{2 \Delta \xi} . \tag{5.17}$$

As we discuss above, in order to maintain inequality (5.13) after each time step if a vector becomes too large we divide it in half; in order that the redefined vectors satisfy (5.13) we require:

$$l^1_{\max} < 2 l^0_{\max} . \tag{5.18}$$

Combining inequalities (5.17) and (5.18) we find:

$$\frac{\alpha \Delta t \mid \vec{v}_0 \mid}{2 \Delta \xi} < l^0_{\max} . \tag{5.19}$$

If inequality (5.19) is satisfied, then $\mid \vec{r}_j^{\,n+1} \mid < 2 l^0_{\max}$ and $h_j > \frac{3}{2 l^0_{\max}}$ for all j.

In order to further investigate the stability of (5.11), we sum the terms of equation (5.14) over the index j. Since the second term on the right side of (5.14) is non-positive, we find

$$\sum_{j=1}^{j=N} h_j \mid \vec{r}_j^{\,n+1} \mid^2 \leq \sum_{j=1}^{j=N} h_j \mid \vec{r}_j^{\,n} \mid^2 + \frac{\alpha \Delta t}{2 \Delta \xi} \vec{v}_0 \cdot \sum_{j=1}^{j=N} (\vec{t}_j \times \vec{t}_{j+1} + \vec{t}_{j-1} \times \vec{t}_j) . \tag{5.20}$$

We consider periodic solutions and since solutions of (5.11) satisfy equation (5.10) the $\vec{r}_j^{\,n}$ form closed polygon curves. The triple product on the right side of (5.20) is unchanged if we

replace the tangent vectors in this sum by the projection of the tangent vectors onto the plane perpendicular to $\vec{v}_0$. Thus we consider the two dimensional closed curve which results by projecting the tangents onto the plane perpendicular to $\vec{v}_0$.

For closed curves in two dimensions $\int_0^L \kappa(s)\, ds = \pm 2\pi m$, $m = 1,2,3, \cdots$, where L is the length of the curve. In two dimensions the curvature can be interpretted as $\frac{d\theta}{ds}$, where θ is the angle between the tangent and any fixed vector. The sum of the cross products in (5.20) can be interpretted in a similar way. For the N-sided polygon which results from projecting the tangent vectors onto the plane perpendicular to $\vec{v}_0$ we have $\sum_{j=1}^{j=N} \theta_j = \pm 2\pi m$, where θ_j is the angle between the j and $j-1$ sides. Since $|\vec{t}_j| = 1$ we have

$$\left| \vec{v}_0 \cdot \sum_{j=1}^{j=N} \vec{t}_{j-1} \times \vec{t}_j \right| \leq |\vec{v}_0| \sum_{j=1}^{j=N} |\sin\theta_j| \leq |\vec{v}_0| \sum_{j=1}^{j=N} |\theta_j| \,. \tag{5.21}$$

If $\vec{t}_j$ is approximating a smooth curve, then $\sum_{j=1}^{j=N} |\theta_j|$ is bounded, but not necessarily equal to a multiple of 2π. Because of numerical results and because of the analytic results for circles, we conjecture, however, that this sum is actually decreasing and that eventually all of the θ_j become positive. If all of the θ_j are positive, then we have: $\sum_{j=1}^{j=N} |\theta_j| = 2\pi m$, $m = 1,2,3, \cdots$. The result of this argument is that we assume

$$\sum_{j=1}^{j=N} |\theta_j| \leq C_0 \,, \tag{5.22}$$

for all n and N. Substituting (5.21) and (5.22) into inequality (5.20) we obtain:

$$\Delta\xi \sum_{j=1}^{j=N} h_j \, |\vec{r}_j^{\,n+1}|^2 \leq \Delta\xi \sum_{j=1}^{j=N} h_j \, |\vec{r}_j^{\,n}|^2 + \alpha\Delta t \, |\vec{v}_0| \, C_0 \,. \tag{5.23}$$

Recalling the definition of h_j, we find

$$|\vec{r}_j^{\,n+1}| - |\vec{r}_j^{\,n}| \leq \frac{\left(|\vec{r}_j^{\,n+1}| + |\vec{r}_j^{\,n}| \right)\left(|\vec{r}_j^{\,n+1}| - |\vec{r}_j^{\,n}| \right)}{|\vec{r}_j^{\,n+1} + \vec{r}_j^{\,n}|} \tag{5.24}$$

$$= \frac{h_j}{2}\left(|\vec{r}_j^{\,n+1}|^2 - |\vec{r}_j^{\,n}|^2 \right) .$$

Combining inequalities (5.23) and (5.24) we obtain the result:

$$\Delta\xi \sum_{j=1}^{j=N} |\vec{r}_j^{\,n+1}| \leq \Delta\xi \sum_{j=1}^{j=N} |\vec{r}_j^{\,n}| + \frac{\alpha\,|\vec{v}_0|\,C_0}{2}\,\Delta t \ . \tag{5.25}$$

Inequality (5.25) implies

$$\Delta\xi \sum_{j=1}^{j=N} |\vec{r}_j^{\,n}| \leq \Delta\xi \sum_{j=1}^{j=N} |\vec{r}_j^{\,0}| + \frac{\alpha\,|\vec{v}_0|\,C_0}{2}\,n\,\Delta t \ , \tag{5.26}$$

and thus the method is stable in the $\mathbf{L}_1$ norm, defined as:

$$|\vec{r}_j^{\,n}|_1 = \Delta\xi \sum_{j=1}^{j=N} |\vec{r}_j^{\,n}| \ .$$

It should be noted that inequality (5.26) is valid when we redefine $\vec{r}_j^{\,n}$ after each time so as to satisfy (5.13) provided that the redefined vectors conserve or decrease the $\mathbf{L}_1$ norm. The simple method which we outline above for redefining $\vec{r}_j^{\,n}$ satisfies this requirement and thus satisfies (5.26).

We discuss further practical restrictions on Δt and $\Delta\xi$ related to the solvability and accuracy of equation (5.11).

In practice we solve equation (5.11) by the method given in equation (2.14) for solving equation (2.2). We briefly review the method. If we are given finite difference equations of the form,

$$\vec{r}_j^{\,n+1} - \vec{r}_j^{\,n} = \Delta t \ f\,(\vec{r}_j^{\,n+1}, \vec{r}_j^{\,n}) \ , \tag{5.27}$$

we form the sequence $\vec{r}_j^{\,k+1}$, where we define the sequence iteratively as

$$\vec{r}_j^{\,k+1} - \vec{r}_j^{\,n} = \Delta t \ f\,(\vec{r}_j^{\,k}, \vec{r}_j^{\,n}) \ .$$

For Δt small enough the sequence converges to a solution of (5.27). We employ this method for solving equations (5.11); we find that a sufficient condition for the sequence to converge is:

$$\frac{\Delta t}{(\Delta\xi)^2} < \frac{1}{4} \ . \tag{5.28}$$

This is the condition that guarantees convergence of the sequence defined in equation (2.14).

We find condition (5.28) to be sufficient provided we require:

$$0.5 \leq |\vec{r}_j^n| \leq \sqrt{2}\,.$$

Inequality (5.19) puts another constraint on Δt and $\Delta\xi$; however, in the limit $\Delta\xi \rightarrow 0$, (5.28) implies (5.19). Furthermore we find that for the range of parameters that we consider, (5.19) is satisfied provided (5.28) is satisfied. There is a more severe restriction, however, which must be placed on $\Delta\xi$. In order to understand this restriction we must discuss in more detail the system we are modeling and the mathematical model we are solving.

5.3 The Reconnection Ansatz

We wish to investigate homogeneous turbulence in superfluid helium. It is conjectured that turbulence in the superfluid is caused by the creation of superfluid vortex tangles. [13] We study systems of vortices evolving according to equation (4.23). The problem with using (4.23) to study systems of vortices is that two vortices will never interact with each other, since equation (4.23) contains terms which only depend on the local geometry of the vortex curve. Feynman [13] suggested a heuristic method for interacting the vortices and Schwarz [39] introduced this method into his numerical algorithm. The algorithm Schwarz introduced is that if two vortices cross each other as they are moving through the fluid, then they should be redefined by reconnecting them as shown in figure 5.1. We shall refer to this interaction as the reconnection ansatz. It should be noted that there is no ambiguity in the redefined vortices since the vortices have a direction associated with them by the direction of the vorticity. In our model of the evolution of superfluid vortices we move the vortices through the fluid according to equation (4.23) and reconnect crossing vortices via the reconnection ansatz. This approximation is in marked contrast to that required for turbulent vortices in an ordinary fluid where non-local interactions cannot be ignored and dominate the local effects. From equation (4.24) we see that the filaments contract near the reconnection point, in marked contrast to the folding and stretching which occurs near a kink in an ordinary vortex [8].

We developed equation (4.23) in order to model the evolution of the vortices under the influence of a uniform background flow field. Experimentally it is observed that the turbulent state is a function of the magnitude of the background flow velocity. In flow through a tube there is a critical velocity, below which the system is not turbulent and above which it is turbulent. Thus numerically we would like to study the properties of the vortices as we vary the magnitude of $\vec{v}_0$. We fix the initial conditions and follow the evolution of the vortex system for different values of $|\vec{v}_0|$. In particular we increase the magnitude of $\vec{v}_0$ and try to observe some characteristic change in the system.

The most obvious approach is to use equation (5.11) by fixing Δt and $\Delta\xi$ so that conditions (5.19) and (5.28) are satisfied and then to let $|\vec{v}_0|$ vary. For instance if we pick $\Delta t = 0.0001$ and $\Delta\xi = 0.02$ and fix $\alpha \leq 1.0$, we find (5.19) is satisfied if $|\vec{v}_0| < 566$, and $\Delta t/(\Delta\xi)^2 = 0.25$.

The reconnection ansatz causes discontinuities in the tangent field which locally look like the self-similar initial conditions given in equation (1.63). If we recall equation (4.24), we see that the vortex should contract in this region of high curvature, provided $\kappa > \vec{b}\cdot\vec{v}_0$. The vortex evolves so as to reduce the curvature locally. In order to capture this local decrease in the arclength of the vortex numerically we must pick $\Delta\xi$ small enough so as to accurately determine this large value of the curvature. Looking at the exact circular solutions given by equations (4.34) and (4.35), we see that all circular solutions decay away in finite time provided that $r\,|\vec{v}_0| < 1$. This suggests that we should measure arclength along the vortex in units of $\frac{1}{|\vec{v}_0|}$; that is we let $\tilde{s} = \gamma s$, where $\gamma \equiv |\vec{v}_0|$. In terms of this new arclength $\tilde{s}$, which we will presently denote in the same way as the old arclength, we find that equation (4.23) becomes:

$$\frac{1}{\gamma^2}\frac{\partial\vec{r}}{\partial t} = g\left(\vec{t}\times\vec{t}\,'' + \alpha\vec{t}\,' \times\frac{\vec{v}_0}{|\vec{v}_0|} + \alpha\vec{t}\,''\right). \tag{5.29}$$

If we redefine our time t, then equations (4.23) and (5.29) are identical except for the fact

that varying the magnitude of $\vec{v}_0$ produces no change in equation (5.29). Varying the magnitude of $\vec{v}_0$ in equation (5.29) changes the size of the system, but not the equation governing the evolution of the system. For instance if we consider the evolution of a system of filaments inside of a unit cube using equation (4.23) and carry out calculations for several different values of γ; the same calculations carried out using equation (5.29) correspond to considering the evolution of a system of filaments inside of a cube whose sides have a length of γ.

Clearly equation (5.11) can be used to approximate either equation (4.23) or equation (5.29); however, keeping Δt and $\Delta\xi$ fixed and varying γ has different meanings in the two cases. Picking $\Delta\xi$ small enough to approximate the large curvatures introduced by the reconnection ansatz means that $\Delta\xi$ should be much less than one when approximating (5.29); whereas the same restriction when applied to approximating equation (4.23) implies that $\Delta\xi$ be much less than $1/\gamma$. If we approximate (4.23) with fixed $\Delta\xi$ and increase γ, we see that eventually our approximation is not fine enough to capture the correct evolution of the singularities introduced by the reconnection ansatz. If we use equation (4.23) we must scale $\Delta\xi$ so that $\gamma\Delta\xi \leq 0.5$, as is shown in the next chapter. In the next chapter we show the results of using these two methods and display the inaccuracy which results when our approximation becomes too coarse. We use both equations (4.23) and (5.29) in chapter six; we could use equation (4.23) throughout and just scale $\Delta\xi$ properly; however, we use (5.29) to emphasis the fact that $\Delta\xi$ should be measured in units of $\frac{1}{\gamma}$.

We obtain an approximate condition for determining the restriction on $\Delta\xi$. We require that the calculated curvature must be able to be larger than γ; thus we see:

$$\frac{h_j}{2\Delta\xi}\left|\vec{t}_{j+1} - \vec{t}_{j-1}\right| > \gamma$$

If we assume that $h_j < 1$ we obtain the following result:

$$\Delta\xi < \frac{1}{\gamma}.$$

We see in chapter six that the actual restriction is more severe. We find that the condition $\gamma\Delta\xi < 0.5$ is sufficient, whereas $\gamma\Delta\xi < 0.8$ is not sufficient for a stable approximation.

We now discuss the implementation of the reconnection ansatz. Since we approximate the position of the vortices at discrete time intervals, there is no simple way to decide exactly when two vortices cross each other. We assume that vortices cross if two points come within a distance $\Delta\xi$, provided that the points are not adjacent approximation points on the same vortex. It often occurs that if one pair of points satisfies the crossing condition, then other pairs of points near the first pair will also satisfy the requirement. If the pairs of possible reconnection points are neighbors it is not reasonable to reconnect all of them; of the possible pairs, we reconnect the pair which is the smallest distance apart. It may occur that a vortex intersects with another vortex in more than one location and thus we must allow some mechanism for deciding when two reconnection pairs are distinct. In order to make the distinction between neighboring reconnection pairs, we say two pairs are not neighbors if they are separated by a distance greater than or equal to $6\Delta\xi$. We choose a distance of $6\Delta\xi$ since this guarantees that the smallest vortex in the system has at least 5 approximation points on it; if a vortex contains fewer points the finite difference equations are no longer applicable. For the same reason, in order for two points on the same vortex to cross we require that the j indices differ by at least six.

We do not check for crossings at each time step. If we were to check for crossings at each time step then certain pairs would reconnect at two consecutive time steps and the same vortex structure as was originally present would occur. In order to reduce the number of pairs which reconnect at consecutive crossings, we only check for crossings on a certain fraction of the time steps. Looking at equation (5.12), we see that approximately the maximum distance $d_{\max}$ a point can move in one time step is given by:

$$d_{\max} = \frac{\Delta t}{\Delta\xi} + \alpha\gamma\Delta t + \frac{\alpha\Delta t}{\Delta s}, \tag{5.30}$$

where we recall that $\gamma = |\vec{v}_0|$. We assume that condition (5.28) is satisfied and define:

$$\lambda = \frac{\Delta t}{(\Delta \xi)^2} \ . \tag{5.31}$$

Substituting (5.31) into (5.30) we obtain:

$$d_{\max} = \lambda \Delta \xi \Big(1 + \alpha(1 + \gamma \Delta \xi) \Big) \ .$$

If we allow a maximum displacement of $\Delta\xi$ before we check for crossings, we determine that we only need check for crossings every $\lambda(1 + \alpha(1 + \gamma\Delta\xi))$ fraction of the time. Usually we pick $\lambda \approx 1/4$ and thus we check for crossings every second to every fourth time step, depending on the value of α. The estimate in equation (5.30) is quite conservative for smooth curves, and therefore it is unlikely that crossings are missed unless the points have just been reconnected; numerical experiments verify this assertion.

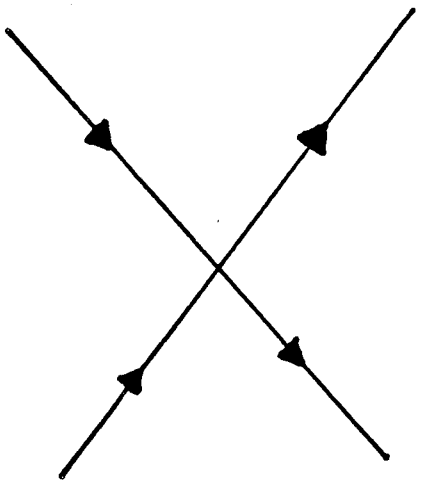

Before the reconnection

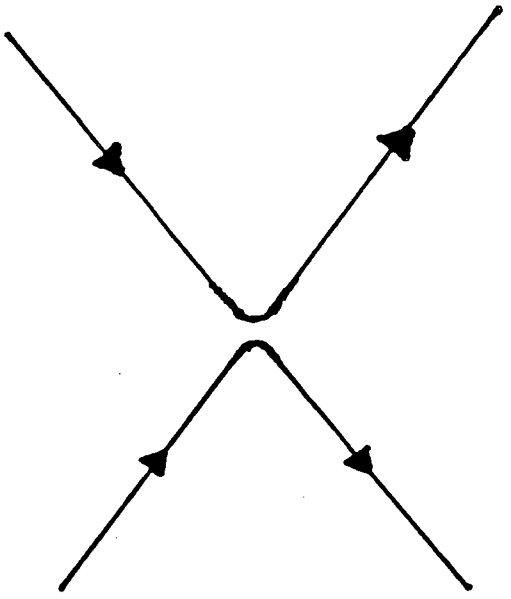

After the reconnection

Figure 5.1

Chapter 6: Numerical Results for Superfluid Helium

In this chapter we discuss the accuracy of the finite difference equation (5.11) when it is used together with the reconnection ansatz introduced in chapter 5. We find that in order for the approximate solutions to be close to the exact solutions, the condition

$$| \vec{v}_0 | \Delta s \leq 0.5 \tag{6.1}$$

must be satisfied. We wish to determine the line density of vortex filaments as a function of γ, where $\gamma = | \vec{v}_0 |$ is the magnitude of the counterflow velocity introduced in chapter four. Following the numerical experiments of Schwarz [39], we solve for the evolution of a system of superfluid vortices and find that the total length of the vortices present in the system reaches an equilibrium value independent of the initial conditions provided that the initial conditions are sufficiently "turbulent". Contrary to Schwarz' conclusions, we find that the turbulence produced is not homogeneous. Furthermore if we carry out the calculations using values of Δs for which the accuracy criteria (6.1) is *not* satisfied, we find that the system of vortices (1) produces homogeneous turbulence and (2) produces the same equilibrium values of vortex line density as those given by Schwarz [39]. We conclude that the model equation we use does not accurately model homogeneous turbulence in superfluid helium.

It is difficult to exhibit the accuracy of equation (5.11) numerically because of the lack of exact solutions of equation (4.21). The only exact solutions we have are given by equations (4.34) and (4.35). These solutions are circular vortices whose radius and binormal are functions of time. We check our approximate solutions obtained with (5.11) and find that they do converge to the exact solutions given by equations (4.34) and (4.35). This convergence check is important in verifying that the constants in equation (5.11) are correct, but the solutions given by circles are of a very special nature and may not be indicative of the performance of the scheme in general. Therefore we apply additional tests in order to check the accuracy of our approximate solutions.

We can be confident of the self-induction part of equation (5.11) because of the numeri-

cal convergence which is demonstrated in chapter 3 for the self-similar solution as well as for the soliton solutions. And if our initial curve is smooth and our approximation is fine enough the circle solutions indicate that equation (5.11) gives a good approximation to (4.21). We must, however, look at initial conditions which have a discontinuity in the tangent field to see how small we must pick Δs in order to adequately resolve the features of solutions of (4.21) for vortex filaments which are not smooth initially.

We choose for initial conditions the vortex filaments pictured in figure 6.1. We allow the filaments to evolve according to (5.11) and allow one reconnection when the curves are appropriately spaced. We then follow the evolution of the filament up to time $t = 1.0$. In figures 6.2 through 6.5 we show the results for different values of Δs. Recall that $\gamma = |\vec{v}_0|$, is the magnitude of the counter flow velocity, and α is defined in equation (5.11). Δt is chosen so that $\frac{\Delta t}{\Delta s^2} < 0.125$. Figures 6.2 through 6.5 show projections of the filament onto the $y-z$ and $x-z$ planes at time $t = 1.0$ We see that there is a drastic change in the filament for $\Delta s < 0.1$. For $\Delta s \leq 0.05$ the solutions appear to converge, and for $\Delta s > 0.05$ the filaments are drastically different from the convergent result; not even the number of loops present in the $y-z$ projection is the same.

In order to further look at the convergence of (5.11) for the given initial conditions, at each time step we calculate the total length of the filament and a quantity we call the total energy E, which we define as

$$E = \int \kappa^2 \, ds \ , \tag{6.2}$$

where κ is the curvature and s is the arclength and the integral is taken along the filament. The energy as defined by 6.2 is not directly related to the physical energy of the filament, but is simply a convenient name.

It is convenient to monitor a singularity by monitoring the energy since the energy is infinite for a filament with a discontinuity in its tangent field. In figures 6.6 through 6.10 we show the length and energy as a function of time for the same values of Δs as used in

figures 6.2 through 6.5. We see that the length is close to the converged result provided $\Delta s \leq 0.05$. The energy, however, has not come close to the converged result until $\Delta s \leq 0.02$. The plots of energy versus time in figures 6.9 and 6.10 are similar; one difference between the two, however, is that the energy in figure 6.10 is monotonically decreasing, whereas the energy in figure 6.9 increases in the time interval from 0.04 to 0.08. We note that in figure 6.9, $\gamma\Delta s = 0.8$, whereas in figure 6.10 $\gamma\Delta s = 0.4$. From the plots of length versus time we would estimate that the results are accurate provided $\gamma\Delta s \leq 2.0$; if we consider the plots of energy versus time we would say that we must require $\gamma\Delta s \leq 0.8$; and if we were very astute observers we may even suspect that the differences between figures 6.9 and 6.10 were indications of non-convergence and require $\gamma\Delta s \leq 0.4$. Since we are primarily interested in the length of the vortex filaments, we feel justified in choosing the restriction $\gamma\Delta s \leq 0.8$ as sufficient for calculating the lengths of vortex filaments. (We shall see shortly this is insufficient.)

We now perform numerical experiments following the work of Schwarz [39], in which we wish to calculate the equilibrium line density for a tangle of superfluid helium vortices as a function of γ, the magnitude of the velocity $\vec{v}_0$. We impose periodic boundary conditions and consider a cube whose sides are of length one. Throughout this chapter we use several different initial conditions. We calculate the evolution of the system of vortex filaments which results from a given initial condition and at each time step we calculate the total length and energy of the system. We say that a system has equilibrated when the total line length begins to oscillate about some average value. We find that the system eventually comes to an dynamic equilibrium for certain initial conditions and for other initial conditions the system decays to a state which contains no interacting vortex filaments. In figure 6.11 we show the length of the vortex filaments and the energy of the filaments as a function of time for a system which has reach equilibrium.

From the length versus time data shown in figure 6.11 we wish to calculate the time

average value of the length. Since we carry out the calculation in a unit cube this average number also gives us the average line length density per unit volume. When we calculate the average line density we do not calculate the average over the whole time interval of the calculation, but we begin to calculate the average after the system has reached equilibrium. For example in figure 6.11 we calculate the average over the interval from $t = 0.5$ to $t = 2.4$. We do not have a definite method for determining when the system has equilibrated, but we generally try to pick the equilibrium point consistently from experiment to experiment.

The choice of parameters for our first experiments is motivated by the results of the calculations summarized in figures 6.6 through 6.10. We choose $\Delta s = 0.02$, $\Delta t = 0.0001$, $\alpha = 0.01$. The initial conditions consist of four circular vortex filaments. We fix all of the parameters except for γ; we calculate the average line length density for several different values of gamma and plot the results in figure 6.12. The first plot in figure 6.12 shows the average length versus gamma and the second plot shows the average length divided by gamma versus gamma. Schwarz [39] argues that if the system of filaments is representative of homogeneous turbulence, the average length should be proportional to gamma squared and thus the second plot should be linear. (See equation (4.22) and the discussion immediately preceding it.)

For $\gamma = 20.0$ no dynamic equilibrium state was reached; the system decayed to a state consisting of two parallel vortex filaments; this fact led us to use initial conditions which were "more turbulent" so we could determine if an equilibrium state were possible for $\gamma \leq 20.0$. For the second initial conditions we use the state obtained from the original initial conditions with $\gamma = 45.0$ and time $t = 0.8$; the system is filled by a vortex tangle initially.

In the first plot of figure 6.13 we show the average line length versus γ. The data points represented by squares are calculated from the first initial conditions and the data

points represented by octagons are calculated from the second initial conditions. The first plot shows two things: (1) that an equilibrium state is possible for most values of γ, provided the initial conditions are sufficiently "turbulent" and (2) that the line length density is independent of initial conditions. It is difficult to say when initial conditions are "turbulent" enough, but care must be taken when one draws conclusions about the existence of an equilibrium state based on calculations of only a single initial condition. Based on the calculations from the first initial condition, we would conclude that a critical velocity exists below which no dynamic equilibrium is possible.

In the second plot of figure 6.13 we plot the length divided by γ versus γ. The main feature of this plot is the fact that the values of the points for which $\gamma \leq 25.0$ are roughly constant or even decrease slightly as γ increases, while the values of the points for which $\gamma > 25.0$ increase linearly as γ increrases. Also a noticeable jump occurs between the point at $\gamma = 25.0$ and the point at $\gamma = 30.0$. The jump is the first indication that the calculations are inaccurate if $\gamma\Delta s > 0.5$.

In order to verify that the jump occuring in figure 6.13 is due to an inaccuracy we must calculate the line densities with values of Δs so that $\gamma\Delta s \leq 0.5$ and see if these values agree with those already calculated. In figure 6.14 we show the line length density versus γ. The data points denoted by squares were calculated with a choice of parameters such that $\gamma\Delta s \leq 0.5$ and those denoted by octagons were calculated with $\gamma\Delta s > 0.5$. From the second plot in figure 6.14 it is clear that the line length density is not proportional to γ^2, but increases even slower than a linear function of α. It is interesting to note that the line densities obtained from the inaccurate calculations are proportional to γ^2; furthermore the line in the second plot of figure 6.14 corresponds to the data presented by Schwarz [39].

In figure 6.15 we show the results of calculations carried out with $\alpha = 0.03$. The points represented by octagons are calculated with $\gamma\Delta s > 0.5$ and the point represented by a square satisfies $\gamma\Delta s = 0.5$. Once again we see that the inaccurate calculation indicates

that the line length density is proportional to γ^2. The line through the data points is the least squares fit of the data to a straight line passing through the origin and the upper line is the data presented by Schwarz [39]. From figures 6.14 and 6.15 we conclude that the calculations performed in reference [39] were carried out with a choice of parameters that do not ensure accuracy.

In figures 6.16 and 6.17 we show the results of calculations with $\alpha = 0.01$ and $\alpha = 0.3$. The data points satisfy the accuracy condition (6.1) and the lines represent the results of Schwarz [39].

We conclude that equation (4.21) does not correctly model homogeneous turbulence in superfluid Helium. The correct functional dependence of the line length density on the magnitude of the counterflow velocity $|\vec{v}_0|$ is obtained when the distance between approximation points is too large; when this occurs the calculated vortices tend to stretch at points of reconnection rather than contract, as the model equation (4.21) requires. This indicates that the problem with model equation (4.21) is that the vortices contract when singularities (kinks) are introduced, whereas there should be stretching occuring at kinks similar to that which occurs in ordinary fluids [8].

figure 6.1

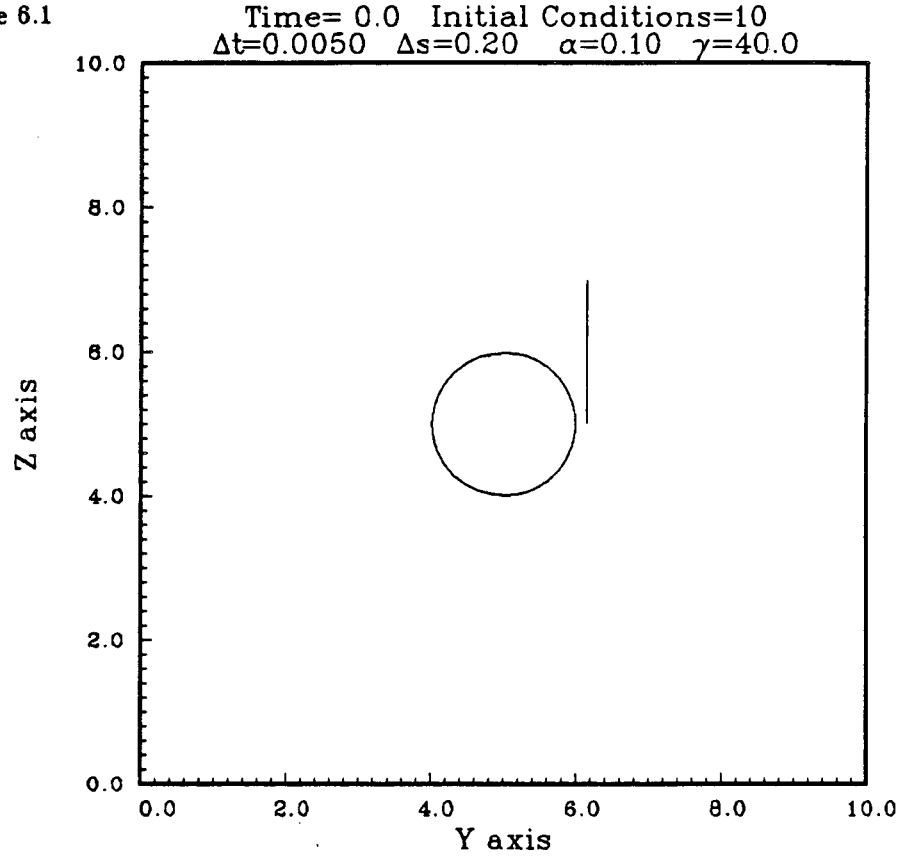
Time= 0.0 Initial Conditions=10
Δt=0.0050 Δs=0.20 α=0.10 γ=40.0
10.0
8.0
6.0
4.0
2.0
0.0
Z axis
0.0
2.0
4.0
6.0
8.0
10.0
Y axis

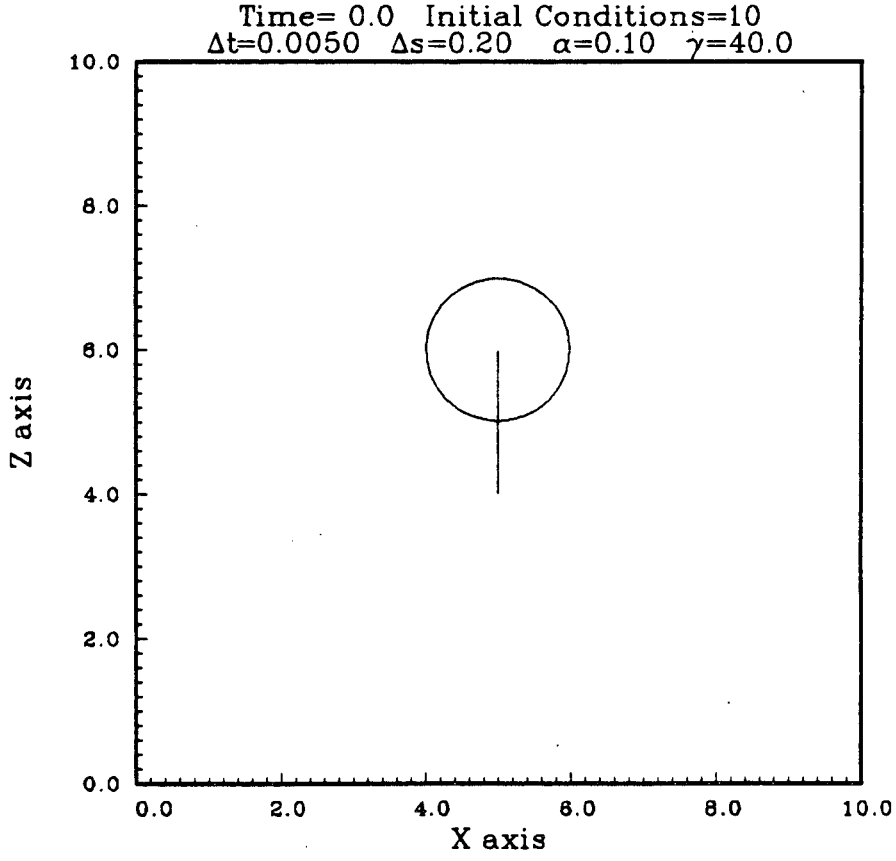
Time= 0.0 Initial Conditions=10
Δt=0.0050 Δs=0.20 α=0.10 γ=40.0
10.0
8.0
6.0
4.0
2.0
0.0
Z axis
0.0
2.0
4.0
6.0
8.0
10.0
X axis

figure 6.2

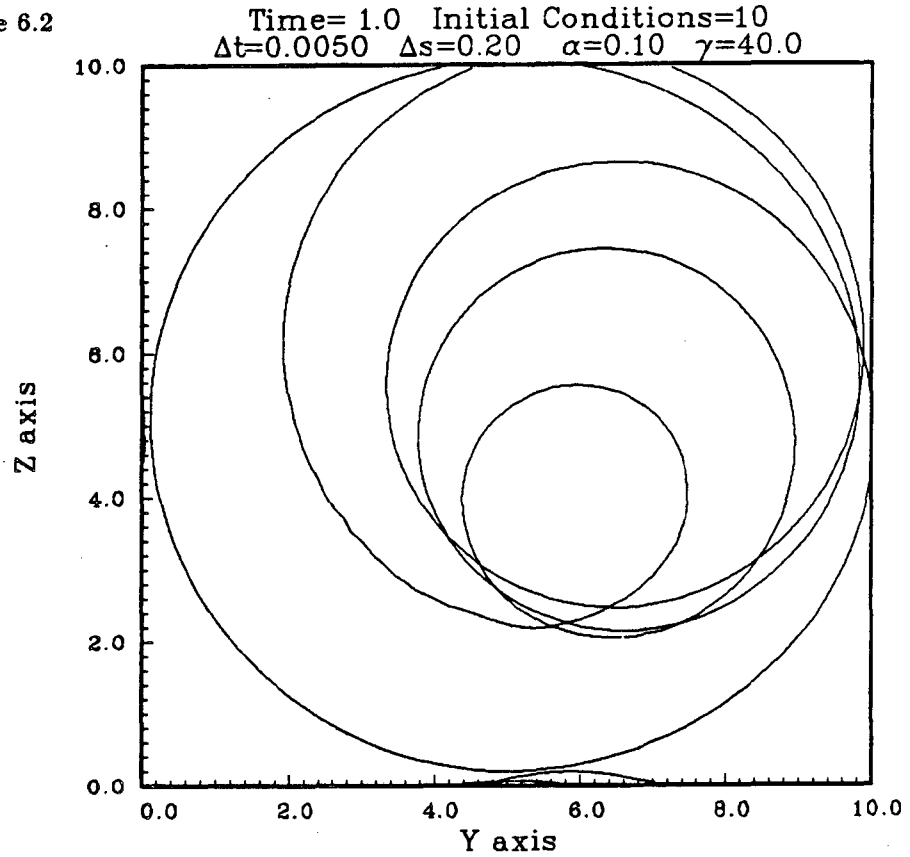
Time= 1.0 Initial Conditions=10
Δt=0.0050 Δs=0.20 α=0.10 γ=40.0
Z axis
Y axis
0.0
2.0
4.0
6.0
8.0
10.0

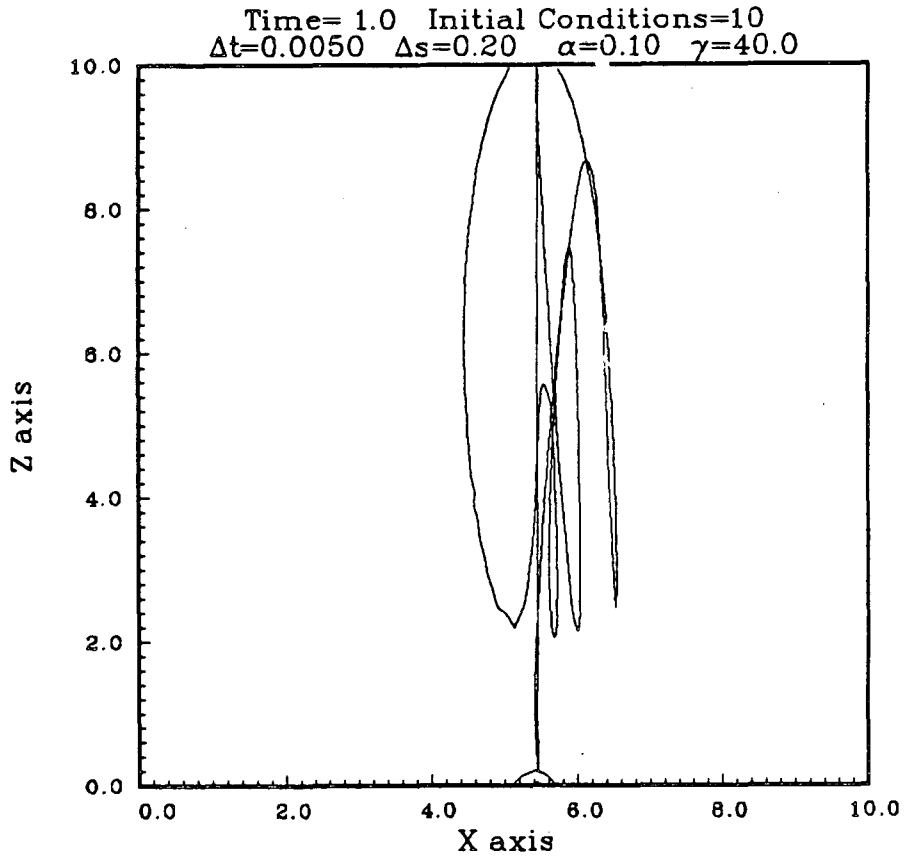
Time= 1.0 Initial Conditions=10
Δt=0.0050 Δs=0.20 α=0.10 γ=40.0
Z axis
X axis
0.0
2.0
4.0
6.0
8.0
10.0

figure 6.3

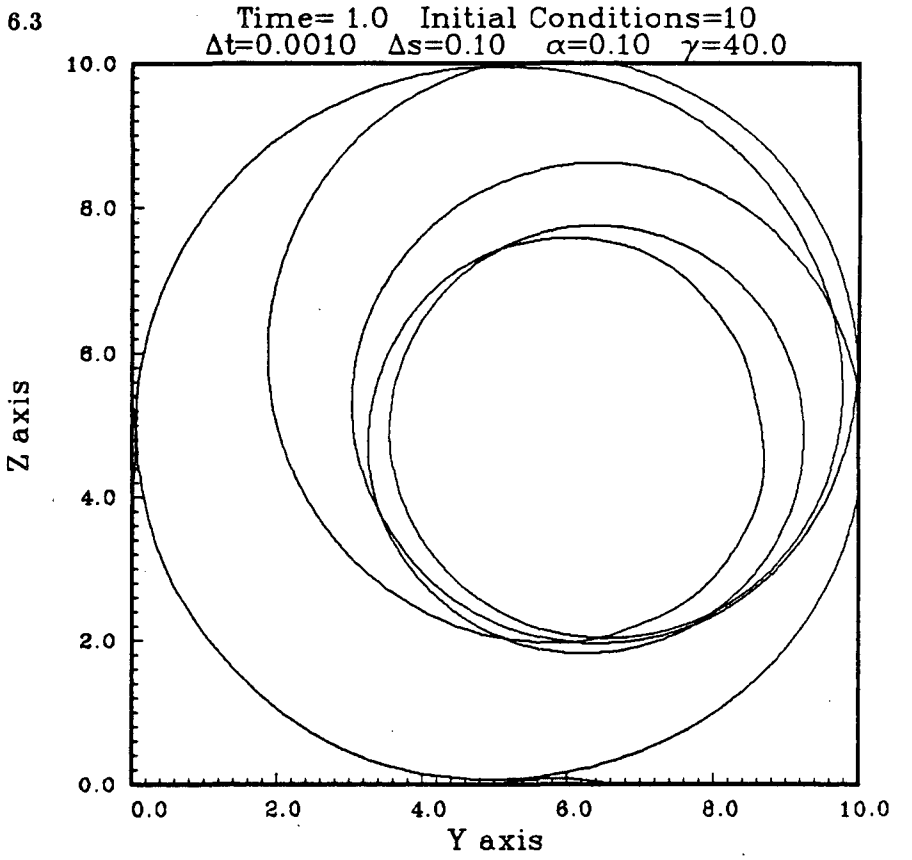
Time= 1.0 Initial Conditions=10
Δt=0.0010 Δs=0.10 α=0.10 γ=40.0
Z axis
Y axis
0.0
2.0
4.0
6.0
8.0
10.0

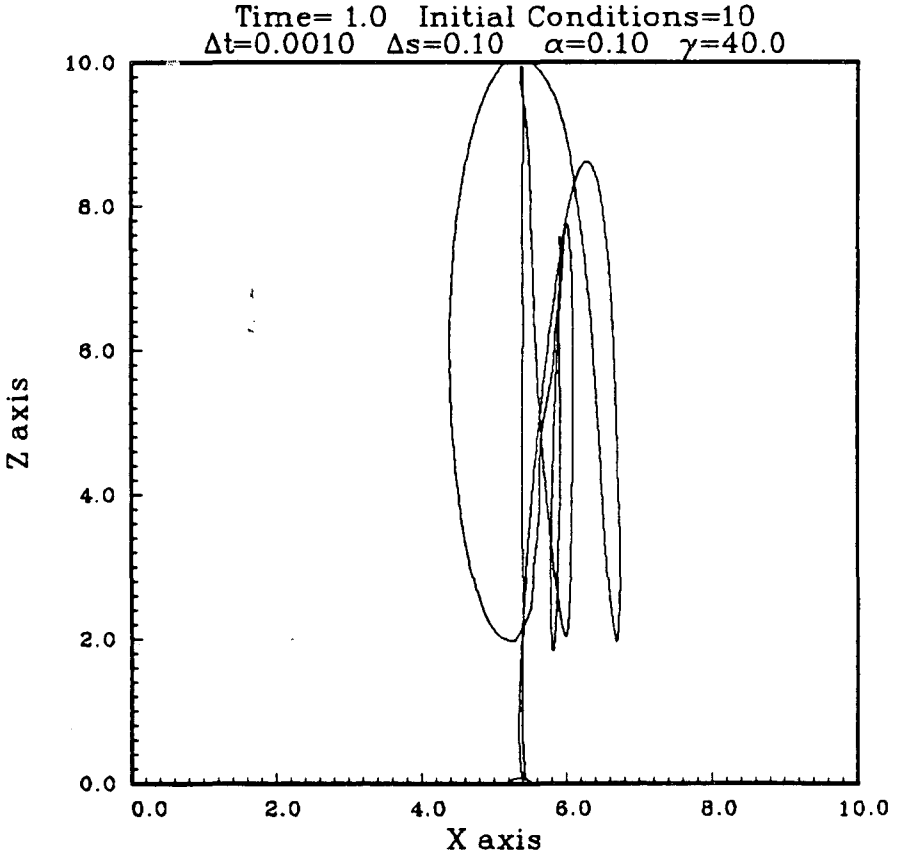
Time= 1.0 Initial Conditions=10
Δt=0.0010 Δs=0.10 α=0.10 γ=40.0
Z axis
X axis
0.0
2.0
4.0
6.0
8.0
10.0

figure 6.4

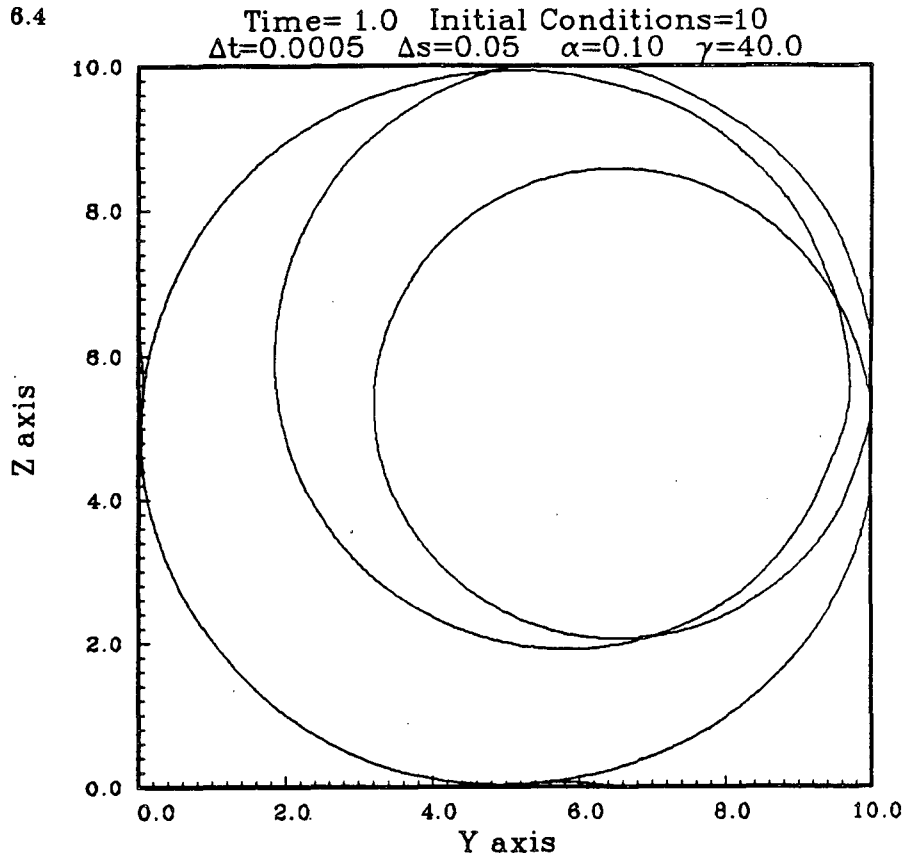
Time= 1.0 Initial Conditions=10
Δt=0.0005 Δs=0.05 α=0.10 γ=40.0
10.0
8.0
6.0
4.0
2.0
0.0
Z axis
0.0
2.0
4.0
6.0
8.0
10.0
Y axis

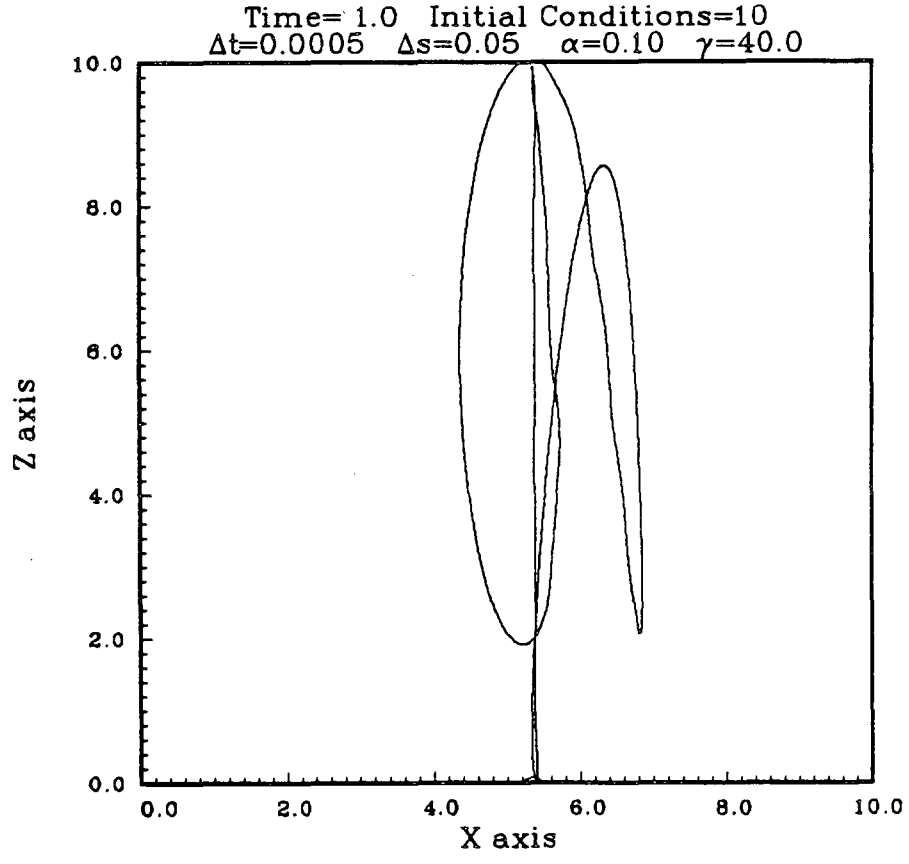
Time= 1.0 Initial Conditions=10
Δt=0.0005 Δs=0.05 α=0.10 γ=40.0
10.0
8.0
6.0
4.0
2.0
0.0
Z axis
0.0
2.0
4.0
6.0
8.0
10.0
X axis

figure 6.5

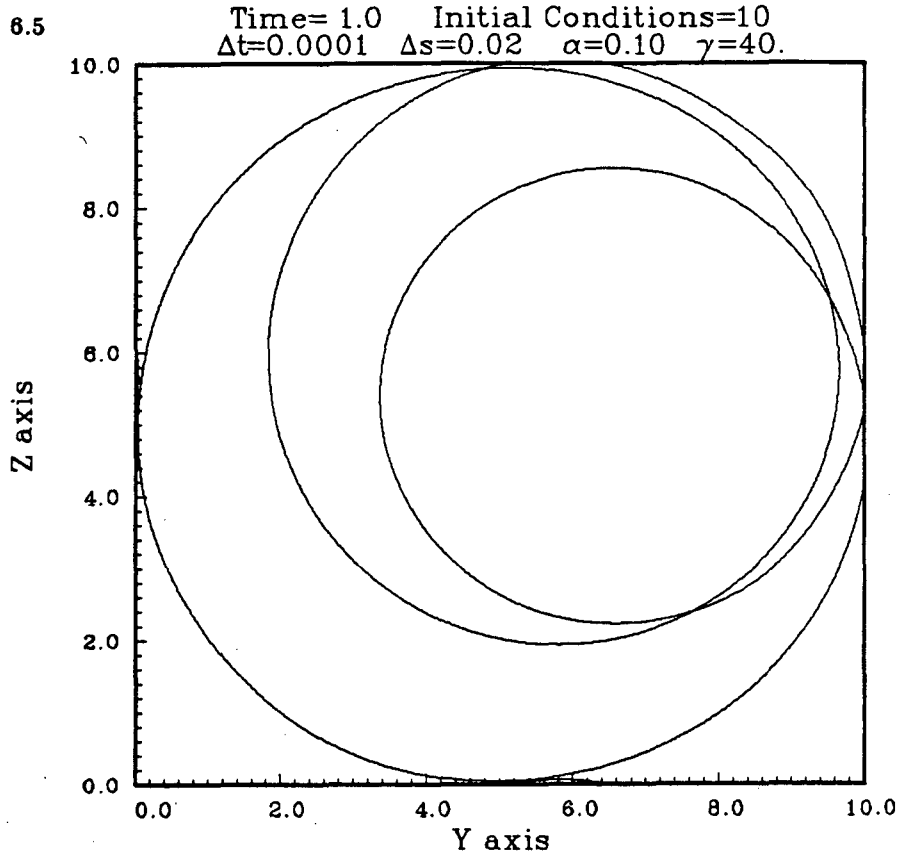
Time= 1.0 Initial Conditions=10
Δt=0.0001 Δs=0.02 α=0.10 γ=40.
10.0
8.0
6.0
4.0
2.0
0.0
Z axis
0.0
2.0
4.0
6.0
8.0
10.0
Y axis

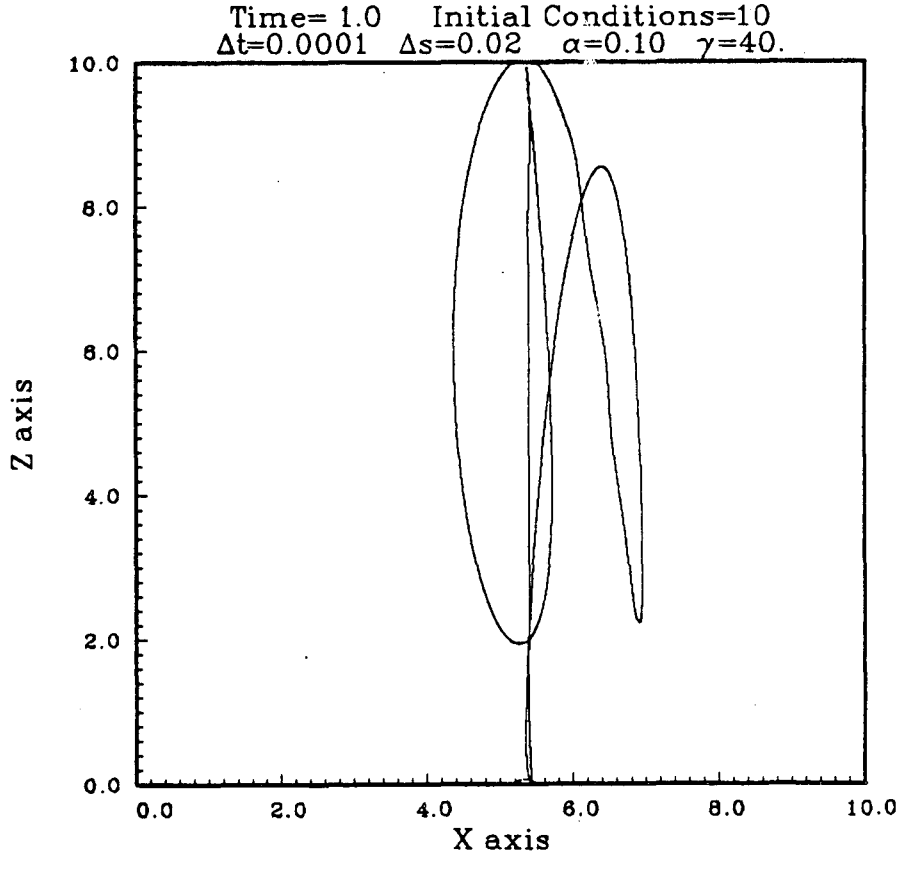
Time= 1.0 Initial Conditions=10
Δt=0.0001 Δs=0.02 α=0.10 γ=40.
10.0
8.0
6.0
4.0
2.0
0.0
Z axis
0.0
2.0
4.0
6.0
8.0
10.0
X axis

figure 6.6

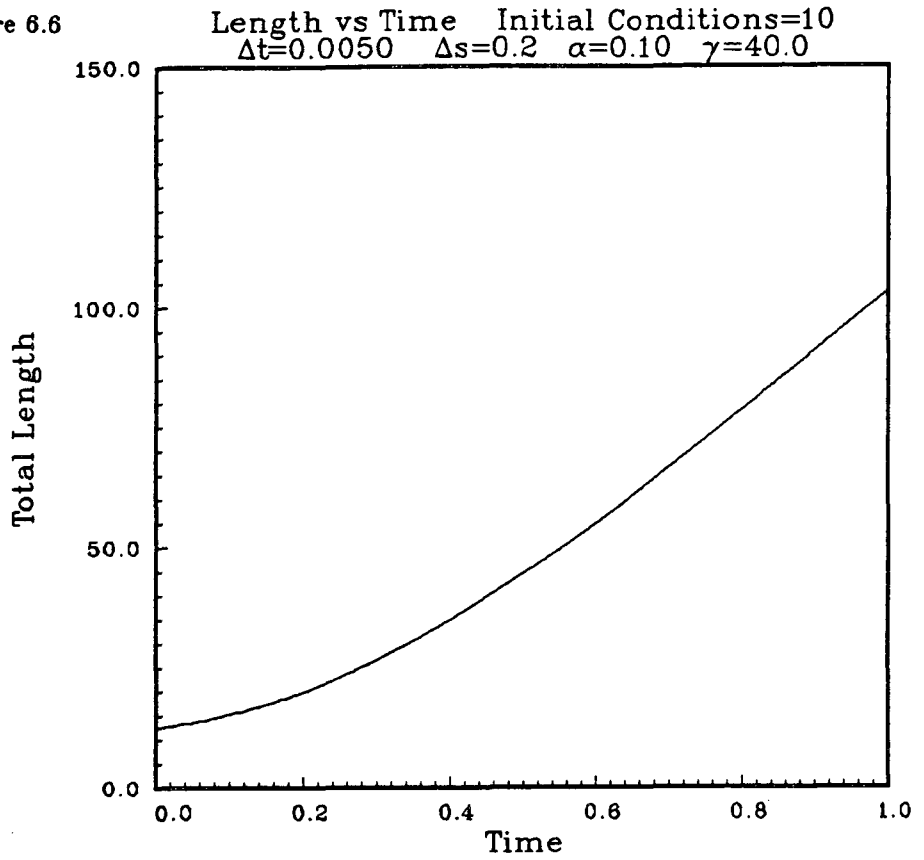
Length vs Time Initial Conditions=10
Δt=0.0050 Δs=0.2 α=0.10 γ=40.0
150.0
100.0
50.0
0.0
Total Length
0.0
0.2
0.4
0.6
0.8
1.0
Time

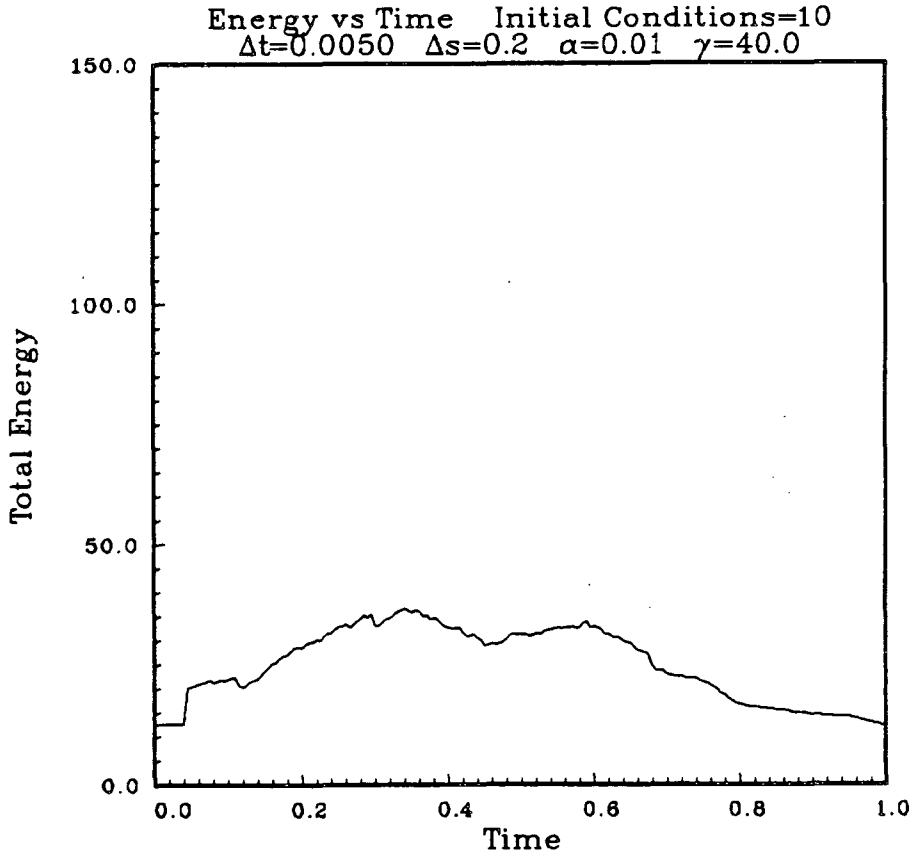
Energy vs Time Initial Conditions=10
Δt=0.0050 Δs=0.2 α=0.01 γ=40.0
150.0
100.0
50.0
0.0
Total Energy
0.0
0.2
0.4
0.6
0.8
1.0
Time

figure 6.7

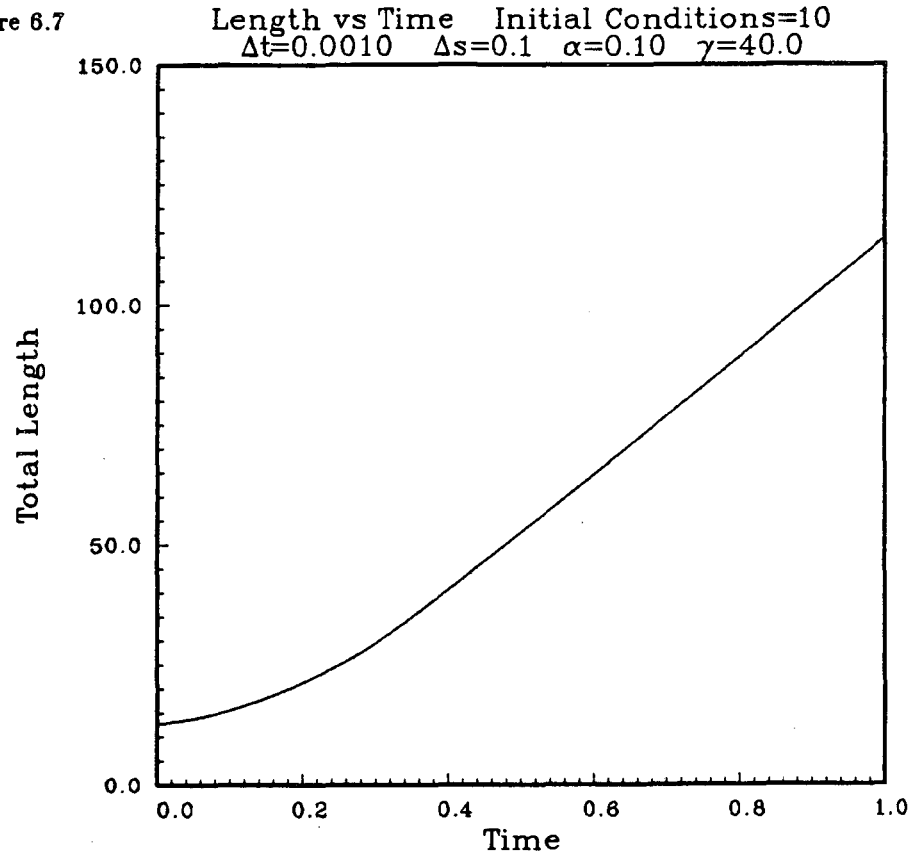
Length vs Time Initial Conditions=10
Δt=0.0010 Δs=0.1 α=0.10 γ=40.0
150.0
100.0
50.0
0.0
Total Length
0.0
0.2
0.4
0.6
0.8
1.0
Time

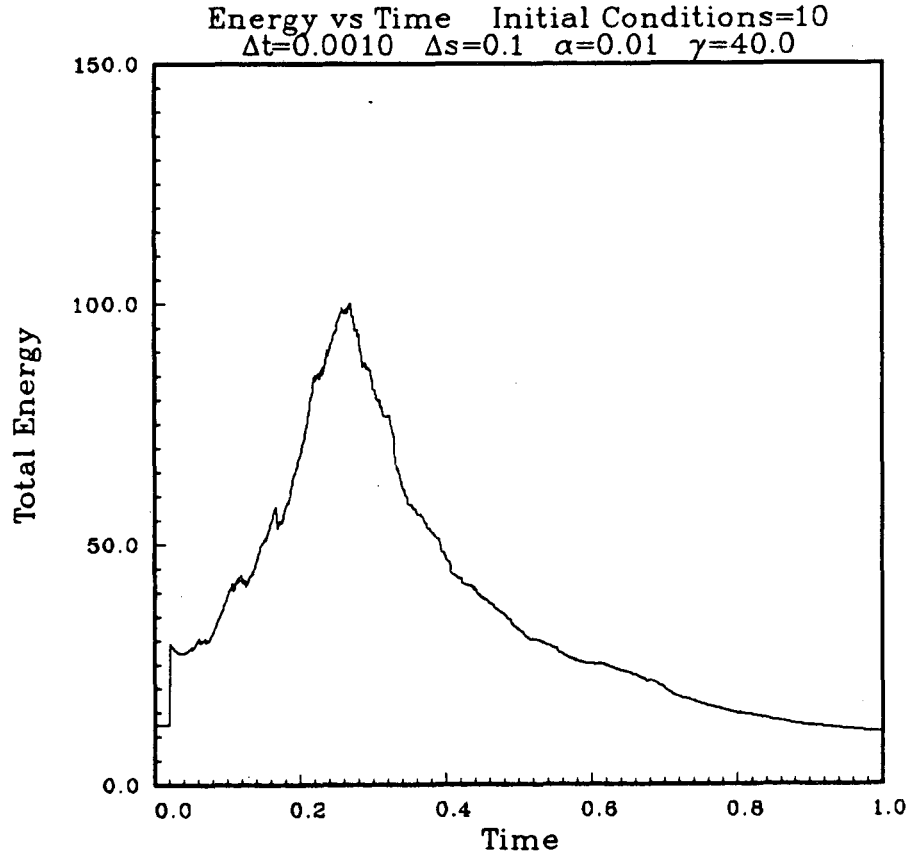
Energy vs Time Initial Conditions=10
Δt=0.0010 Δs=0.1 α=0.01 γ=40.0
150.0
100.0
50.0
0.0
Total Energy
0.0
0.2
0.4
0.6
0.8
1.0
Time

figure 6.8

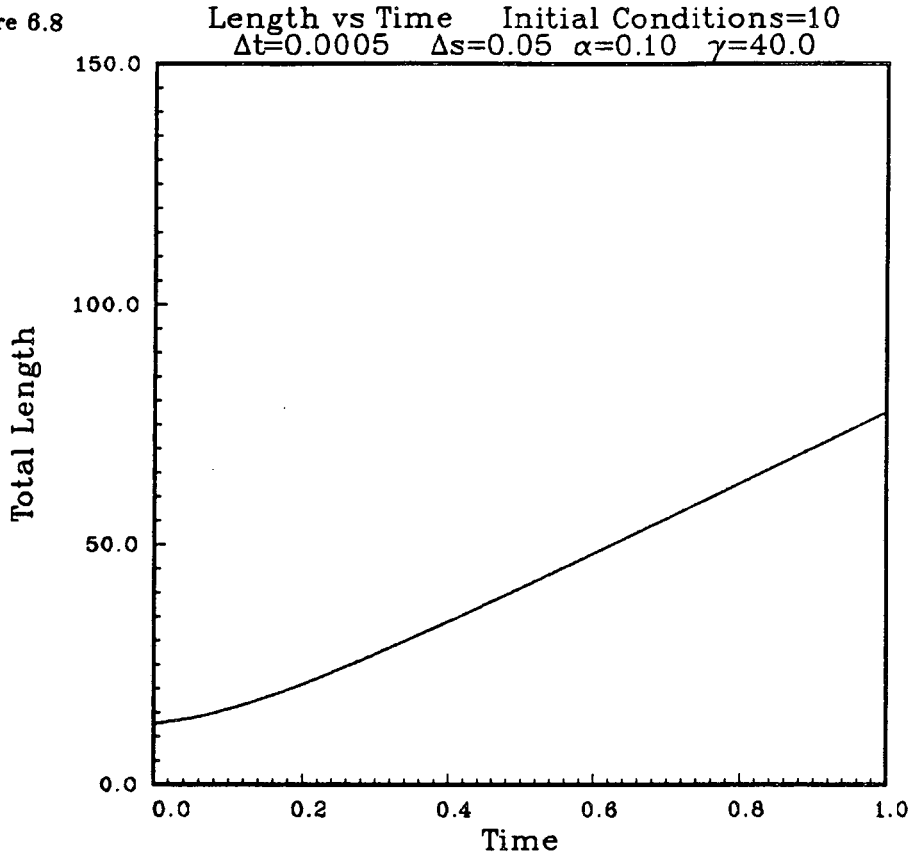
Length vs Time Initial Conditions=10
Δt=0.0005 Δs=0.05 α=0.10 γ=40.0
150.0
100.0
50.0
0.0
Total Length
0.0
0.2
0.4
0.6
0.8
1.0
Time

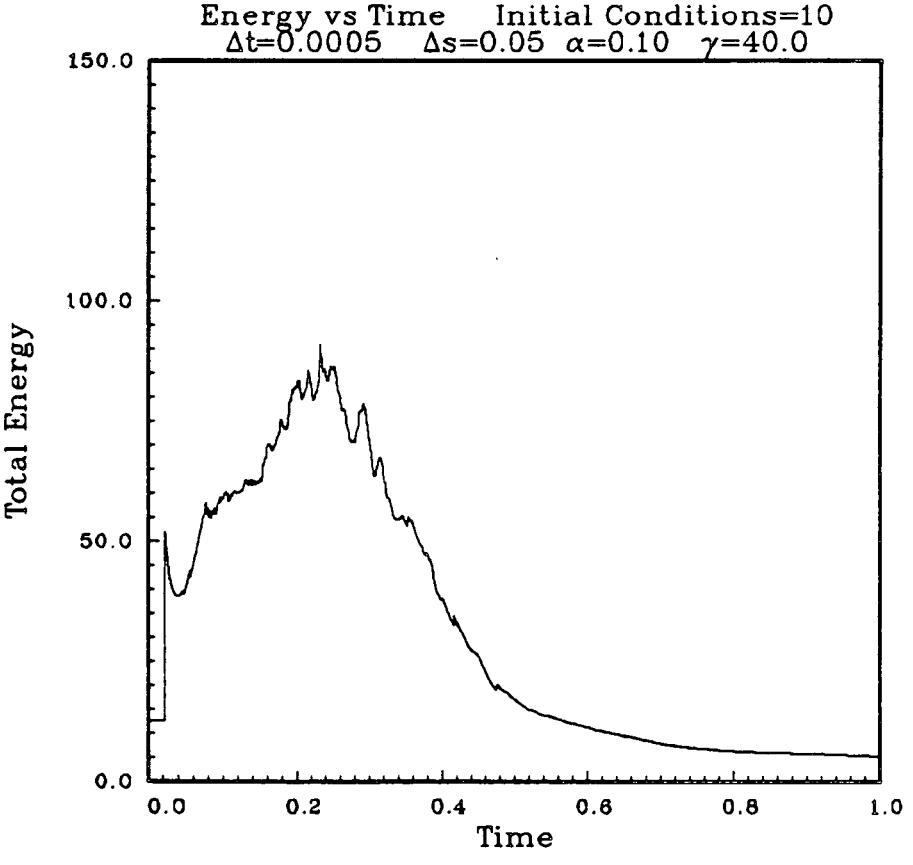
Energy vs Time Initial Conditions=10
Δt=0.0005 Δs=0.05 α=0.10 γ=40.0
150.0
100.0
50.0
0.0
Total Energy
0.0
0.2
0.4
0.6
0.8
1.0
Time

figure 6.9

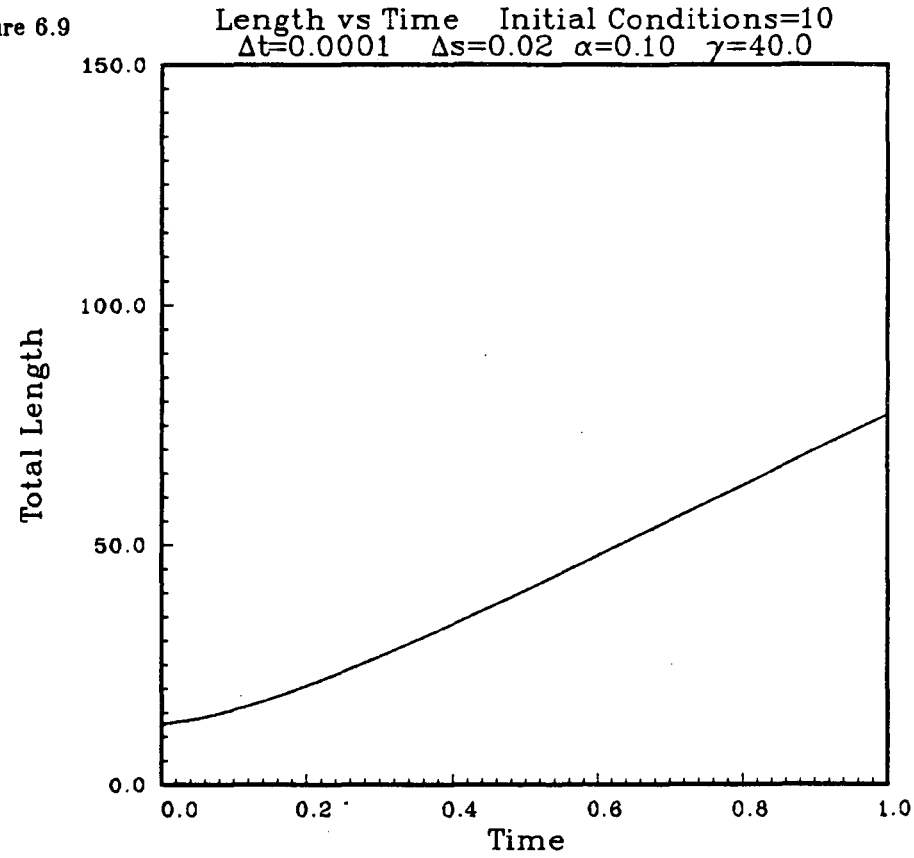
Length vs Time Initial Conditions=10
Δt=0.0001 Δs=0.02 α=0.10 γ=40.0
150.0
100.0
50.0
0.0
Total Length
0.0
0.2
0.4
0.6
0.8
1.0
Time

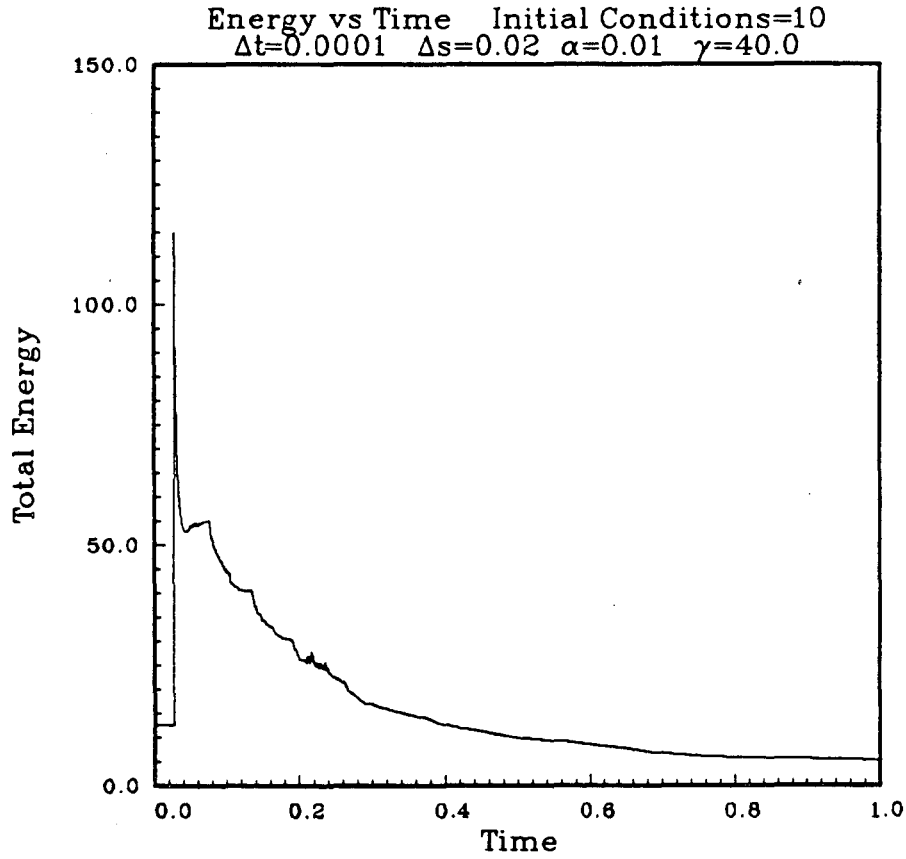
Energy vs Time Initial Conditions=10
Δt=0.0001 Δs=0.02 α=0.01 γ=40.0
150.0
100.0
50.0
0.0
Total Energy
0.0
0.2
0.4
0.6
0.8
1.0
Time

figure 6.10

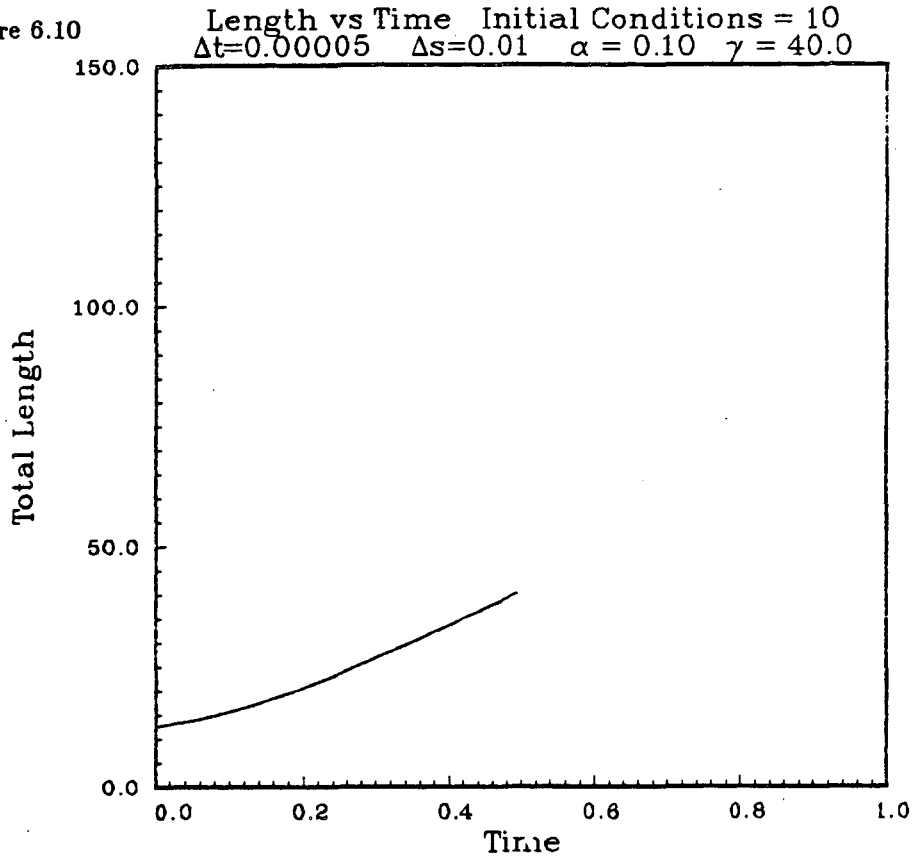
Length vs Time Initial Conditions = 10
Δt=0.00005 Δs=0.01 α = 0.10 γ = 40.0
150.0
100.0
50.0
0.0
Total Length
0.0
0.2
0.4
0.6
0.8
1.0
Time

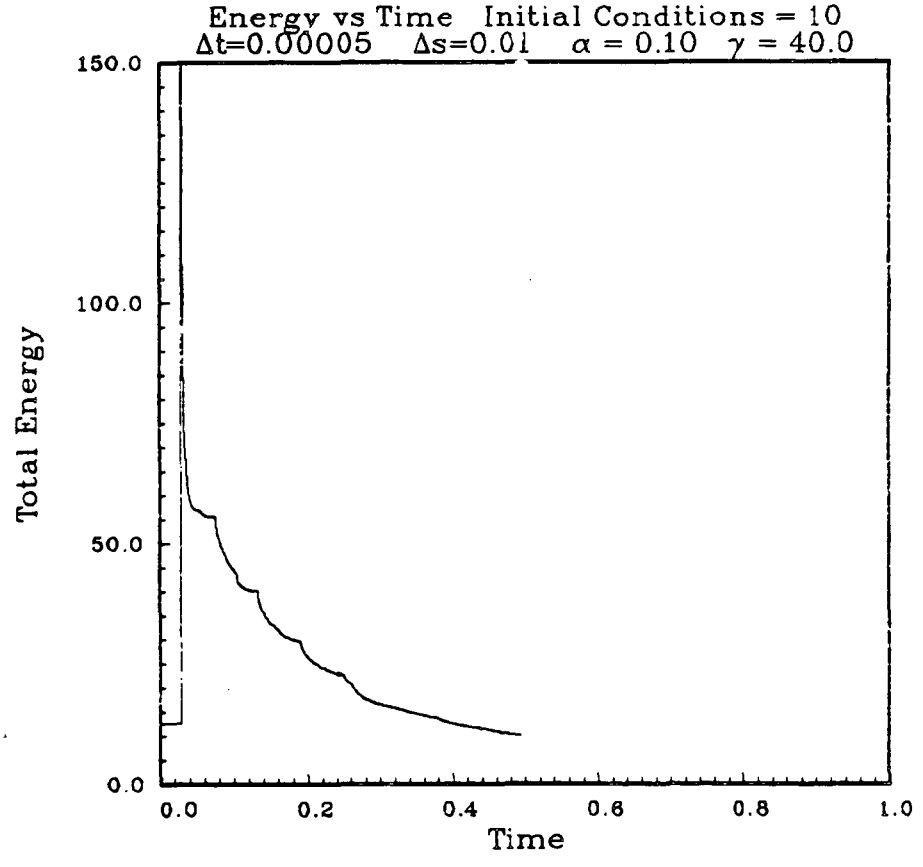
Energy vs Time Initial Conditions = 10
Δt=0.00005 Δs=0.01 α = 0.10 γ = 40.0
150.0
100.0
50.0
0.0
Total Energy
0.0
0.2
0.4
0.6
0.8
1.0
Time

figure 6.11

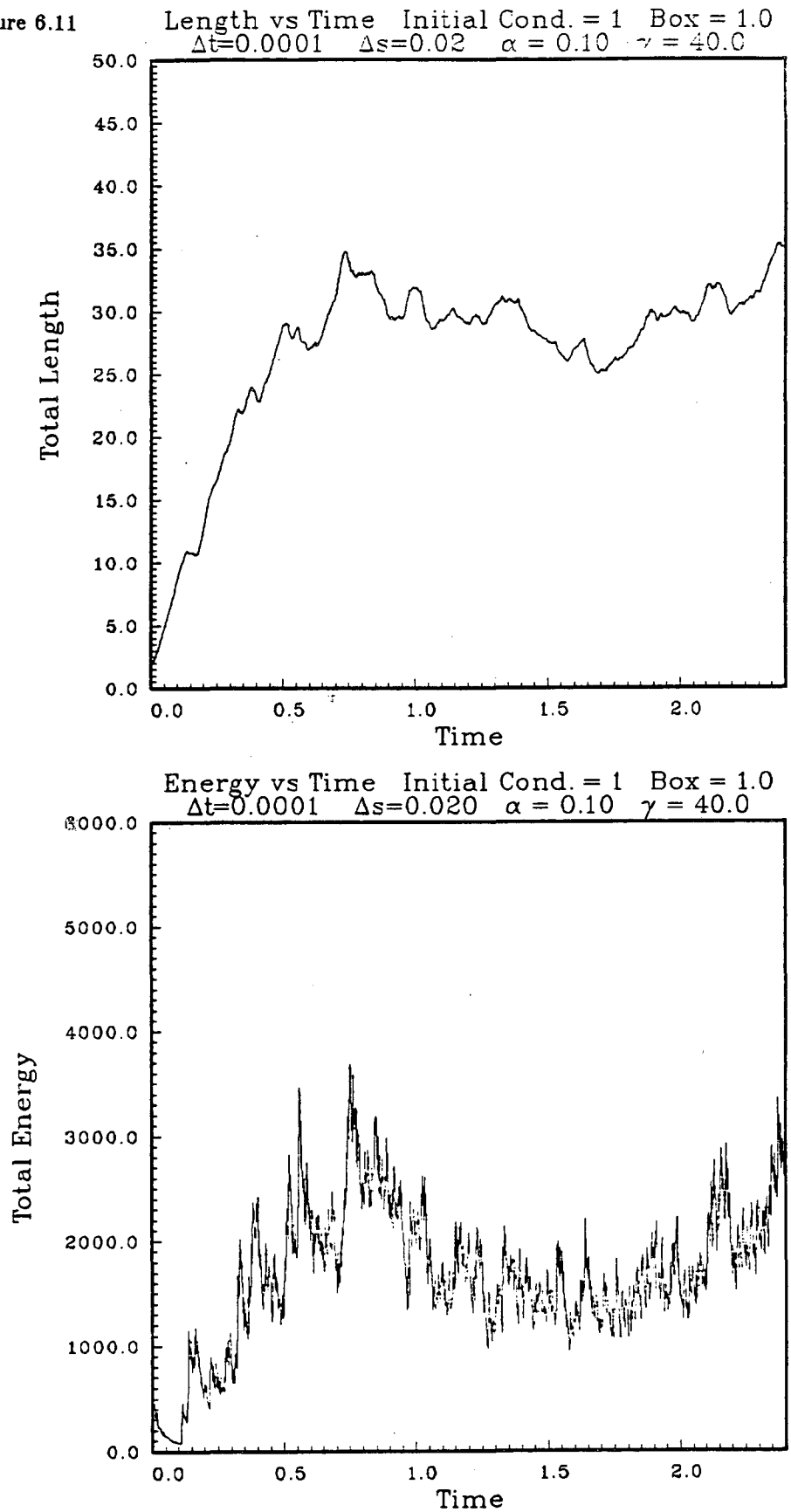
Length vs Time Initial Cond. = 1 Box = 1.0
Δt=0.0001 Δs=0.02 α = 0.10 γ = 40.0
Total Length
Time
0.0
5.0
10.0
15.0
20.0
25.0
30.0
35.0
40.0
45.0
50.0
0.5
1.0
1.5
2.0
Energy vs Time Initial Cond. = 1 Box = 1.0
Δt=0.0001 Δs=0.020 α = 0.10 γ = 40.0
Total Energy
Time
1000.0
2000.0
3000.0
4000.0
5000.0
6000.0

figure 6.12

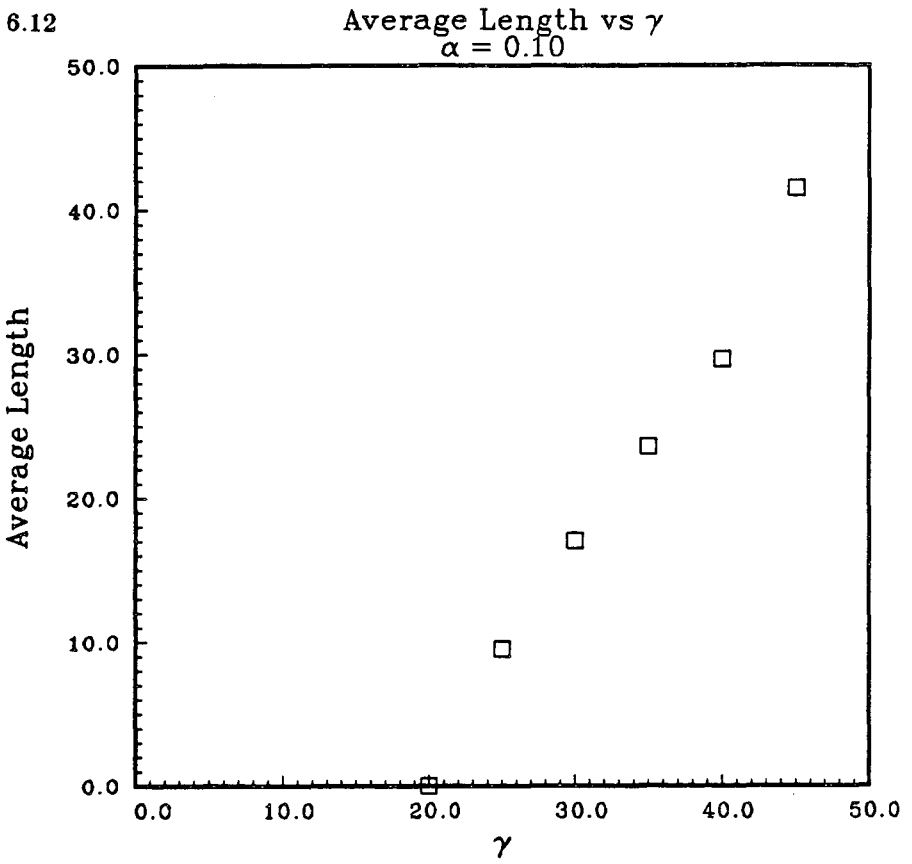
Average Length vs γ
α = 0.10
Average Length
γ
0.0
10.0
20.0
30.0
40.0
50.0

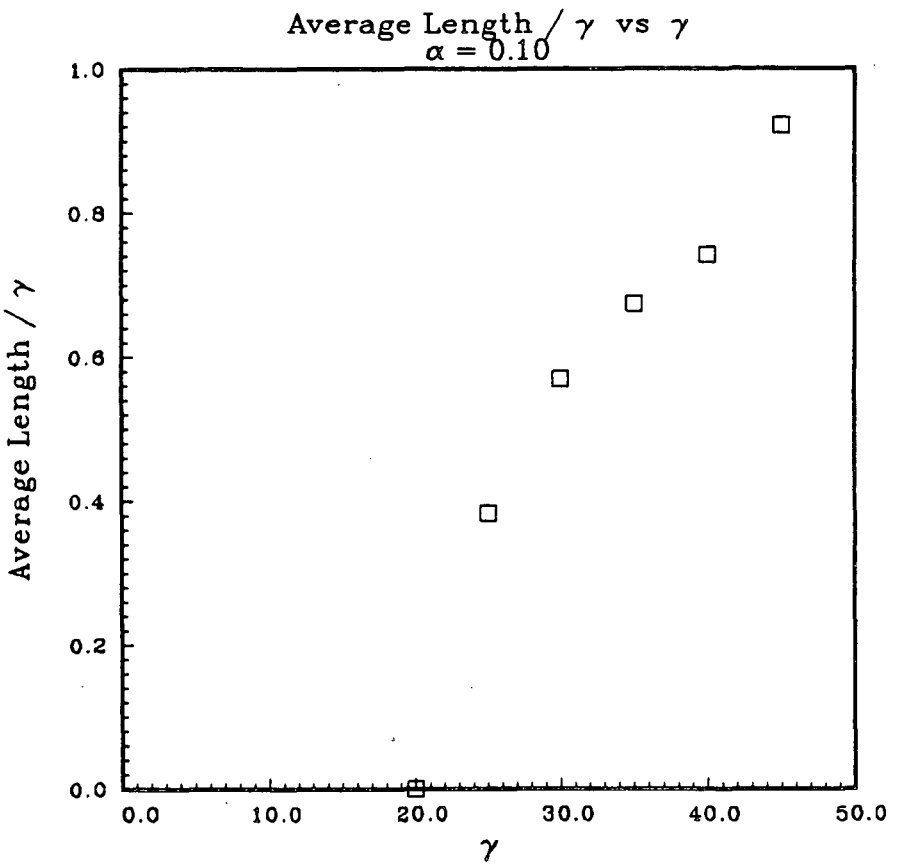
Average Length / γ vs γ
α = 0.10
Average Length / γ
γ
0.0
0.2
0.4
0.6
0.8
1.0
10.0
20.0
30.0
40.0
50.0

figure 6.13

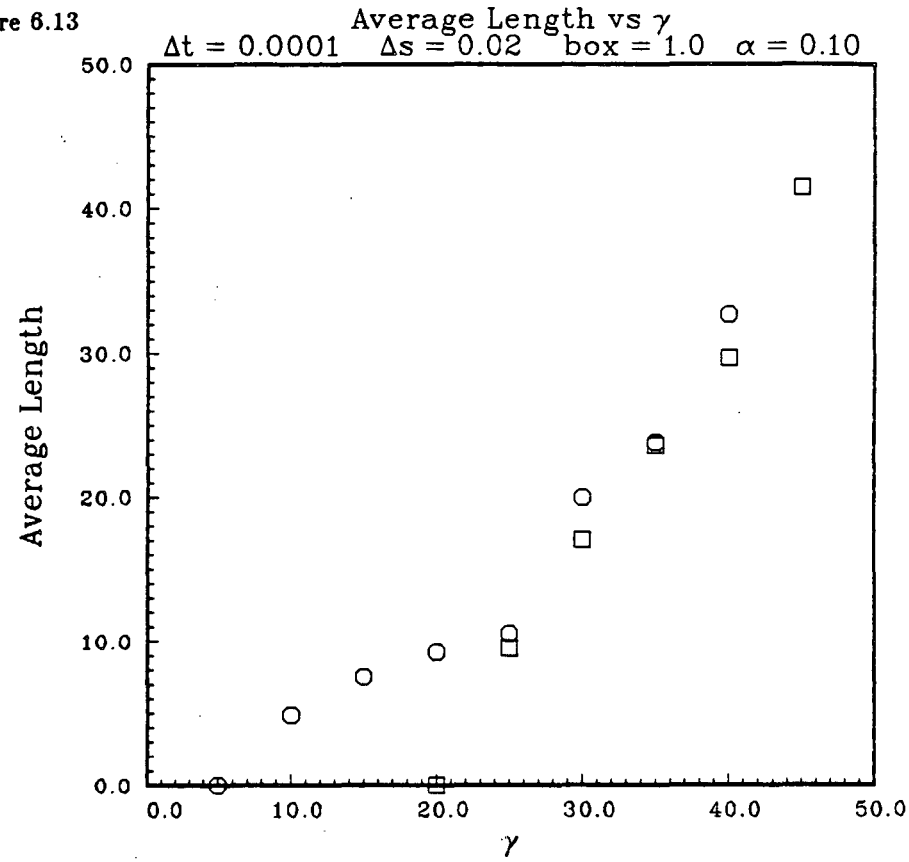
Average Length vs γ
Δt = 0.0001 Δs = 0.02 box = 1.0 α = 0.10
Average Length
γ
0.0
10.0
20.0
30.0
40.0
50.0

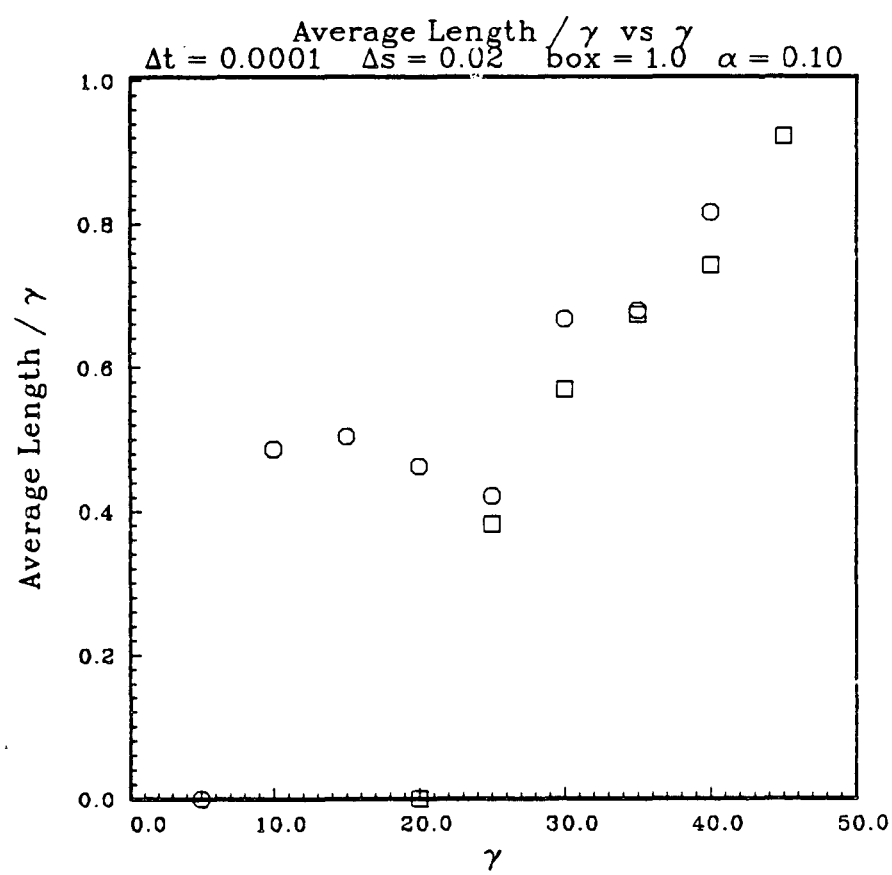
Average Length / γ vs γ
Δt = 0.0001 Δs = 0.02 box = 1.0 α = 0.10
Average Length / γ
γ
0.0
0.2
0.4
0.6
0.8
1.0
10.0
20.0
30.0
40.0
50.0

figure 6.14

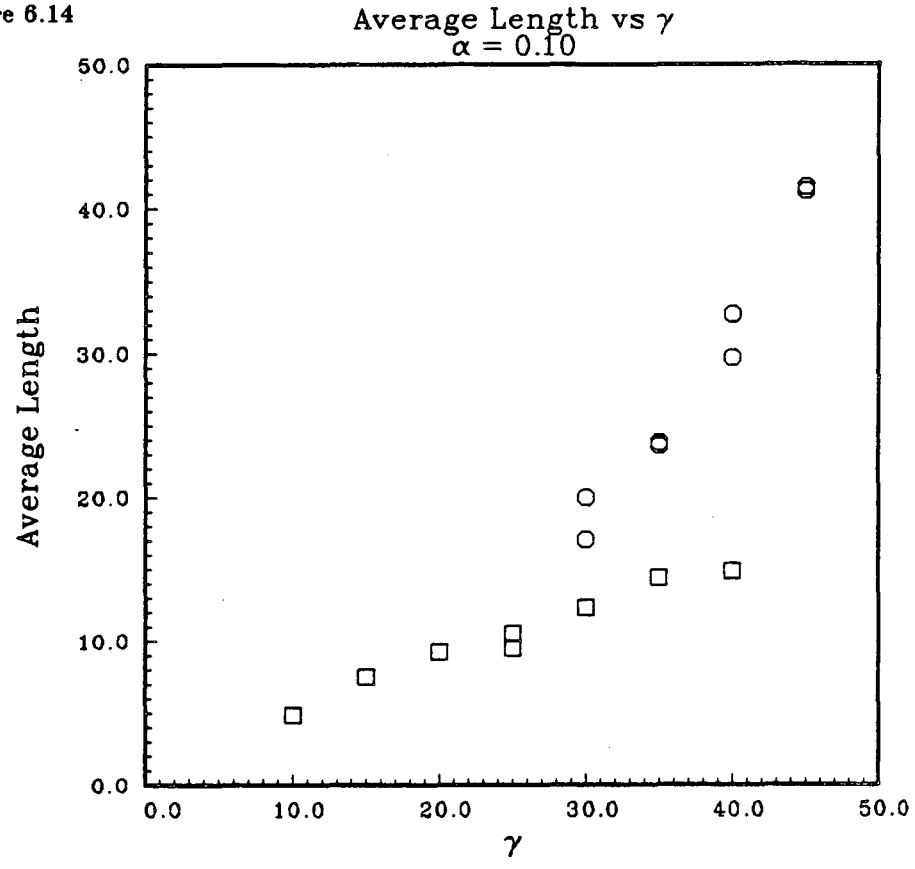
Average Length vs γ
α = 0.10
Average Length
γ
0.0
10.0
20.0
30.0
40.0
50.0

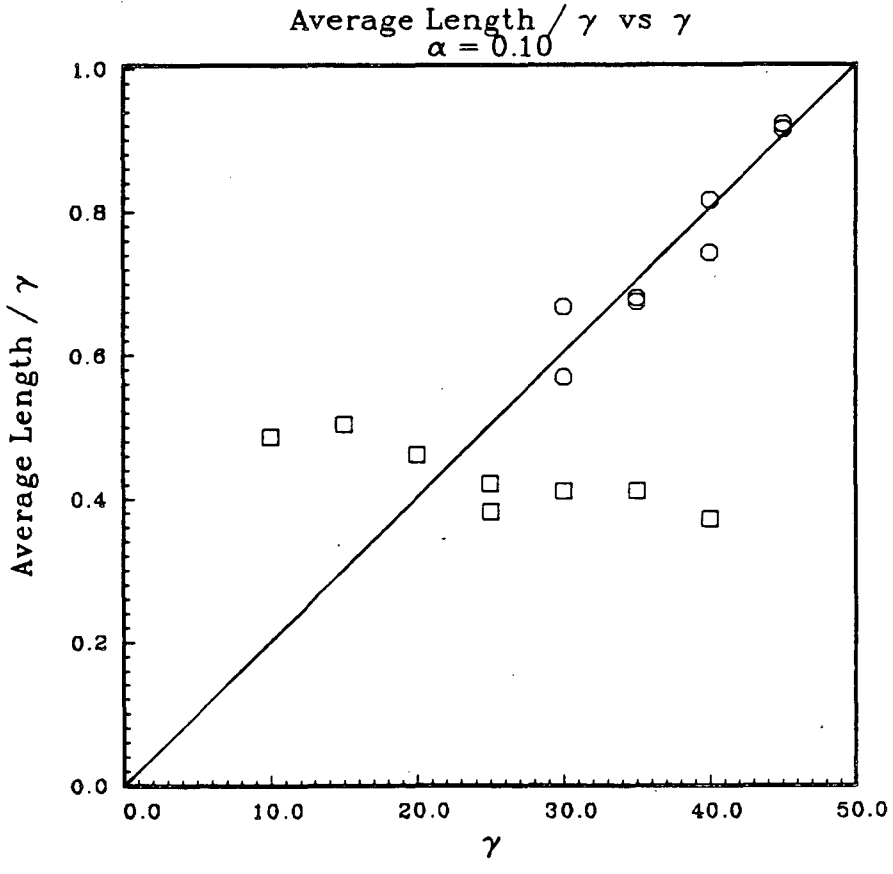
Average Length / γ vs γ
α = 0.10
Average Length / γ
γ
0.0
0.2
0.4
0.6
0.8
1.0
10.0
20.0
30.0
40.0
50.0

figure 6.15

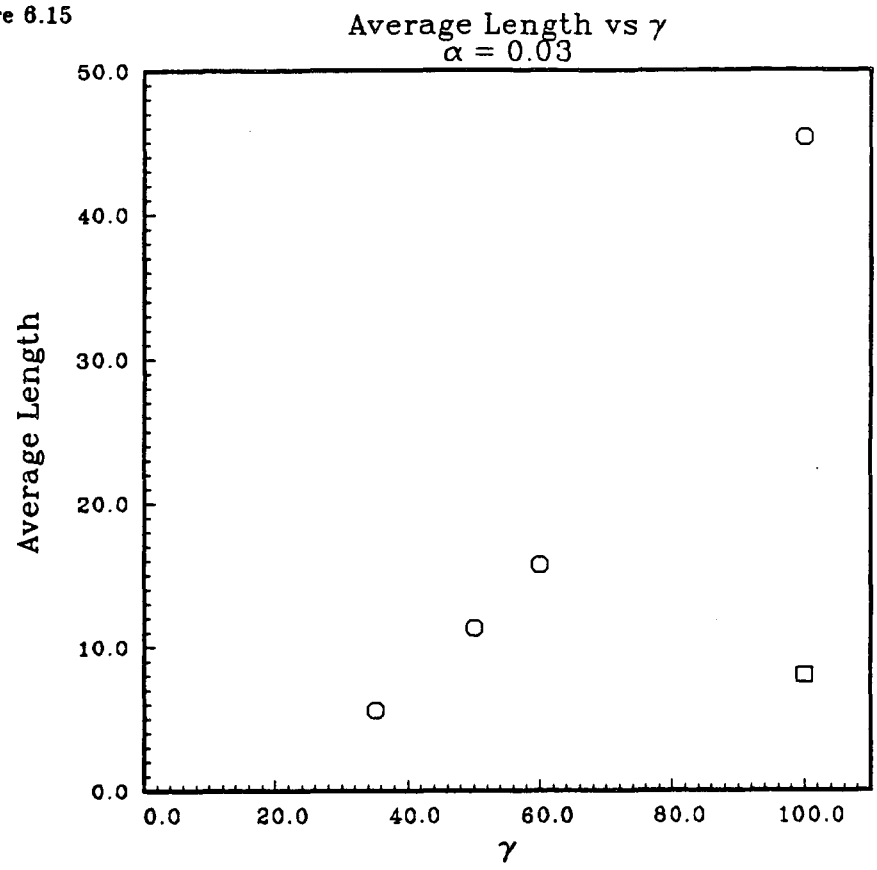
Average Length vs γ
α = 0.03
Average Length
50.0
40.0
30.0
20.0
10.0
0.0
0.0
20.0
40.0
60.0
80.0
100.0
γ

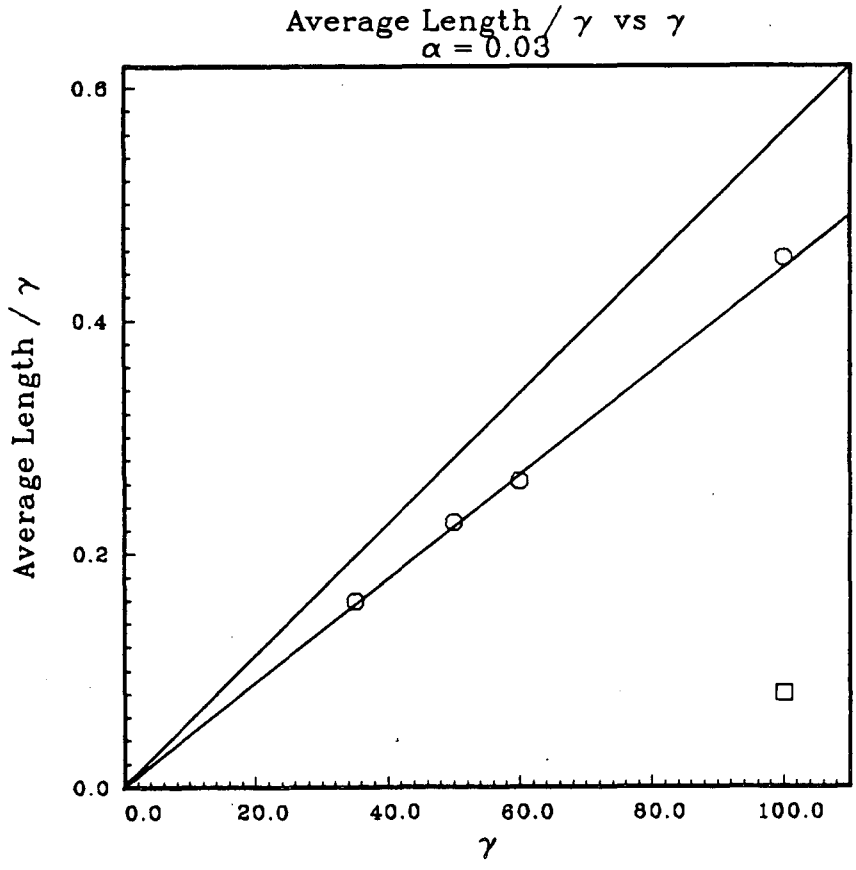
Average Length / γ vs γ
α = 0.03
Average Length / γ
0.6
0.4
0.2
0.0
0.0
20.0
40.0
60.0
80.0
100.0
γ

figure 6.16

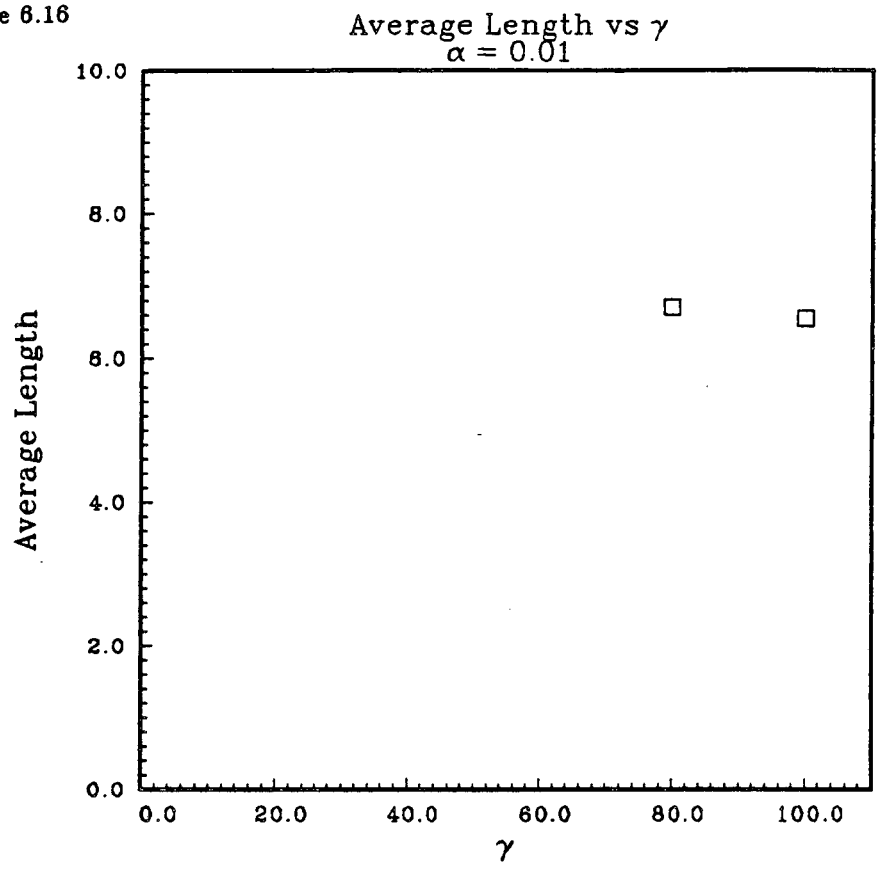
Average Length vs γ
α = 0.01
Average Length
10.0
8.0
6.0
4.0
2.0
0.0
0.0
20.0
40.0
60.0
80.0
100.0
γ

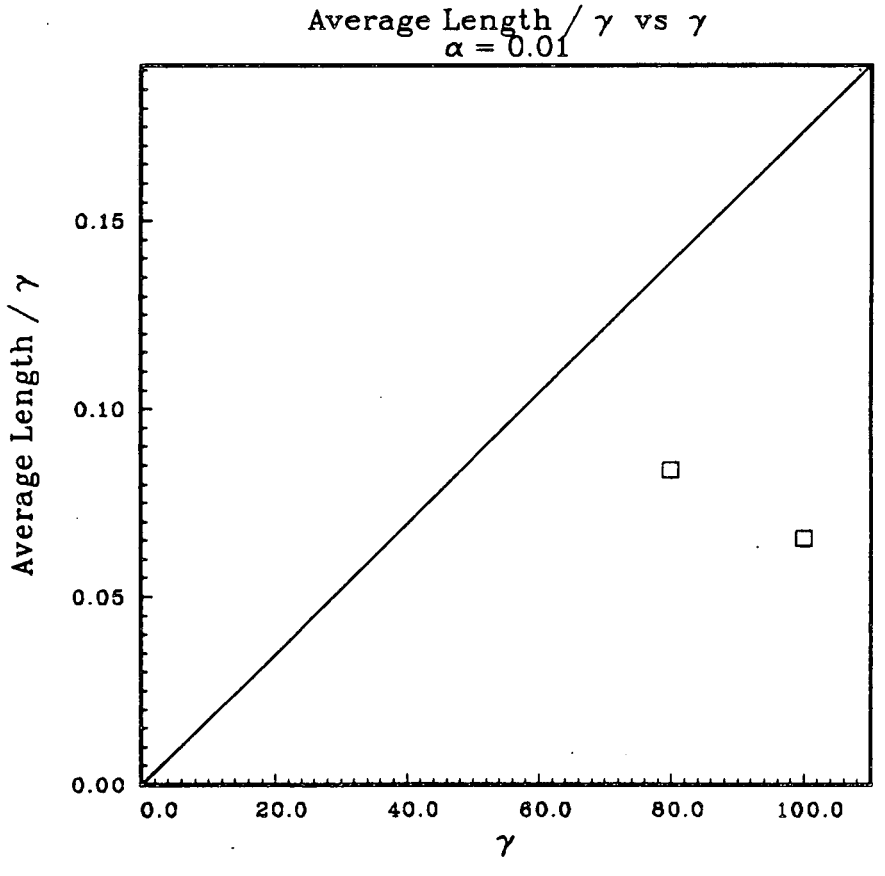
Average Length / γ vs γ
α = 0.01
Average Length / γ
0.15
0.10
0.05
0.00
0.0
20.0
40.0
60.0
80.0
100.0
γ

figure 6.17

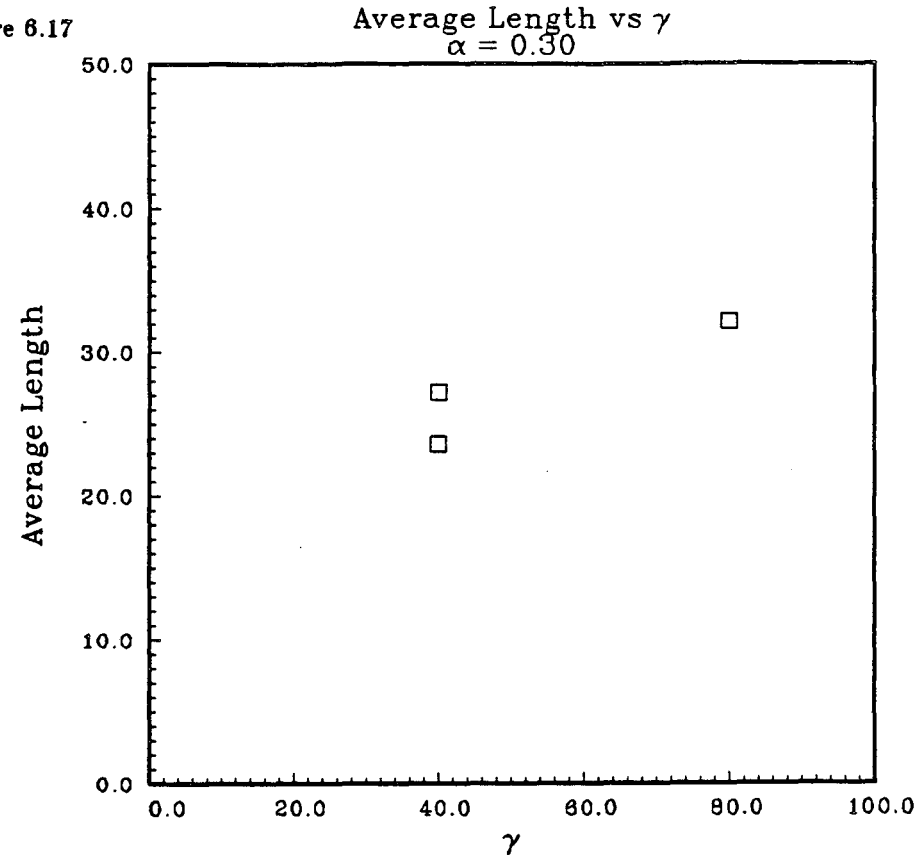
Average Length vs γ
α = 0.30
Average Length
50.0
40.0
30.0
20.0
10.0
0.0
0.0
20.0
40.0
60.0
80.0
100.0
γ

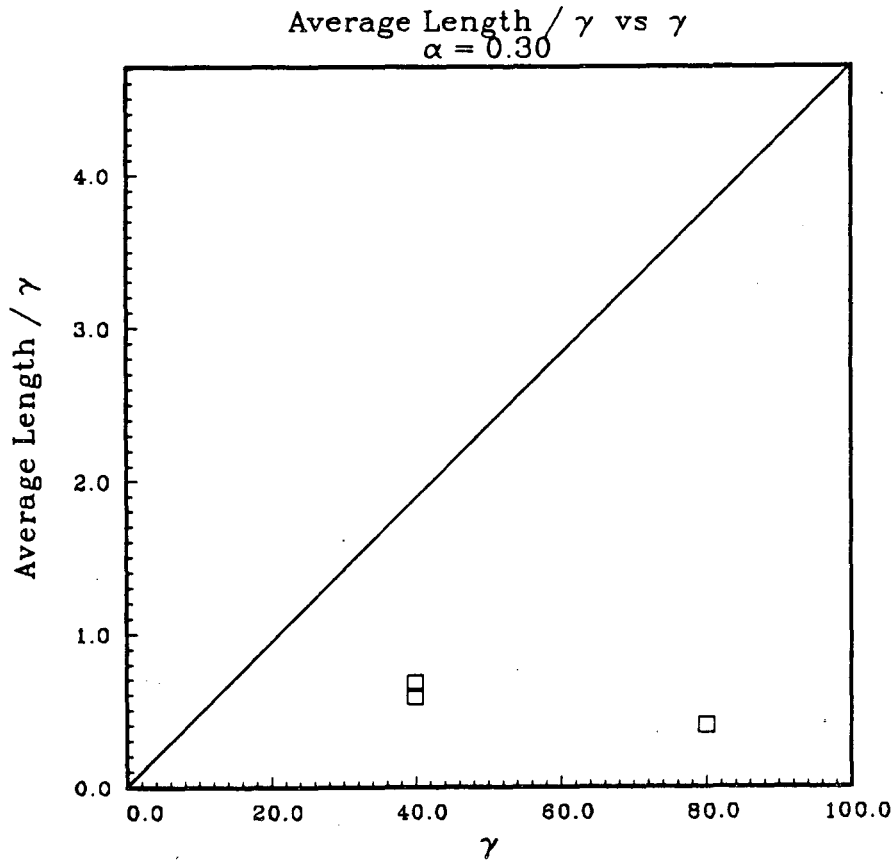
Average Length / γ vs γ
α = 0.30
Average Length / γ
4.0
3.0
2.0
1.0
0.0
0.0
20.0
40.0
60.0
80.0
100.0
γ

Bibliography

[1] C. Anderson and C. Greengard, On Vortex Methods, SIAM J. Numer. Anal., 22 (1985), pp. 413-440.

[2] H. Aref and E. P. Flinchem, Dynamics of vortex filament in a shear flow, J. Fluid Mech., 148 (1984), pp. 477-497.

[3] C. F. Barenghi, R. J. Donelly, and W. F. Vinen, Friction on Quantized Vortices in Helium II. A Review, J. Low Temp. Phys., 52 (1983), pp. 189-247.

[4] G. K. Batchelor, *An Introduction to Fluid Dynamics,* Cambridge University Press, London, 1967.

[5] R. Betchov, On the curvature and torsion of an isolated vortex filament, J. Fluid Mech., 22 (1965), pp.471-479.

[6] A. J. Chorin, *Course notes for advanced numerical analysis,* Mathematics Dept., Univ. California, Berkeley, 1972

[7] A. J. Chorin, Estimates of Intermittency, Spectra, and Blow-Up in Developed Turbulence, Comm. Pure. Appl. Math., 34 (1981), pp. 853-866.

[8] A. J. Chorin, The Evolution of a Turbulent Vortex, Commun. Math. Phys., 83 (1982), pp. 517-535.

[9] A. J. Chorin, Numerical Estimates of Hausdorff Dimension, J. Comp. Phys., 46 (1982), pp. 390-396.

[10] A. J. Chorin and J. Marsden, *A Mathematical Introduction to Fluid Mechanics,* Springer-Verlag, New York, 1979.

[11] S. C. Crow, Stability Theory for a pair of trailing vortices, AIAA J., 8 (1970), pp. 2172-2179.

[12] M. Delfour, M. Fortin, and G. Payre, Finite-Difference Solutions of a Non-linear Schrödinger Equation, J. Comp. Phys., 44 (1981), pp. 277-288.

[13] R. P. Feynman, Application of Quantum Mechanics to Liquid Helium, in *Progress in Low Temperature Physcs,* Volume 1, North-Holland, 1955.

[14] C. W. Gear, *Numerical Initial Value Problems in Ordinary Differential Equations,* Prentice-Hall, Englewood Cliffs, N. J., 1971.

[15] J. Ginibre and G. Velo, On a class of non-linear Schrödinger equations. III. Special theories in dimensions 1, 2 and 3, Ann. Inst. Henri Poincaré, 28 (1978), pp. 287-316.

[16] C. A. Greengard, Three Dimensional Vortex Methods, Ph.D. Thesis, University of California, Berkeley, California, 1984.

[17] O. H. Hald, *Course notes for advanced numerical analysis,* Mathematics Dept., Univ. California, Berkeley

[18] O. H. Hald and V. Mauceri Del Prete, Convergence of Vortex Methods for Euler's Equations, Math. Comp., 32 (1978).

[19] H. E. Hall, The Rotation of Liquid Helium II, Advances in Physics, 9 (1960), pp. 89-146.

[20] H. E. Hall and W. F. Vinen, The rotation of liquid helium II: I. Experiments on the propagation of second sound in iniformly rotating helium II, Proc. R. Soc. A, 238 (1956), pp. 204-214.

[21] H. E. Hall and W. F. Vinen, The rotation of liquid helium II: II. The theory of mutual friction in uniformly rotating helium II, Proc. R. Soc. A, 238 (1956), pp. 215-234.

[22] F. R. Hama, Progressive Deformation of a Curved Vortex Filament by its Own Induction, Phys. Fluids, 5 (1962), pp. 1156-1162.

[23] F. R. Hama, Progressive Deformation of a Perturbed Line Vortex Filament, Phys. Fluids, 6 (1963), pp. 526-534.

[24] H. Hasimoto, A soliton on a vortex filament, J. Fluid Mech., 51 (1972), pp. 477-485.

[25] P. L. Kapitza, Heat Transfer and Superfluidity of Helium II, J. Phys. USSR, 5 (1941), pp. 59-69.

[26] I. M. Khalatnikov, *Introduction to the Theory of Superfluidity,* Benjamin, New York, 1965.

[27] H. O. Kreiss, Über die Stabilitätsdefinition für Differenzengleichungen die Partielle Differentialgleichungen Approximieren, BIT 2 (1962), pp. 153-181.

[28] L. D. Landau, The Theory of Superfluidity of Helium II, J. Phys. USSR, 5 (1941), pp. 71-90.

[29] L. D. Landau and E. M. Lifshitz, *Fluid Mechanics,* Pergamon, London, 1959.

[30] D. Laugwitz, *Differential and Riemannian Geometry,* Academic Press, New York, 1965.

[31] S. Leibovich and K. Stewartson, A sufficient condition for the instability of a columnar vortex, J. Fluid Mech., 126 (1983), pp. 335-356.

[32] A. C. Newell, *Solitons in Mathematics and Physics,* SIAM, Philadelphia, 1985.

[33] L. Onsager, Statistical Hydrodynamics, Nuovo Cimento Suppl., No. 2, Vol. 6, (1949), pp. 279-287.

[34] S. J. Putterman, *Superfluid Hydrodynamics,* North-Holland, Amsterdam, 1974.

[35] R. D. Richtmyer and K. W. Morton, *Difference Methods for Initial-Value Problems,* John Wiley, New York, 1967.

[36] P. H. Roberts and R. J. Donelly, Superfluid Mechanics, Annu. Rev. Fluid Mech., 6 (1974), pp. 179-225.

[37] M. Rosenlicht, *Introduction to Analysis,* Scott Foresman, Glenview, Illinois, 1968.

[38] K. W. Schwarz, Turbulence in superfluid helium: Steady homogeneous counterflow, Phys. Rev. B, 18 (1978), pp. 245-262.

[39] K. W. Schwarz, Generation of Superfluid Turbulence Deduced from Simple Dynamical Rules, Phys. Rev. Let., 49 (1982), pp. 283-285.

[40] K. W. Schwarz, Critical Velocity for a Self-Sustaining Vortex Tangle in Superfluid Helium, Phys. Rev. Let., 50 (1983), pp. 364-367.

[41] K. W. Schwarz, Three-Dimensional Vortex Dynamics in Superfluid ^{4}He. I. Line-Line and Line-Boundary Interactions, Phys. Rev. B, 31 (1985), pp. 5782-5804.

[42] E. Siggia, Collapse and amplification of a vortex filament, Phys. Fluids, 28 (1985), pp. 794-804.

[43] E. Siggia and A. Pumir, Incipient singularity in the Navier-Stokes equations, Phys. Rev. Letters, 55 (1985), pp. 1749-1750.

[44] M. Spivak, *Calculus on Manifolds; a modern approach to classical theorems of advanced calculus*, Benjamin, New York, 1965.

[45] V. E. Zakharov and A. B. Shabat, Exact Theory of Two-Dimensional Self-Focusing and One-Dimensional Self-Modulation of Waves in Nonlinear Media, Soviet Phys. JETP, 34 (1972), pp. 62-69.

This report was done with support from the Department of Energy. Any conclusions or opinions expressed in this report represent solely those of the author(s) and not necessarily those of The Regents of the University of California, the Lawrence Berkeley Laboratory or the Department of Energy.

Reference to a company or product name does not imply approval or recommendation of the product by the University of California or the U.S. Department of Energy to the exclusion of others that may be suitable.

LAWRENCE BERKELEY LABORATORY
TECHNICAL INFORMATION DEPARTMENT
UNIVERSITY OF CALIFORNIA
BERKELEY, CALIFORNIA 94720